CZECH TECHNICAL UNIVERSITY IN PRAGUE

Faculty of Electrical Engineering

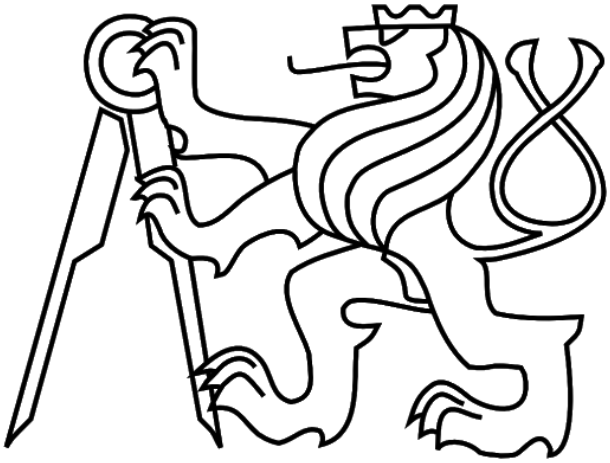

Diploma Thesis

Space mission analysis of a CubeSat satellite in VLEO using an air-breathing ion thruster

Author: Bc. David Hladík

Supervisor: Doc. RNDr. René Hudec CSc.

Prague, 2021

ZADÁNÍ DIPLOMOVÉ PRÁCE

I. OSOBNÍ A STUDIJNÍ ÚDAJE

Příjmení: **Hladík** Jméno: **David** Osobní číslo: **424401**

Fakulta/ústav: **Fakulta elektrotechnická**

Zadávající katedra/ústav: **Katedra měření**

Studijní program: **Letectví a kosmonautika**

Studijní obor: **Avionika**

II. ÚDAJE K DIPLOMOVÉ PRÁCI

Název diplomové práce:

Analýza kosmických misí malých satelitů CubeSat na VLEO s využitím air-breathing iontového pohonu.

Název diplomové práce anglicky:

Space mission analysis of a CubeSat satellite in VLEO using an air-breathing ion thruster

Pokyny pro vypracování:

Description:
Recent advances in space technology have enabled the design of space missions in very low space orbits using small CubeSats 6U to 16U with its own propulsion based on an Atmosphere-Breathing Electric Propulsion (ABEP) with a focus on air-breathing ion thrusters. These studies are based on the experiments and projects of FEE CTU in the field of X-ray monitors, both for space applications and applications of observation of high-energy phenomena in the Earth's atmosphere. This work aims to study the feasibility of a small satellite mission for observing X-ray and high-energy emissions in the Earth's atmosphere in a very low orbit using the ABEP. It should include basic analyzes, specification of parameters and studies for the mission design of a future air-breathing ion-powered satellite.
Tasks:
Create a tool for analyzing the usage of air-breathing ion thruster for very low earth orbit (VLEO) space missions. It should be able to determine the values of drag, power and needed thrust for given space mission parameters. It will also calculate the molecular flow of atomic oxygen for further determination of material degradation. Subsequently, use the data obtained from the tool for a feasibility study and space mission design to study X-ray emissions in the atmosphere (eg in the polar region and in the area of tropical thunderstorms for TGF (Terrestrial Gamma Ray Flashes)). Finally, design and optimize the power system for a small CubeSat satellite, which will be used for this mission.
- Identify and carry out a discussion of general risks related to the operation of a satellite in VLEO
- Create a tool for the analysis of space missions in VLEO with an ABIT propulsion system that will determine the values of drag, power and needed thrust for given space mission parameters. It will also calculate the molecular flow of atomic oxygen for further determination of material degradation.
- Use the space mission analysis tool to design a space mission in VLEO for the study of X-ray sources in the low atmosphere (e.g. TGF, polar regions). Payload of the satellite will be a scientific experiment based on X-ray monitors developed at CTU FEE with lobster eye optics and Timepix detector.
- Design and optimize power system for small CubeSat satellite in very low orbit that is using an ABIT propulsion system.
- Verify the partial functions of the created tool on available data.

Seznam doporučené literatury:

[1] Turner M. J. L.: Rocket and Spacecraft Propulsion Principles, Practice and New Developments, 2nd edition, Praxis Publishing Ltd, UK, 2005, ISBN 3-540-22190-5
[2] Larson W. J., Wertz, J. R.: Space Mission Analysis and Design, Microcosm Inc., Netherlands, 3rd ed. , 1999, ISBN 1-881883-10-8
[3] Edgar Y. Choueiri: Electric Propulsion, Princeton university, 2003
[4] Fortescue P., Swinerd G., Stark J.: Spacecraft Systems Engineering, 4th edition, John Wiley & Sons, Inc., UK, 2011, ISBN 978-0-470-75012-4
[5] Wu J., Zheng P., Zhang Y., Wu B.: A Comprehensive Review of Atmosphere-Breathing Electric Propulsion Systems, International Journal of Aerospace Engineering, 2020
[6] F. Romano, G. Herdrich, S. Fasoulas, T. Schönherr, et al.: "Performance Evaluation of a Novel Inductive Atmosphere-Breathing EP System". 35th International Electric Propulsion Conference (IEPC), Atlanta, USA, October 2017, IEPC-2017-184.
[7] https://www.nasa.gov/smallsat-institute/space-mission-design-tools

Jméno a pracoviště vedoucí(ho) diplomové práce:

doc. RNDr. René Hudec, CSc., katedra radioelektroniky FEL

Jméno a pracoviště druhé(ho) vedoucí(ho) nebo konzultanta(ky) diplomové práce:

Datum zadání diplomové práce: **25.01.2021** Termín odevzdání diplomové práce: _____

Platnost zadání diplomové práce:
do konce letního semestru 2021/2022

doc. RNDr. René Hudec, CSc. podpis vedoucí(ho) práce	podpis vedoucí(ho) ústavu/katedry	prof. Mgr. Petr Páta, Ph.D. podpis děkana(ky)

III. PŘEVZETÍ ZADÁNÍ

Diplomant bere na vědomí, že je povinen vypracovat diplomovou práci samostatně, bez cizí pomoci, s výjimkou poskytnutých konzultací. Seznam použité literatury, jiných pramenů a jmen konzultantů je třeba uvést v diplomové práci.

. _____ Datum převzetí zadání

_____ Podpis studenta

Abstrakt

Diplomová práce se zabývá využitím Air-Breathing Ion Thruster pro kosmické mise na orbitě pod 300 km, neboli VLEO (z angl. *Very Low Earth Orbit*). V teoretické části jsou podrobně rozebrány klíčové pojmy a náležitosti kosmické mise, technologie klasické i vzduch-dýchající elektrické propulze v kosmických systémech, rizika spojená s VLEO oblastí a rentgenové detekce. V druhé části práce je provedena analýza kosmických misí se vzduch-dýchajícím iontovým pohonem, jeho využití a limitace spojené s provozem na VLEO. V rámci analýzy je též představena kosmická mise monitorování vysokoenergetických efektů v zemské atmosféře, kde došlo k návrhu energetického systému vhodného pro správný chod družice CubeSat se vzduch-dýchajícím pohonem.

Klíčová slova

vzduch-dýchající iontový pohon, VLEO, elektrická propulze, CubeSat, aerodynamický odpor, kosmická mise

Abstract

The diploma thesis is dealing with the usage of an Air-Breathing Ion Thruster for space missions below the orbit altitude of 300 km, so-called Very Low Earth Orbit (VLEO) region. The theoretic part introduces the key components of a space mission, the technology of electric propulsion in space systems, the description of air-breathing ion thruster and x-ray detection. The second part of the thesis is focused on performing an analysis of space missions with an Air-Breathing Ion Thruster, its feasibility and limitation. As part of the analysis, the space mission is designed to perform an X-ray monitoring using CubeSat satellite. The design of power system that is capable of supporting the propulsion of a CubeSat unit is included in the space mission design.

Key words

air-breathing ion engine, VLEO, electric propulsion, CubeSat, atmospheric drag, space mission design

Prohlášení

Prohlašuji, že jsem předloženou práci vypracoval samostatně a že jsem uvedl veškeré použité informační zdroje v souladu s Metodickým pokynem o dodržování etických principů při přípravě vysokoškolských závěrečných prací.

V Praze, dne . . . .

podpis autora práce

Declaration

I declare that this thesis has been composed solely by myself and that it has not been submitted, in whole or in part, in any previous application for a degree. Except where states otherwise by reference or acknowledgment, the work presented is entirely my own.

In Prague, ...

signature

Poděkování

Chtěl bych velmi poděkovat vedoucímu mé diplomové práce doc. RNDr. René Hudcovi Csc., za trpělivost s mými otázkami a poskytnutí jeho znalostí. Zároveň jsem vděčný panu Mgr. Adamu Obrusníkovi, Ph.D., a celému týmu lidí z firmy SpaceLab, za poskytnutí konzultací a dat z jejich výzkumu. V neposlední řadě chci poděkovat panu doc. Ing. Janu Kolářovi, CSc., za ochotnou konzultaci a nasměrování správným směrem při tvorbě této práce.

Acknowledgements

I would like to thank the supervisor of my diploma thesis doc. RNDr. René Hudec, Csc., for being patient with my questions and providing his knowledge. At the same time, I am grateful to Mgr. Adam Obrusník, Ph.D., and the entire group of people from SpaceLab, for providing consultations and data from their research. Last but not least, I would like to thank doc. Ing. Jan Kolář, CSc., for his willing consultation and for showing me the right direction in the making of this diploma thesis.

Contents

Nomenclature

AB	Air-Breathing
ABEP	Air-Breathing Electric Propulsion
ABIT	Air-Breathing Ion Thruster
CTU	Czech Technical University
ECR	Electron Cyclotron Resonance
FEEP	Field Emission Electric Propulsion
FOV	Field of View
HET	Hall Effect Thruster
LEO	Low Earth Orbit
MPPTC	Max Power Point Tracking Converter
PCC	Power Conditioning Converter
PPT	Pulse Plasma Thruster
T/D	Thrust-to-Drag ratio
T/P	Thrust-to-Power ratio
VLEO	Very Low Earth Orbit

Chapter 1

Introduction

Contents

1.1 Motivation

Since the late 1950s, when space exploration began with the first satellite Sputnik, mankind has launched thousands of satellites into space with roughly 3 300 active satellites orbiting the Earth at this moment, while the number is growing every day [1] [2]. However, even after more than 60 years of continuous space exploration, there is still one region that remains relatively unexplored.

The vast majority of these satellites and inactive objects, such as space debris, are concentrated in the so-called Low Earth Orbit (LEO), ie in orbits between 300 km and 2000 km. The remaining satellites and objects inhabit higher orbits, which are used mainly for geostationary or geosynchronous orbits. On the other side of the scale, there is the so-called Very Low Earth Orbit (VLEO), ie an orbit below 300 km in which there are essentially no flying objects on stable orbits at all [4].

The VLEO region, approximately from 100 km to 300 km, is still barely accessible, despite technological progress and great scientific efforts. This is due to numerous aspects, but mostly atmospheric drag, which negatively affects the flying body velocity and is, therefore, one of the biggest aspects that affect the lifetime of the satellite. The lower the orbit, the greater the atmospheric drag and the shorter the lifetime of the satellite. The force that slows down an orbiting satellite is quantified by the so-called ballistic coefficient. It depends on the shape, size, and weight of the satellite used. Therefore, the attention is shifting to new solutions in VLEO exploration. The recently most used solution is the usage of CubeSat satellites. Their small dimensions in the tens of centimeters and low production costs are good prerequisites for exploring this area. However, even with small dimensions, the atmospheric drag is a persistent problem and the lifetime of CubeSats orbiting below 250 km can be counted in the units of days, see fig. 1.1.

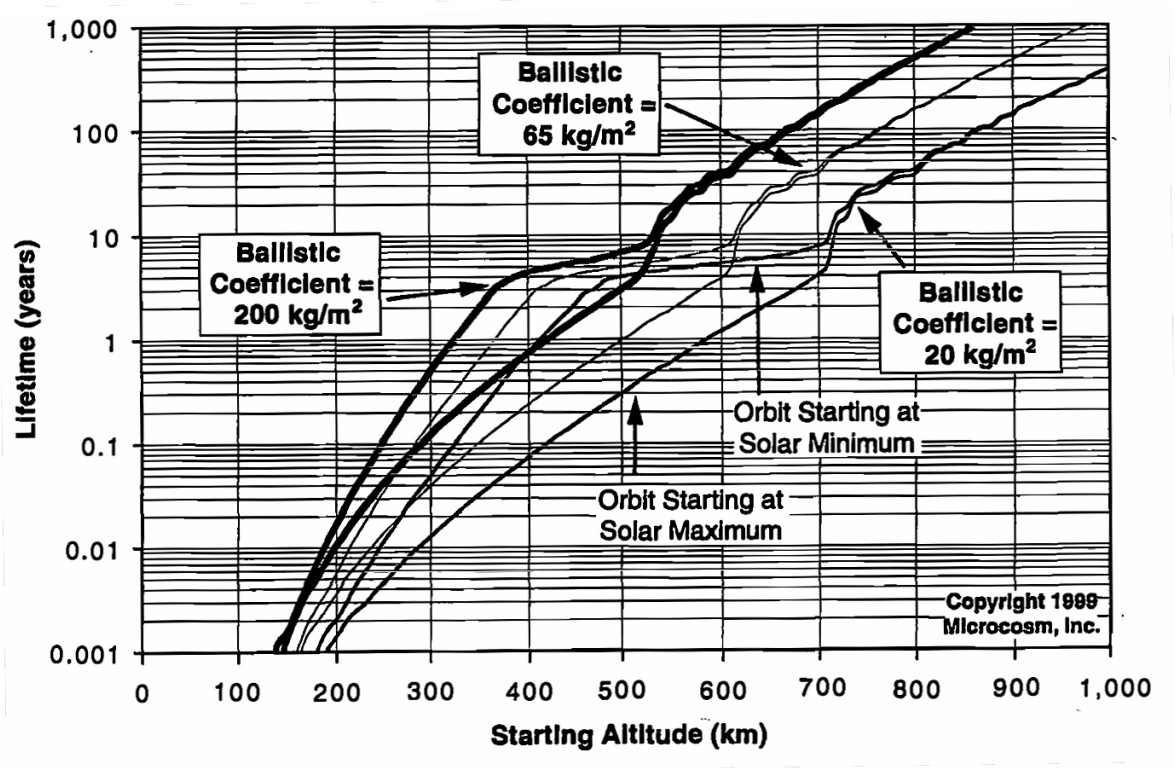

Figure 1.1: Lifespan of a satellite in orbit plotted against the orbit altitude and for different drag coeficients [6]

It is obvious that for the meaningful use of such low orbits, a satellite with its own propulsion is needed. The propulsion system will act against atmospheric drag and prolong the lifetime of a mission. The two questions arise. What is the ideal shape and size of a satellite for missions on VLEO? And what kind of propulsion is most effective for these purposes?

As mentioned, small CubeSats seem to be a suitable choice at first glance. However, it is necessary to be aware of what types of propulsion are available and if it is possible to build them in such small dimensions that they can serve the CubeSats. For a comprehensive overview, it is good to recall all the traditional options and then choose those that can be used or at least theoretically applicable for CubeSats. The types of propulsion systems can be divided into three large groups. Propulsion based on a simple physical principle (pressurized water propulsion, gas nozzles), chemical energy (solid and liquid propulsion), and electrical energy.

Compressed gas propulsion is widely used on both rocket launchers and spacecrafts. They are very reliable, easy to manufacture, and can be manufactured in dimensions small enough to be suitable for CubeSats. However, their specific impulse is one of the lowest, around 70 s [7]. Thus, they are primarily used for attitude control, where short and accurate pulses are required and efficiency is not taken into account.

Chemical rocket propulsion dominates the rocket launcher segment, as it is the only one with a sufficient thrust-to-weight ratio (T/W) to overcome the Earth's gravity and dense atmosphere near the Earth's surface. Their modified versions can also be used effectively in a vacuum, where they are often used to guide satellites into transfer orbits. Solid propulsion is again structurally simple to manufacture and has high reliability. There are also examples with a size of a few centimeters and their specific impulse is already many times higher than gas thrusters - about 280 s (version modified for vacuum reaches up to 300 s) [8]. However, it still does not reach values that would be usable to maintain a permanent orbit in a longer period of time. A major disadvantage of solid propulsion systems is also the impossibility of re-ignitions. In addition, experiments are still being carried out to determine the harmfulness of the particles, which could be released into the upper atmosphere during the continuous firing of solid chemical rockets [5]. Liquid propulsion would theoretically be a more suitable candidate as it has a higher specific impulse, can be ignited repeatedly and with a suitable propellant combination do not produce any toxic or greenhouse gases [9]. However, their complex design makes it almost impossible to reduce the size enough to be used for CubeSat missions.

The last category that remains is electric propulsion. It contains dozens of different propulsion concepts, which have one thing in common. High values of a specific impulse (Isp), which is many times higher than of the previously described types, and thus high efficiency, when the usage of a little amount of propellant can produce the same or even higher amount of energy. The values of Isp for electric propulsion reach up to thousands of seconds [10]. Although the concept of electric propulsion has been known for several decades, it was not until the end of the millennium that it became widely used. At first for the mere station keeping of orbits in geostationary satellites, then for interplanetary flights, and nowadays, it is often used even for changes in orbits around the Earth. This progress is due to endless research, which continues to increase reliability and efficiency. Currently, research on electric propulsion is focused on two directions. Increasing dimensions and power, where the goal is to achieve power over 100 kW (from today's maximum units of kilowatts [12]). Such a large engine could already be considered for use with large satellites or even manned vehicles. On the other hand, designers are trying to reduce the dimensions and thus the power usage so that it is possible to use electric propulsion for small and nanosatellites. This effort has been successful and there are already electric drives with a radius in millimeters [13].

Despite the high specific impulse and ideal dimensions, there is always room for improvement of this technology. The current situation allows to extend the lifetime of a mission in VLEO from several hours to days or even months [28]. But for a truly long-term mission, there is a limitation in the form of the need to carry its own propellant, where its volume is again limited by the size of the satellite used. For this reason, since the start of the new millennium, scientists have been trying to develop an electric drive that will be able to use particles from the residual atmosphere as a propellant. This concept is called *air-breathing electric propulsion (ABEP)* (also referred to as *atmospheric-breathing electric propulsion*).

1.2 Contribution

This work has been created in cooperation with the Czech company SpaceLab, which is developing a new air-breathing electric propulsion drive. The work aims to:

- Analyze and design a suitable space mission for a small CubeSat satellite in Very Low Earth Orbit (VLEO) using an air-breathing electric propulsion (ABEP) drive.
- Carry out a feasibility study of ABEP propulsion and comparison to classical electric propulsion.

1.3 Overview

The first part of the thesis describes the principles of maintaining the satellite on VLEO. Therefore, it is necessary to have an overview of the classical electric propulsion, which is described in the Chapter 2. It is followed by an explanation of the principles of an air-breathing electric propulsion and a description of the VLEO environment in the Chapter 3.

The second part is focused on explaining the principles of X-ray detection and describing the Lobster Eye detector in the Chapter 4. At the same time, the Chapter 5 provides a brief summary of the space mission design process.

The third part is devoted to the design of a specific space mission with a CubeSat satellite and air-breathing propulsion unit in the VLEO region. In the Chapter 6 simple algorithm with interactive plots that was used to perform the analysis is described, and in the Chapter 7 space mission for X-ray monitoring is designed. It includes ABIT analysis and power system design. Authors own results are presented within these chapters.

At last, the conclusion and the discussion can be found in the Chapter 8.

Data plots throughout the whole thesis (namely in Chapters 3, 6 and 7), if not marked with a reference or stated otherwise, are the author's work.

Chapter 2

Electric Propulsion

Contents

2.1 Brief history

As in the case of chemical propulsion, the beginnings of electric propulsion date back to the 1920s to two men who are referred to as the fathers of rocketry. Robert H. Goddard and Konstantin Eduardovich Ciolkovsky (sometimes in English literature as Konstantin Eduardovitch Tsiolkovsky). These two gentlemen independently came up with an idea that accelerated particles could be used to move objects based on Newton's laws [14]. Out of this idea came not only today's chemical rocket engines, but also the first suggestions on how to use accelerated electrons (and later ions) for the propulsion purposes. In 1920, Robert H. Goddard published his first documents describing the design of an electrostatic thruster.

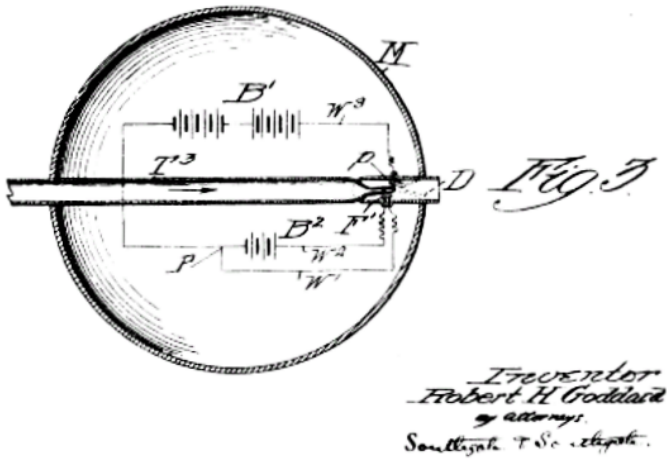

Figure 2.1: The first design of an electrostatic thruster patented by Robert H. Goddard in 1920 [14]

Further development of electric propulsion continued a few decades later, in the early 1950s. The reason behind the wide gap was both political, where most of the world was occupied with World War II, and the technical limitations in the associated industries. For thorough testing, a high vacuum was (and still is) required, which was not achievable with the technology of that time. At the same time, chemical rockets, despite enormous advancement during the war, still did not reach such a level as to launch a spacecraft into orbit [14]. For these reasons, all efforts were focused on improving chemical propulsion first.

With the first successes in the field of rocketry in the 1950s, scientists returned to the concept of electric propulsion. Three basic building blocks have been discovered, on which modern concepts still stand [5].

- The need for high atomic number propellant for the most efficient use of accelerated particles
- The need for a neutralizating beam that ”injects” electrons into the exhaust gases
- The usage of two accelerating grids placed in close proximity for the generation of strong electric field

The first experiments in space took place in the early 1960s in both the United States and the Soviet Union. At first only to provide station keeping maneuvers, which it serves reliably

to this day. Subsequently, in the 1990s, electric propulsion became relevant for commercial purposes and, over time, for guidance in transfer orbits and space missions such as Deep Space 1, launched in 1998 to demonstrate new ion propulsion technologies. During this mission, the value of $\Delta v = 4500$ m/s was achieved with only 70 kg of propellant [15]. To date, electric propulsion is widely used for most of the standard orbital maneuvers. It is worth noting the growing constellation of Starlink satellites by SpaceX, which uses krypton ion thrusters to raise and maintain its orbit.

2.2 Division of Electric Propulsion

As there is large number of different concepts of electric propulsion drives, it is important to outline at least a basic division. There is still disagreement among the authors as to which key to use when dividing the different types of electric propulsion. However, most publications sticks to the division, based on different principles that are used to accelerate the particles. In this case, it is possible to divide it into three large groups [16].

- Electrostatic
- Electromagnetic
- Electrothermal

In each of these groups, it is still possible to subsequently divide the types according to the way ions are generated and a number of other subcategories. However, such a detailed division is not essential for this work. Out of dozens of concepts, only the most relevant and used types of electric propulsion were selected for further discussion.

2.2.1 Electrostatic propulsion

The principle of electrostatic propulsion is simple and of all the other principles the most researched. Appropriately selected propellant is ionized and the resulting charged ions are

accelerated by a strong electric field. The ejected ions generate thrust according to the Newton's third law. In practice, two charged grids placed in close proximity to each other are often used to generate a strong electric field, thus creating a large voltage potential difference. The resulting flow of charged particles behind the grids is further neutralized by a beam of electrons to prevent the accumulation of a positive charge on the outside of the satellite. Rare gases such as argon, xenon or cesium are most often chosen as propellant [17]. This is a consequence of trade-offs between the value of an atomic number, where the aim is to have the highest possible value for the highest possible thrust, price and good properties for long-term storage.

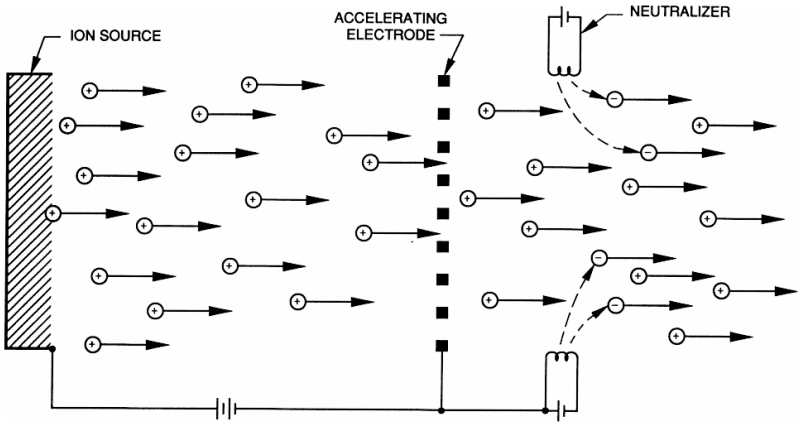

Figure 2.2: Diagram of simple electrostatic propulsion system that is using an electric field to accelerate charged ions [20]

The biggest limiting factors are heat losses and, in the case of grid design, material degradation. Heat losses occur in the ionization chamber during the ionization process and can therefore be influenced by a suitably selected ionization system. On the other hand, the grid electrodes and cathode wear out due to erosion during ion impacts at high velocities. This is a limiting factor that has a very negative effect on the lifetime of the entire system. Material erosion can be reduced by using modern materials such as carbon or by better hole layout for easier ion ejection [17].

The most known examples of electrostatic propulsion are *Ion Thruster* and *Field Emission Electric Propulsion (FEEP)*.

2.2.1.1 Ion Thruster

Ion thruster (sometimes reffered to as *Gridded Ion Thruster*) is one of the most researched concepts of an electrostatic or perhaps even electric propulsion systems. It is popular mainly due to its proven long lifetime of over 20 000 hours, high efficiency (around 65 %), exhaust velocity of up to 30 000 m/s and power levels between 50 W- 200 kW [17]. The basic concept of ion thruster consists of three common elements.

- Ion source
- Acceleration grid
- Neutralizer

Ion source

Ion source contains the whole system of ionization of the propellant. The most used principles of ionizating the propellant are electron bombardment, contact ionization using a cesium-tungsten surface and ionization using microwave or radio waves [20].

The electron bombardment principle is based on a cathode that emits the electrons into the ionization chamber, which is filled with propellant and has walls behaving as an anode. By means of a strong magnetic field in the chamber, the electron is swirled from the cathode to the anode by a swirling motion, where it strikes atoms of the propellant and ionizes them along the way.

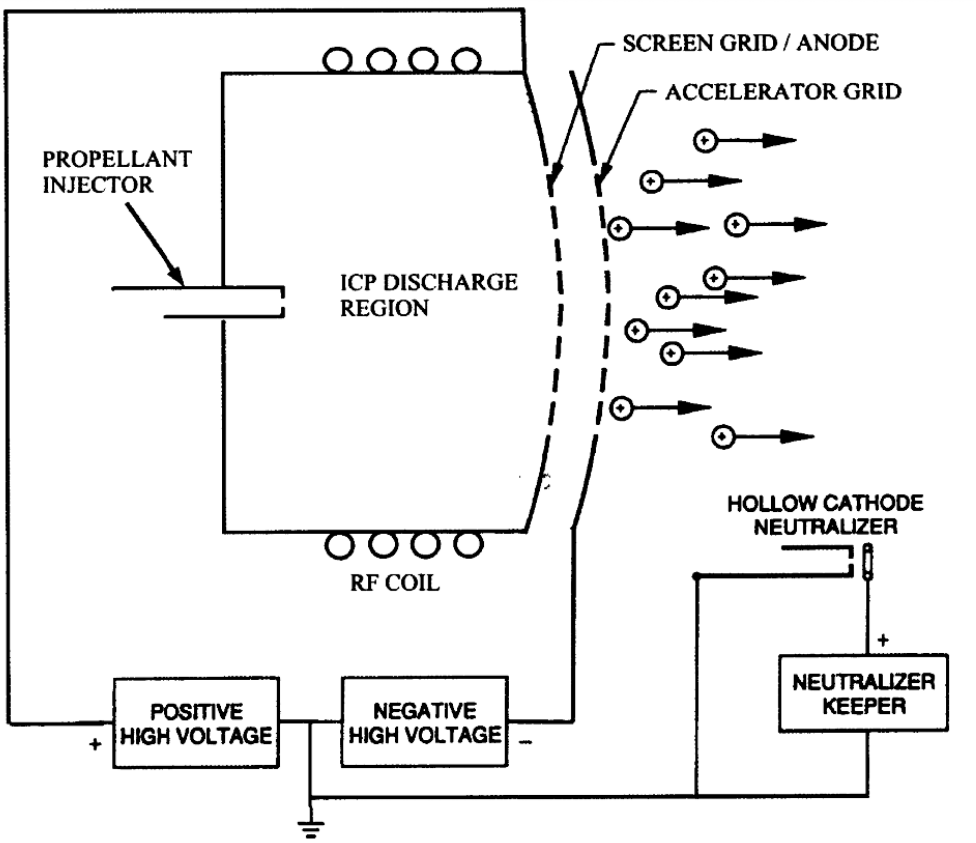

Figure 2.3: Ion Thruster diagram that is using ion bombardment to ionize the propellant [18]

The magnetic field, which permeates the entire ionization chamber, is created by three ring magnets, which were empirically chosen so that the resulting field supports ionization and discharge stability as much as possible. A typical value of the magnetic field is about 0.25 T and the voltage between the cathode and the anode is about 30 V when xenon is used as a propellant. Contact ionization is not used very often, because ionization degrades the tungsten layer, which in turn significantly reduces the ionization efficiency [20].

Ionization by radio waves is in principle very similar to the already mentioned electron bombardment. The only difference is that the discharge is driven inductively by radio waves, so it is a so-called cathode-free concept. It is gaining in popularity in recent years, mainly in Europe. A similar concept is also used in Japan, where they mostly utilize microwave range of spectrum. These electromagnetic waves can create and maintain plasma in the ionization chamber due to a phenomenon called *Electron Cyclotron Resonance (ECR)* [21].

The supplied microwaves or radio waves have a corresponding cyclotron resonant frequency based on a magnetic field in the vessel. The frequency is chosen to be synchronous with the

Larmor radius of the electrons in the ionization chamber. Due to resonance effects the energy of electrons rises, which subsequently causes ionization of the surrounding elements.

Acceleration grids

As was mentioned above, acceleration grids are placed behind the ionization chamber as shown in the figure 2.3. They fulfill the simple task of accelerating positively charged ions from the ionization chamber to the required velocities so that there are as few ion impacts on the grid material as possible. The grid perforations are empirically configurated to minimize the number of ion impacts on the material and the voltage levels are set to precise values that increase the beam density and thus the efficiency of the whole system [20].

The rate at which ions shoot out of the ionization chamber is determined mainly by the decrease in potential between the ion source and the plane of effective neutralization and the so-called charge-to-mass ratio. Commonly achieved velocities are up to 10^5 m/s [20]. The equation 2.1 shows how is the power level dependant on the exhaust velocity.

$$m_p = \alpha P = \frac{\alpha T v_e}{2\eta} = \frac{\alpha \dot{m} v_e^2}{2\eta} \tag{2.1}$$

Here m_p denotes the mass of the electric source, α is the ratio of mass to unit of power, η is the efficiency of the thruster, T is the thrust, $\dot{m}$ is the mass flow of the propellant and v_e is the exhaust ion velocity. At the same time, it is important to be aware of the seriousness of the issue of the density of the outgoing beam. Ideally, it is necessary to achieve the highest possible density, which can be expressed by the equation 2.2.

$$j = \frac{4\epsilon}{9}\left(\frac{2q}{M}\right)^{1/2}\frac{V^{3/2}}{d^2} \tag{2.2}$$

Where j is the beam density, d is the size of the gap between the grids, V is the voltage, ε is the dielectric permittivity and q/M is the charge-to-weight ratio. The maximum thrust density can be subsequently derived.

$$\frac{T}{A} = \frac{\dot{m}v_e}{A} = \frac{jMv_e}{q} = \frac{8\epsilon}{9}\left(\frac{V}{d}\right)^2 \tag{2.3}$$

Where *A* is the area of the nozzle and v_e is expressed as a function of the voltage on the grids and the charge-to-mass ratio of the ion.

$$v_e = \left(\frac{2qV}{M}\right)^{1/2} \tag{2.4}$$

Using real values of *V, d* and *q/M* it can be obtained that it is possible to achieve a thrust of units of newton per square meter with the required power level of up to 10^5 W [20].

Neutralizer

After the release of positive ions from the ionization chamber, a negative charge accumulates around the entire propulsion system. In order to avoid retaining the positive ion beam at the surface of the drive, a neutralizer is present which electrostatically neutralizes the outgoing beam immediately after passing through the acceleration grids. Another hollow cathode, similar to the one used to ionize the propellant, is used for this purpose [19].

2.2.1.2 Field Emission Electric Propulsion - FEEP

For missions where a long-term thrust impulse is not required, it is possible to omit all complex elements of the ion thruster, such as a source of bombarding electrons, grids for precise ion beam directing or electromagnets. If an electric field with a high concentration is generated around the outlet of the capillary tube, it is possible to ionize a propellant such as liquid metal directly using this field. The ions formed from direct ionization can be electrostatically accelerated. This system, shown in 2.4, is called *Fiel Emission Electric Propulsion* or FEEP.

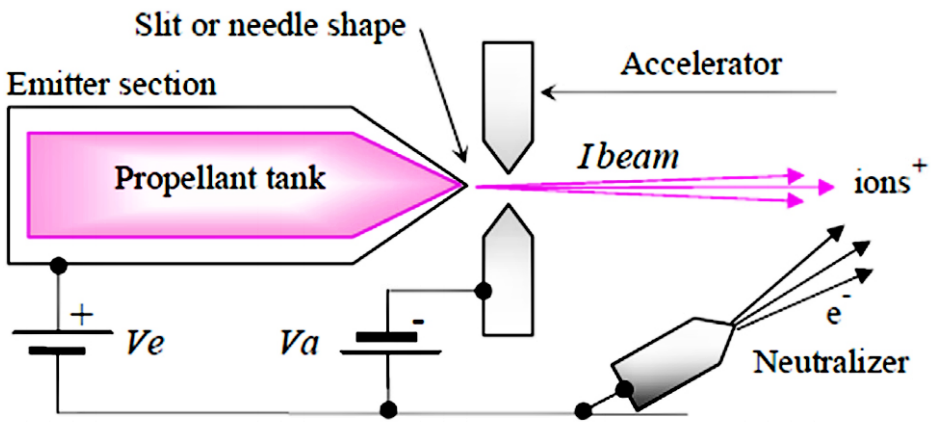

Figure 2.4: Field Emission Electric Propulsion drive diagram. [23]

Typically, cesium is used as a propellant for this type of propulsion. It is stored in a tank, from which it is let into a micro millimeter capillary tube at the end of which it is ionized by a strong electric field. When the electric field reaches the order of 10^9 V/m, ions are emitted directly from the propellant at the endpoint of the capillary tube. The subsequently accelerated ion beam must again be neutralized by a similar neutralizer as in the case of the ion thruster.

For commonly used voltage values around 10 kV, the exhaust velocity is up to 100 000 m/s and the efficiency is very close to 100 %. Although the exhaust velocity is up to three times higher than in the case of ion thruster, there is a disadvantage in low thrust, which reaches values of about 16 µN/W. However, there are FEEP drive concepts that achieve a ratio of up to 5 mN/W [20].

FEEP drives are most often used for short, maximum several minutes long ignitions, where a high degree of accuracy and efficiency is required. However, since cesium is used as a propellant, there are still many problems associated with exhaust gases and, in general, contamination by the propellant, which will need to be addressed before the use of this type of propulsion becomes standard.

2.2.2 Electromagnetic propulsion

Electromagnetic propulsion uses the properties of plasma as a conductive medium. The basic principle is the interaction of an electric current that passes through an ionized propellant with a magnetic field. This interaction creates a Lorentz force that accelerates the propellant out of the chamber. Electromagnetic systems can produce exhaust velocities significantly higher than electrothermal propulsion systems and the thrust density is much higher than in the case of electrostatic systems. It is also important to realize that the used plasma, despite its conductivity, is externally neutral, so the electromagnetic system is not limited by the charge imbalance as electrostatic systems are.

Two basic models of electromagnetic propulsion systems are *Hall Effect Thruster (HET) and Pulse Plasma Thruster (PPT)*.

2.2.2.1 Hall Effect Thruster - HET

Hall Effect Thruster is in the spectrum of an electric propulsion right between electrostatic and electromagnetic propulsion systems. Its principle is similar to ion thruster propulsion, however, it does not use any accelerating grids and the acceleration of ions is done exclusively by the Lorentz force created by an electromagnetic field in the plasma. Due to the conductivity of the plasma and the presence of an external magnetic field, the Hall effect is strongly manifested, when the ions are swirled away perpendicular to the present magnetic field, ie out of the chamber. Ionization is also performed by the Lorentz force. Injected electrons begin to orbit freely around the axial component of the electric field. During this movement, they collide with the atoms of the propellant, most often xenon, which is injected through the anode and ionize it. The strength of the magnetic field is chosen so that the electrons remain in a swirling motion with a minimal axial speed component and thus can ionize longer. On the other hand, heavier ions are drawn out of the chamber by the electric field and create thrust.

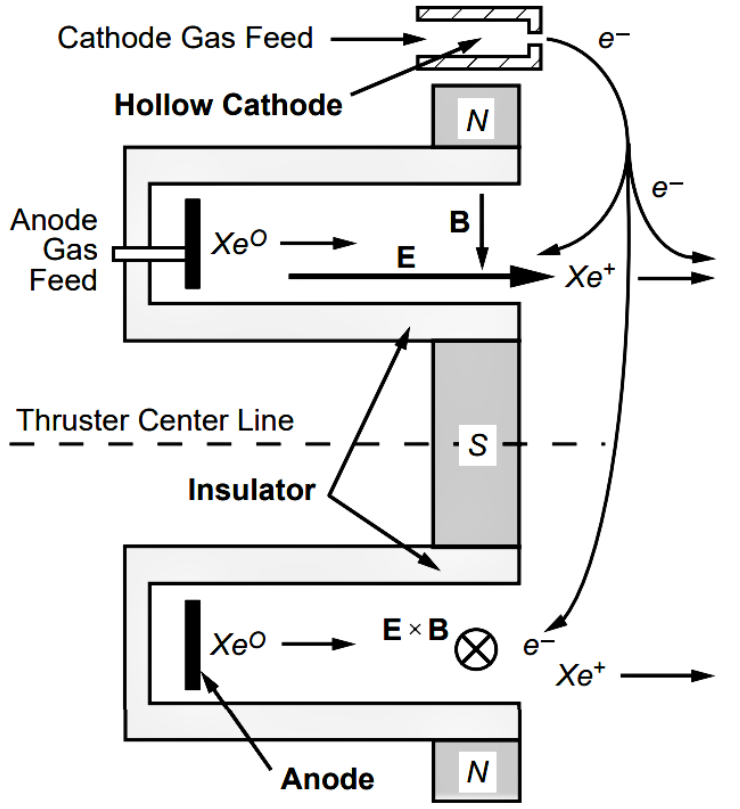

Figure 2.5: Hall Effect Thruster diagram. [11]

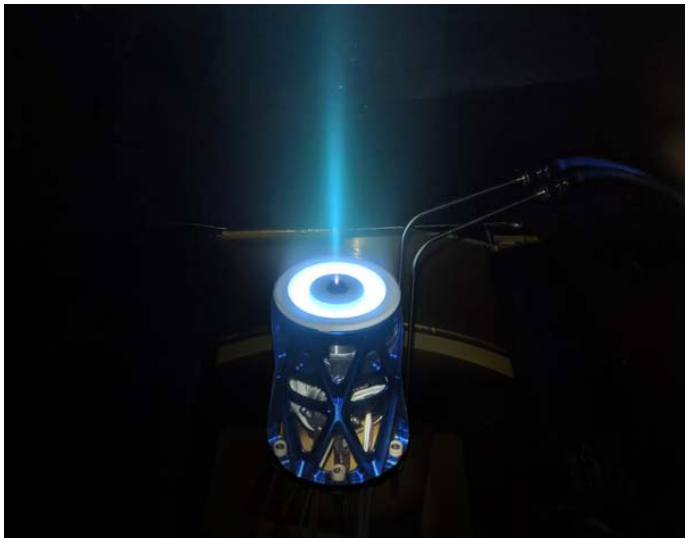

Figure 2.6: Real photo of an active HET. [22]

The nominal values of a typical xenon Hall Effect Thruster are up to 80 mN of thrust with exhaust velocity of 16 000 m/s, an applied voltage of 300 V and an efficiency up to 70 % [20] [12].

2.2.2.2 Pulse Plasma Thruster - PPT

Like FEEP, the pulsed plasma thruster is based on short (approximately 10 µs) energy pulses of up to 10 MW. A system of capacitors is most often used to store this energy. PPT systems can be divided into two different concepts. One uses a gas propellant and is called GF-PPT (*Gas-fed Pulsed Plasma Thruster*). The second is based on solid propellant and is called APPT (*Ablative Pulsed Plasma Thruster*) [25].

GF-PPT systems were developed in the early 1960s and operate on the principle of high-frequency injection of small doses of gas propellant between two electrodes, where an energy pulse occurs and the gas is ionized. Subsequently, a pinch effect occurs, which uses the Lorentz force to push the ionized gas out of the chamber (more on the issue of electromagnetic pinch can be found, for example, in the book *P. Kubes*, [24]). In the 1960s, efficiencies were reaching values over 20 % and specific impulses were as high as 5,000 s [20]. Futher development was suspended at the time, because of limited capability of manufactoring large and high quality capacitors. Another problem occured with the lifetime and precision of valves used to distribute the propellant.

For these reasons, a simplified concept of APPT (Ablative Pulse Plasma Nozzle) was made. It uses ablation of a solid material, most often Teflon, instead of gas as a propellant. Teflon is evaporated by an electrical impulse and the resulting plasma is, as in the previous case, expelled from the chamber by the Lorentz force. Thanks to this concept, the problem with a lifetime of valves has been eliminated and the overall reliability of the entire system has been increased. On the other hand, such a solution has a much lower efficiency (below 15 %) and a satellite contamination from exhaust gases created by Teflon ablation is present. [20].

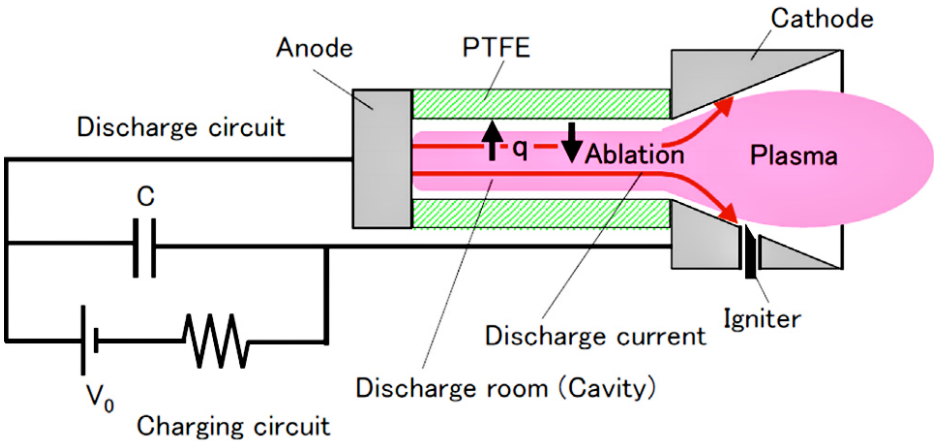

Figure 2.7: APPT diagram. [23]

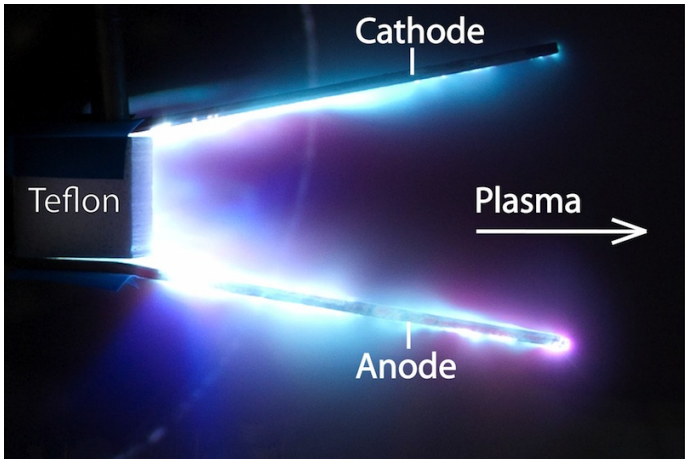

Figure 2.8: Real photo of an active APPT. [26]

Nowadays, the scientific segment of high-energy pulses is developing fast and experimental data on the behavior of such discharges are being refined, which is reflected in the renewed interest in GF-PPT.

2.2.3 Electrothermal propulsion

Electrothermal propulsion is conceptually the simplest. The principle is in heating the propellant, raising its pressure and then releasing it through a suitably shaped thruster. Electrothermal drives are further divided according to the method of transferring thermal energy to the propellant.

- Resistojets
- Arcjets
- Induction and radiation heated devices

For all three methods applies that they remove the limiting factor of chemical propulsion that the combustion process is necessary. Thus the propellant can be chosen purely on the basis of their physical properties and not the chemical one. On the other hand, there are several limitations during the heating process and their gross power is strictly limited by the maximum exhaust velocity. Exhaust velocity of electrothermal propulsion systems is given by the equation 2.5 [19].

$$v_e \leq \sqrt{2(h_t h_e)} \tag{2.5}$$

where h_t enthalpy of heated propellant and h_e is nozzle exit enthalpy.

Therefore, the ideal gas for the propellant would be hydrogen. However, the problem of hydrogen storage reduces its attractiveness for this method of propulsion. Nowadays, gases such as ammonia and hydrazine are widely used due to their dissociation properties into low mass molecules and its high thermal capacity.

2.2.3.1 Resistojets

Resistojets use direct contact between the heater and the propellant to heat it. A tungsten chamber is often used as a heater, through which the propellant passes before being ejacted from the nozzle. Resistojets are strictly limited by the heat resistance of the material that was used to construct the chamber. Most often, the upper temperature limit is around 3000 K and thus the exhaust velocity is limited to maximum values of about 10 000 m/s. Even so, these are two to three orders of magnitude higher exhaust velocities than conventional chemical propulsion can achieve [38]. Other limiting factors include the resistance of the insulators and heating surfaces exposed to high temperatures for long periods of time, while minimizing viscous and radiant heat losses.

On the other hand, due to their design simplicity and great similarity to the widely used compressed gas thrusters, they have been used frequently and reliably since the mid-1960s. The difference between compressed gas thruster (called *cold thrusters*) and resistojets (*hot thrusters*) can be simplified to a mere addition of the heating system. The specific impulse of such an improvement will increase up to ten times. For better understanding of their performance, typical values of hydrazine resistojet achieves exhaust velocity up to 3500 m/s, a thrust of 0.3 N with an efficiency of 80 % and a power consumption of about 750 W [20].

2.2.3.2 Arcjets

To increase the performance of an electrothermal propulsion system, higher exhaust velocity is required, ie higher propellant temperatures. However, as already mentioned, this is limited by the heat resistance of the engine chamber. Therefore, for higher temperatures, it was necessary to develope a system in which there is no contact between the hot propellant and the chamber wall. Such a system is called an *Arcjet* and uses an electric arc in a suitably chosen configuration to heat the propellant. A direct current of tens or hundreds of amperes is released between the cathode and the anode. The resulting electric arc reaches a temperature of up to tens of thousands of degrees Kelvin. The propellant is then injected perpendicular to the arc. By a combination of thermodynamic and ionization processes it is swirled along the arc into a nozzle and fired at an average speed of up to tens of thousands of meters per second. Although the walls of the chamber and the electrode are protected from high temperatures, the electrodes erode and thus the lifetime of the entire drive is severely limited. At present, hydrazine arcjets have an exhaust velocity of about 6000 m/s with an efficiency of up to 40 % [20].

2.2.3.3 Induction and radiation heating

Due to the limiting factor of arcjet, their electrodes, there was a great effort to find a solution that would work without any electrodes. The methods of such heating vary greatly in the energy required, the geometry, the propellants used and the method of energy transfer from

low frequency waves (radio waves) to the microwave region. The heated propellant is then often confined by means of an electrostatic or electromagnetic field and ejected from the nozzle. Induction and radiation electrothermal drives can, in fact, be considered as a kind of hybrids between all three categories of electrical propulsion - electrothermal, electrostatic and electromagnetic.

The biggest disadvantage of induction drives lies in the low efficiency of electromagnetic wave generation. For these reasons, it is still a concept that is only tested in laboratories. However, it turns out that these drives could be advantageous on a smaller scale, around a power level of 100 W and below [20].

2.3 Summary

Electric propulsion is divided into three large groups - Electrostatic, electromagnetic, and electrothermal. Each group includes a large number of different drive concepts, which differ mainly in their efficiency expressed by a specific impulse, the amount of achievable thrust, lifetime, and power consumption. The table 2.1 summarizes the basic types of electric engines mentioned in the previous sections, and the following figure 2.9 provides comprehensive graphic overview of the thrust and specific impulse values for each engine type, including chemical rocket engines.

	Thrust [mN]	Isp [s]	Efficiency	Lifetime [h]	Power [W]
Arcjet	100-250	480 - 700	up to 40 %	1200	750 - 2000
Resistojet	**300-400**	300	**80 - 90 %**	400	500 - 800
PPT	0.1 - 2	500 - 1000	under 20 %	X	**10 - 100**
FEEP	0.001 - 1	**6000 - 10 000**	up to 50 %	X	X
HET	80 - 100	1600 - 2000	up to 50 %	7000	1300 - 1500
Ion Thruster	5 - 40	2500 - 3800	up to 65 %*	**25 000***	200 - 4000*

Table 2.1: The summary of the most important parameters of all the discussed propulsion types [38]. The best values for every parameter are shown in bold. Parameters signed with * refers to *Choueiri, 2003* [20].

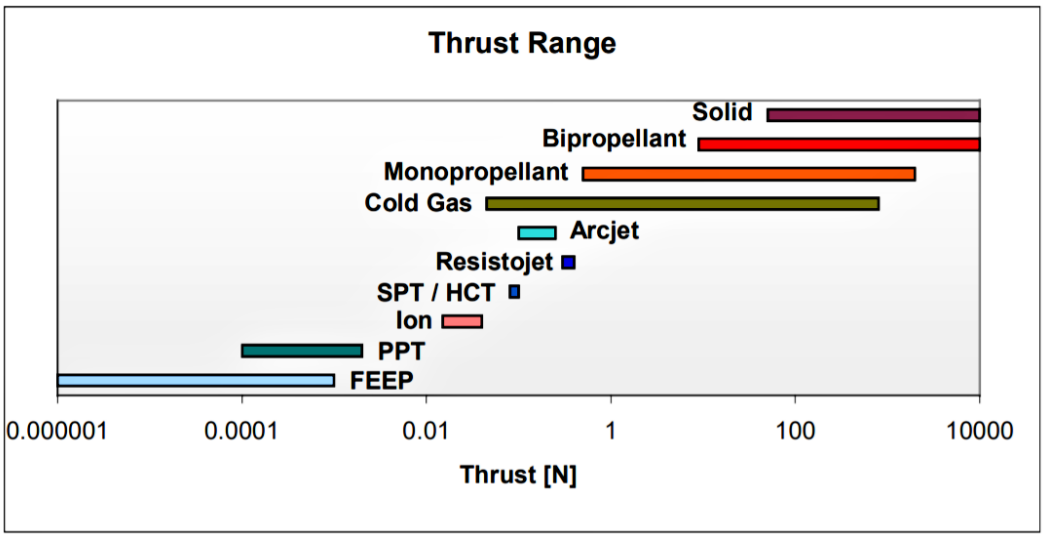

(a) Overview of thrust values for individual types of propulsion systems

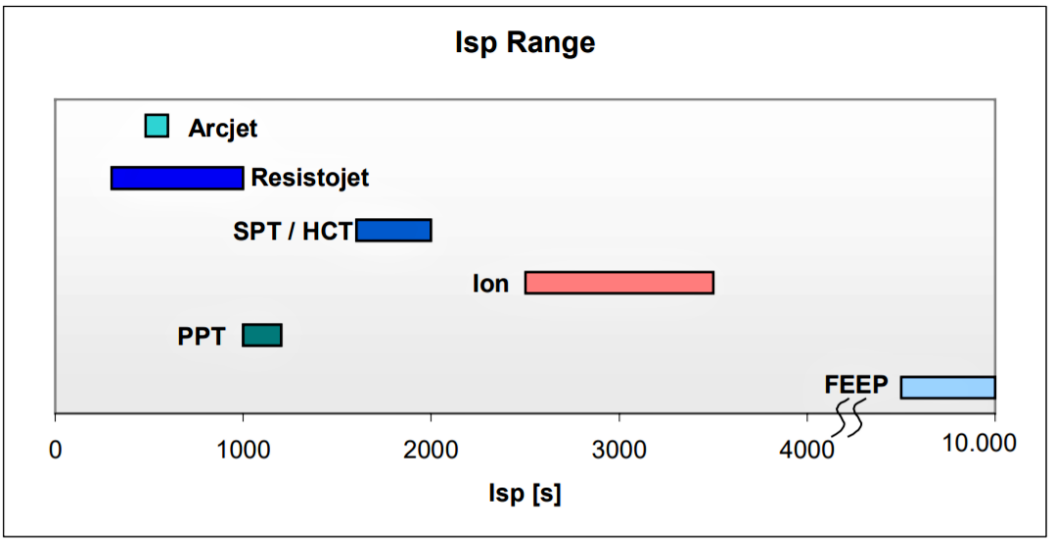

(b) Overview of Isp values for individual types of electric propulsion systems

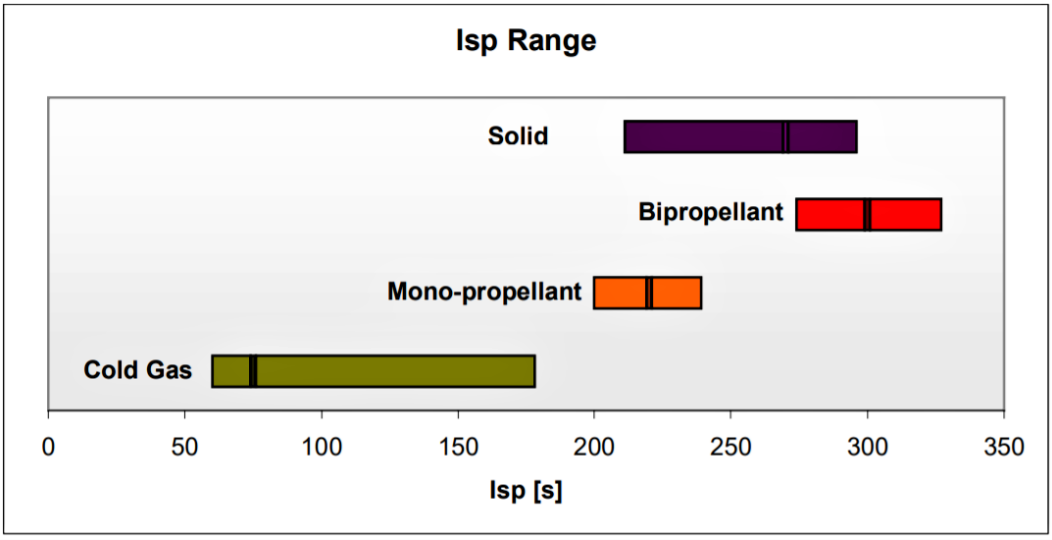

(c) Overview of Isp values for individual types of classic chemical propulsion systems

Figure 2.9: Overview graphs of thrust and Isp values for individual types of propulsion systems including classic chemical propulsion units [38]

Chapter 3

Air-Breathing Ion Thruster

Contents

In the introductory paragraphs, it was already indicated that even the best propulsion system (electric or other type) is insufficient for space missions in orbits below 300 km. This is not due to low efficiency or physical limitations, but purely from the fact that keeping a satellite on such a low orbits requires a lot of energy and therefore a lot of propellant, which the satellite must naturally carry.

Several missions were carried out at orbits below 300 km, but mostly without its own propulsion system for compensating the atmospheric drag. The lifespan of such missions

was therefore of the order of only a few hours, a maximum of days. However, in 2009 ESA launched the GOCE satellite (*The Gravity Field and Steady-State Ocean Circulation Explorer*). This satellite had an ion propulsion system made by QinetiQ, which was able to develop a thrust of up to 22 mN with a power consumption of about 1 kW and 40 kg of xenon as a propellant [27]. The goal of the ion thruster was to keep the satellite in orbit at 254 km for a minimum of 20 months. Due to low solar activity the mission was extended to the final 55 months when the propellant finally ran out.

When increasing the volume of propellant tanks, the breaking point will sooner or later occur, when it is no longer economically feasible to further increase its volume. Higher volume of propellant means higher mass and insufficient space for the payload of the mission and the overall enlargement of the satellite will negatively affect the life of the mission and it is therefore necessary to add propellant again. The current state-of-the-art technology of conventional electric drives can compensate atmospheric drag below 250 km for a maximum of 2 years [28]. A possible solution to this situation lies in a propulsion system that could use the residual atmospheric gases present at altitudes between 100 km and 300 km as propellant. This would eliminate the problem of a limited amount of propellant in the satellite and the lifetime of a space mission could theoretically be dependant only on the lifetime of the individual mechanical parts.

Project Discoverer [29], supported by European Union, brings together several major European universities that are working in the field of space engineering, to develop funcional and ready-to-use propulsion system based on so-called *Air-Breathing* technology. The direction of research is determined by three fundamental questions.

- How to increase the level of understanding and use of orbital and aerodynamic properties of the object in the low layers of the atmosphere, for the attitude control?
- Is there a suitable propulsion system that is able to use residual atmospheric gases as its propellant to compensate for atmospheric drag and thus eliminate the mission lifespan limitation?
- Are there materials and manufacturing processes that can reduce the effects of atmospheric drag on the surfaces of a spacecraft?

Several experiments have already been performed within the project and countless works have been published, which to a greater or lesser extent answer these key questions. It is possible to list a few publications that will be mentioned within the framework of this diploma thesis. *Investigation of Novel Drag-Reducing and Atomic Oxygen Resistant Materials in Very Low Earth Orbit using SOAR (Satellite for Orbital Aerodynamics Research)* [30], *The Benefits of Very Low Earth Orbit for Earth Observation Missions* [31], *Modeling and Simulation of Very Low Earth Orbits* [32], *RF helicon-based inductive plasma thruster (IPT) design for an Atmosphere-Breathing Electric Propulsion system (ABEP)* [33].

ESA air-breathing propulsion study, conducted in 2007, addressed the issue of the usability of AB drives in comparison with conventional versions of electric propulsion. This study deals mainly with the technologies for large satellites with usable power in hundreds of watts, up to units of kilowatt. An important conclusion of the study is the altitude range definition of applicability for AB drives. The bottom line is limited by the available power and thrust capabilities of the satellite and is set to 200 km [28]. For the upper limit, it has been found that from the altitude of about 250 km above sea level there is a so-called *Propellant break-even point*, which indicates the point beyond which it is economically more advantageous to use a classical electric propulsion system for atmospheric drag compensation [28]. Both of these limits will be analyzed in the upcoming chapters and results will be compared.

To understand the issues of Air-Breathing technology, it is necessary to explain the properties of the environment at given altitudes and its effects on the spacecraft, outline suitable propulsion systems that can be adapted to the usage of residual gases of the atmosphere and finally a detailed description of one selected engine concept.

3.1 Environment Properties

The Earth's atmosphere, composed of various types of gases, reaches a height of about 10 000 km above the Earth's surface. Due to gravitational forces, most of the atmospheric matter is kept close to the surface and it is stated that up to 75 % of the total atmospheric mass is in the first 11 km [34]. The internationally recognized boundary of space, the so-called Karman's line, is set at an altitude of 100 km above the surface of the ocean. This is only a theoretical line, because, as has been said, the atmosphere continues for thousands of kilometers. Only the decrease in the density of particles is very steep. Even though the concentration of particles above the 100 km line is small compared to lower layers of the atmosphere, it still fundamentally influences the behavior of flying bodies that move there at high orbital velocities.

3.1.1 Residual atmosphere

The atmospheric model NRLMSISE-00 (*Naval Research Laboratory Mass Spectrometer and Incoherent Scatter Radar*) developed in 2000 is used for accurate particle density calculations [35]. This model also takes into account the specific day, month of the year and the corresponding solar and geomagnetic activity, which strongly affect the density of the atmosphere in the upper atmospheric layers. Solar and geomagnetic activity changes periodically and has been intensively studied for the last decade. Detailed values are provided by NOAA (*National Oceanic and Atmospheric Administration*) available at [36].

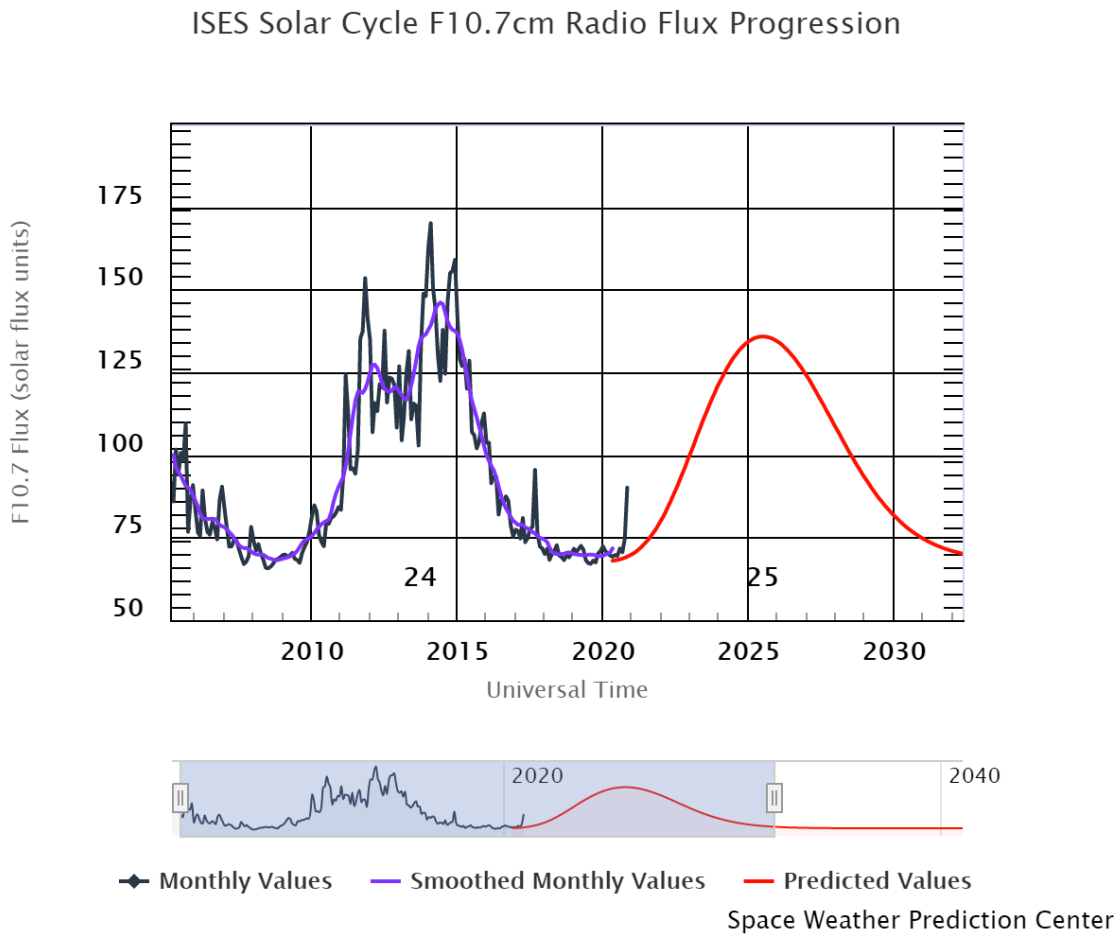

Figure 3.1: Solar activity for the past 20 years and its prediction for upcoming solar cycle. [36]

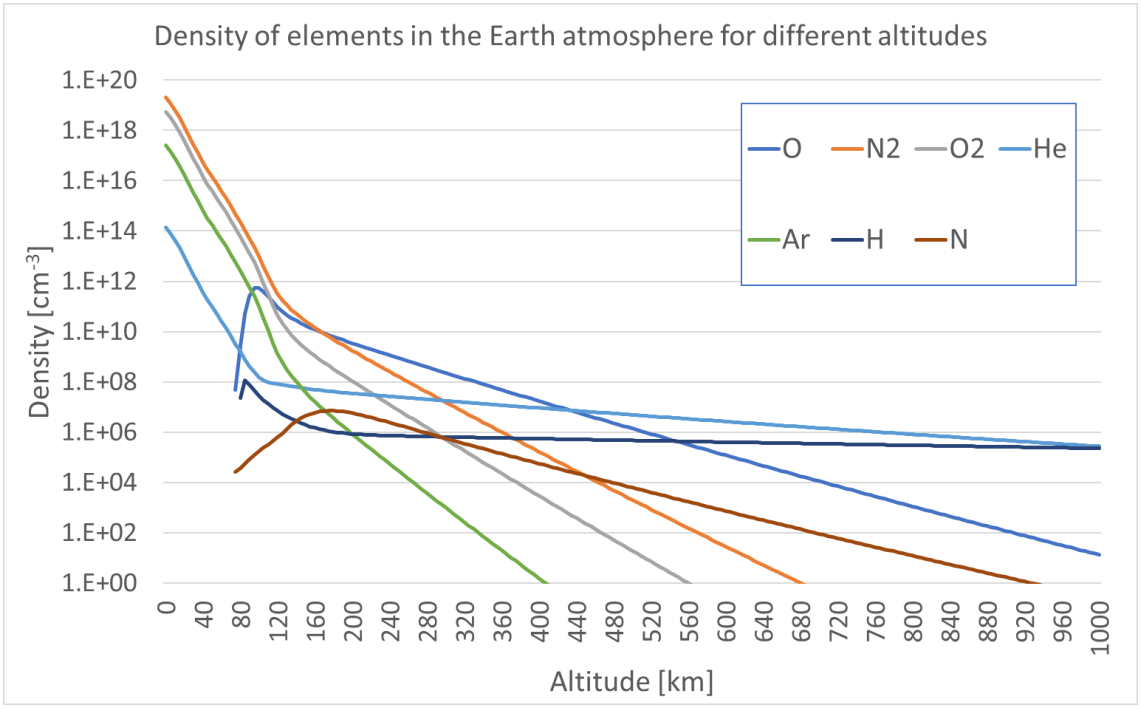

Figure 3.2: Density of different atmospheric elements for different altitudes. Data aquired from NRLMSISE-00 [35].

From the figure 3.2 it is evident that around the Karman line oxygen and nitrogen molecules with a density of 10^{13} particles per cm^3 still predominate. However, the density of both elements decreases rapidly with an altitude and around the altitude of 170 km atomic oxygen begins to dominate and keeps being the main element of the atmosphere up to an altitude of about 500 km, where it is replaced by hydrogen and helium with a density of 10^6 particles per cm^3. Knowledge of these values is crucial for the design and operation of an electric propulsion engine that should use residual atmospheric gases, not only in terms of available gases to generate thrust, but also because of chemical interactions that can adversely affect satellite material. And last but not least, to calculate the force that will act on the satellite.

To derive the drag of the environment, it is necessary to know the relative velocity between the spacecraft and the molecules of the atmosphere. Assuming a circular orbit, the orbital velocity can be derived from the laws of gravity by the equation 3.1 and subsequently graph of velocities for different orbits can be plotted.

$$v = \sqrt{\frac{GM_z}{R_z + h}} \tag{3.1}$$

where G is the gravitational constant, M_z is the mass of the Earth, R_z is the radius of the Earth and h is the altitude of the orbit.

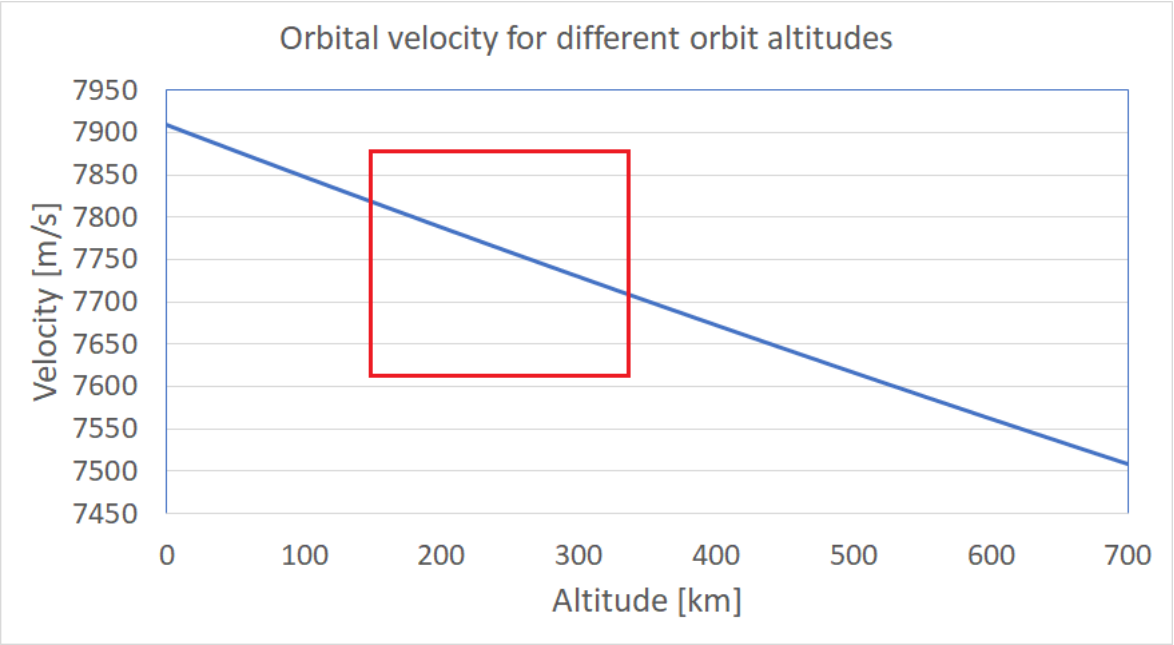

Figure 3.3: The dependence of the orbital velocity on the altitude of a given orbit. VLEO area is marked in red.

As seen from the graph the orbital velocity in VLEO is around 7.8 m/s. For altitudes above 1500 km, thermal velocity of particles becomes an important factor when computing interactions between flying body and its surrounding [37]. Given the focus of this diploma on VLEO region, it is possible to neglect this phenomenom. Thus, the relative velocity at which the molecules hit the spacecraft is considered as the velocity of the spacecraft itself, i.e. 7.8 m/s.

3.1.2 Drag

For every space mission at VLEO, i.e. below 300 km, drag is the main factor that affects its lifespan. It can be described as a force that acts on the spacecraft against the direction of its movement, regardless of whether the spacecraft moves relative to the environment or vice versa. To calculate this force, it is necessary to know the velocity v, the diameter of the spacecraft in the direction of a motion A, the density of the environment ρ and the coefficient of drag C_d. The value of the drag coefficient is set to $C_d = 2.2$ for most calculations in orbital mechanics, and for orbits below 400 km this number is accurate with a deviation of $\pm$ 10 % [37].

The calculation of aerodynamic drag varies greatly depending on the nature of the environment. An important parameter in this decision is the Knudsen number, which indicates whether the environment is perceived as a continuum flow or the free molecular flow. This determines the forces acting on the flying body. The Knudsen number depends on the molecular composition of the medium, as well as on its particle density. And since the particle density in the atsmophere are again strongly dependent on altitude and solar activity, the Knudsen number is also affected by these values. According to *Jackson, 2017* [5], above the altitude of 100 km the Knudsen number is > 1, indicating that the environment is perceived as a free molecular flow. Dependence on solar activity is notable only in higher layers of the atmosphere, roughly above 250 km. However, free molecular flow model is quite complex and computationally demanding. At the same time, using a model for the continuum flow is an optimal simplification, while maintaining high accuracy. Therefore, it is not necessary to deal with the model of free molecular flow for the calculation of drag in this work. The continuum flow model describes aerodynamic drag by the equation 3.2

$$D = \frac{1}{2}\rho C_D A v^2 \tag{3.2}$$

Using this equation, it is finally possible to plot the dependence of the aerodynamic drag of the spacecraft on the altitude of the orbit. Due to the characteristics of the space mission, which will be discussed in a later chapter, the plot of the drag for the relevant sizes of CubeSat satellites are shown in Fig. 3.4, i.e. 3U, 6U, 8U, 12U and 27U (ram area of 0.01 m^2, 0.02 m^2, 0.04 m^2, 0.04 m^2 and 0.09 m^2).

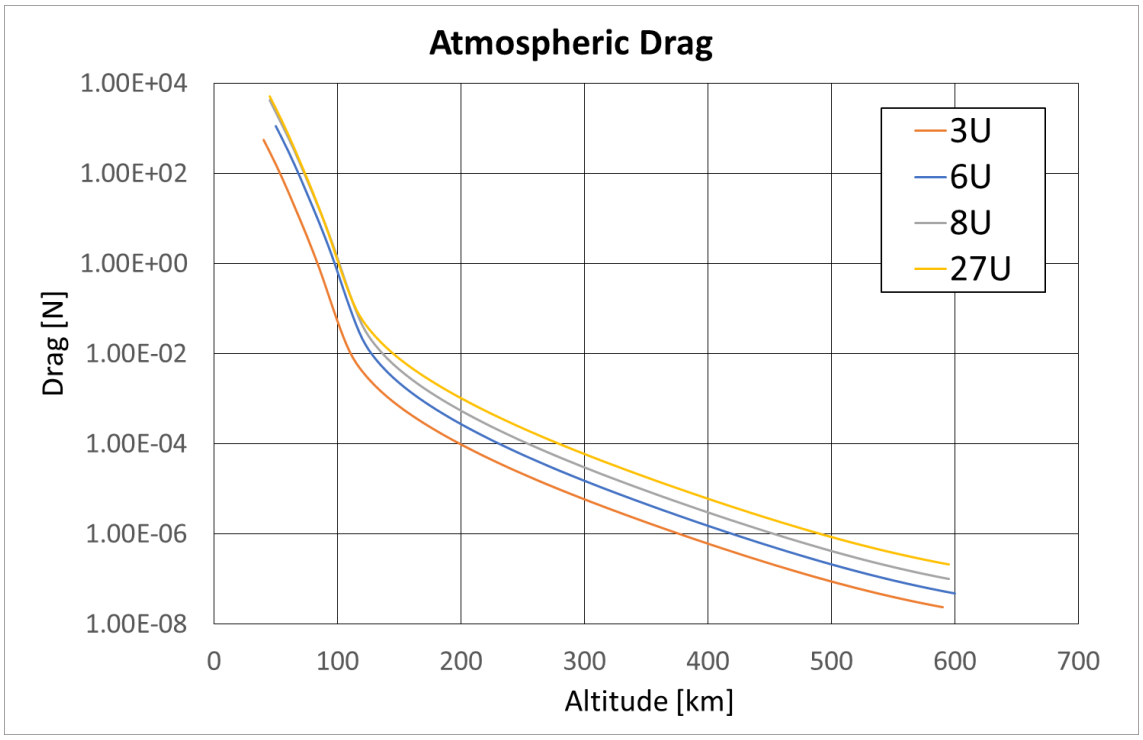

(a)

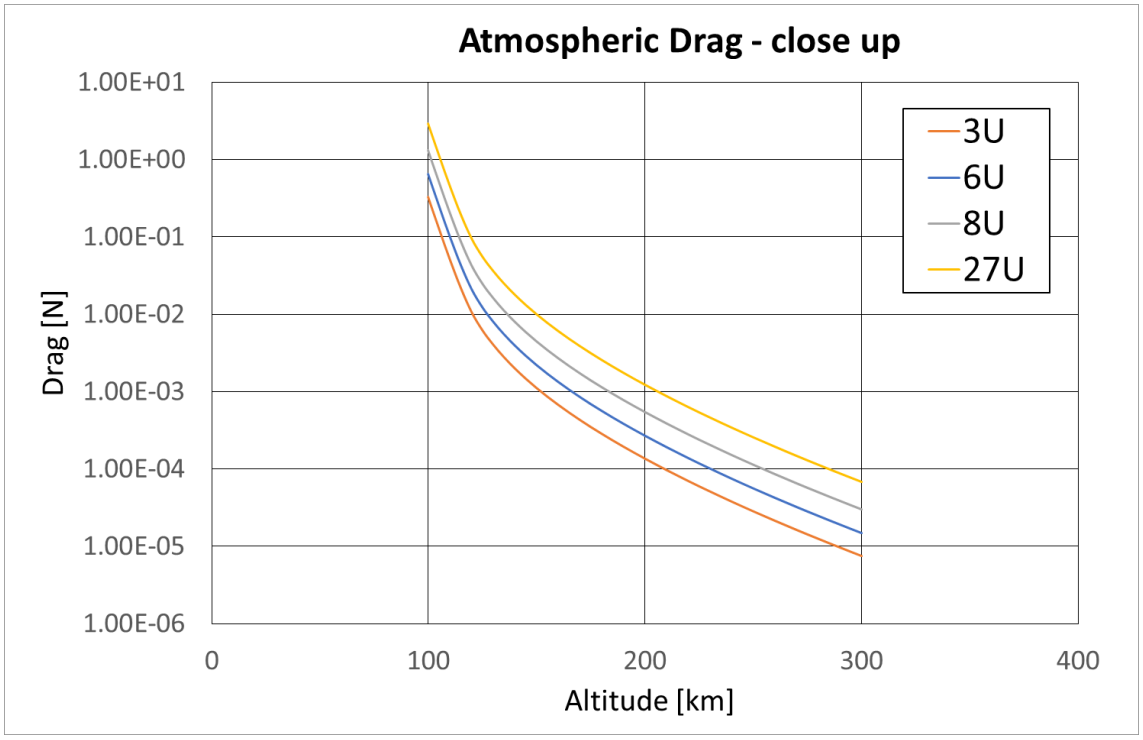

(b) Close up for the altitudes below 300 km

Figure 3.4: Aerodynamic drag plotted against the orbit altitude.

3.1.3 Atomic oxygen

In addition to aerodynamic drag, another issue arises at orbital velocities and altitudes of VLEO associated with the presence of gas molecules, especially atomic oxygen. As explained in the previous section, from a certain line, the environment is seen as the flow of free molecules and the interaction with the flying body is thus different. Instead of flowing around a body like water around a stone, collisions with individual molecules are happening like bullets hitting a wall. Particles are reflected from the surface of the body and energy is transferred. Under standard conditions of an ideally smooth material, we can speak of a specular reflection, where the particle bounces at the same angle as it hit the material with a minimum of energy loss. However, highly chaotic and accidental reflections were found when observing the spacecrafts in orbit.

It was concluded from experiments and observations that the surface of the body flying in the residual atmosphere is initially clean and the reflection is almost specular [39]. However, atomic oxygen particles and other molecules are absorbed into the material of a spacecraft over time. Its surface structure changes and the impinging particles are reflected diffusely, i.e. in all directions, and with a loss of energy which is transferred to the spacecraft. Most of this phenomenon is observed at altitudes between 100 km and 300 km, where the highest concentration of atomic oxygen is. The effect of diffuse reflection, the same as aerodynamic drag, contributes to a shorter satellite lifespan, but is very difficult to simulate.

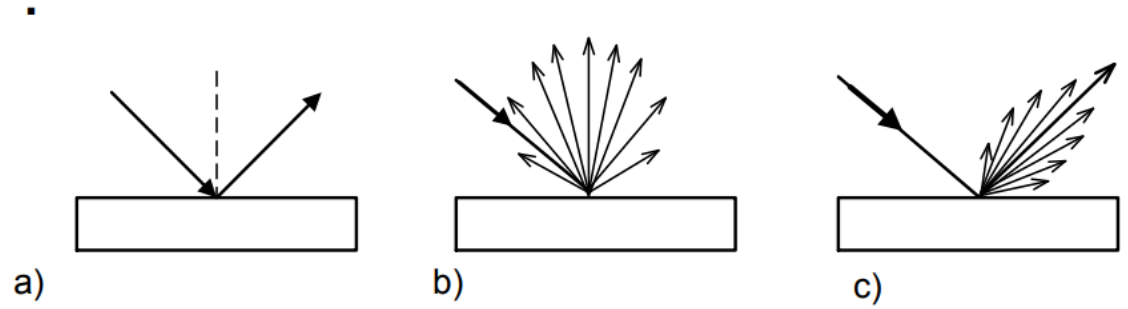

Figure 3.5: Reflection of particles a) specular b) diffuse c) quasi-specular [40]

Increased aerodynamic drag is not the only problem associated with atomic oxygen. As has been stated, atomic oxygen is highly reactive and interacts with the material of the flying

body, changing its physical and chemical properties. This is the so-called contamination of the material. Diffuse reflection of particles from contaminated material is one of the manifestations. Another outcome of the contamination may be the reaction of atomic oxygen with silicon, from which essential components such as solar panels are often made. A thin layer of SiO_x is formed on the surface of the solar panels, which reduces the efficiency of the solar cells [41]. At the same time, an analysis of materials obtained from the MIR space station and the LDEF satellite, both of which have spent several years in low orbit, shows that atomic oxygen can enter the satellite's interior and contaminate it, including the payload [41]. Subsequently, oxygen atoms cause the degradation of optical elements, where, for example, in the Hubble telescope, the sensitivity to UV radiation is reduced by up to 15 % per year [42].

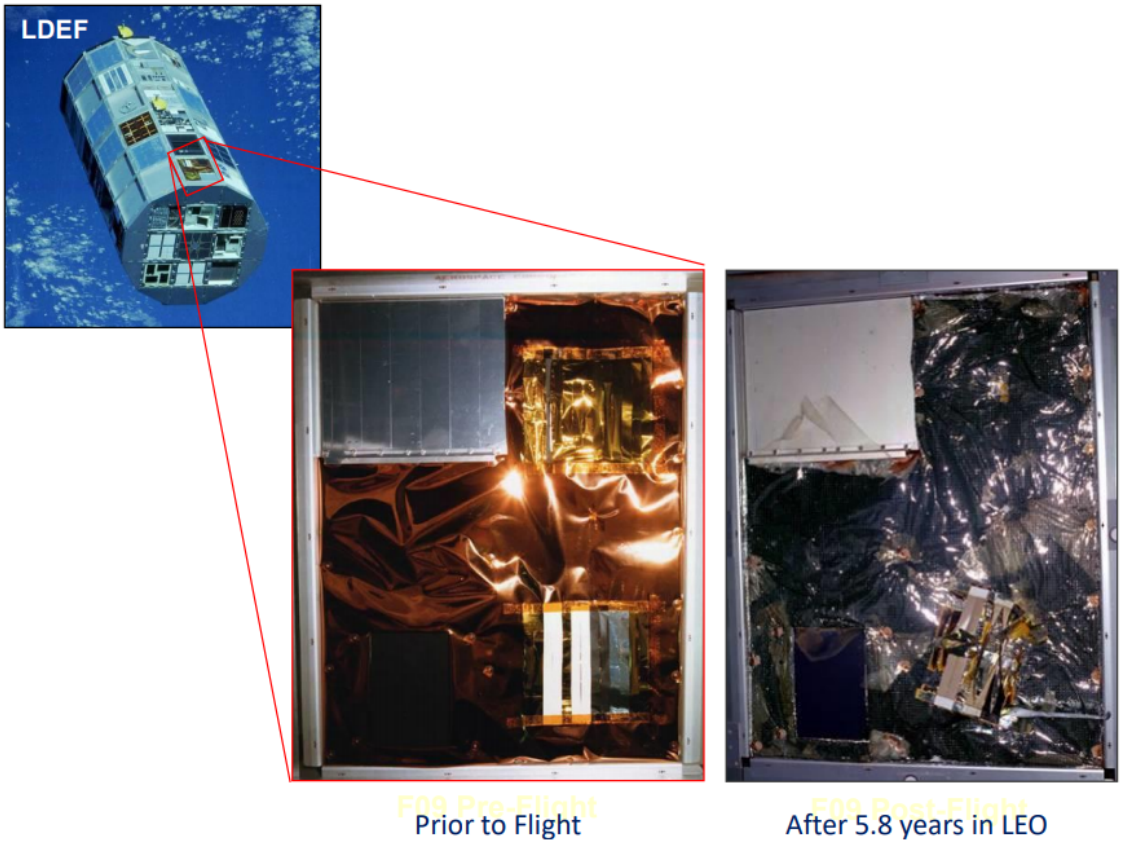

Figure 3.6: Photographs of the panel from the LDEF satellite before the flight and after 5.8 years in LEO.[42]

It is possible to protect the surface from atomic oxygen with an added coating, which is less reactive. However, due to inhomogeneous application caused by, for example, dust particles or microscopic mechanical cracks, part of the protected material is always exposed.

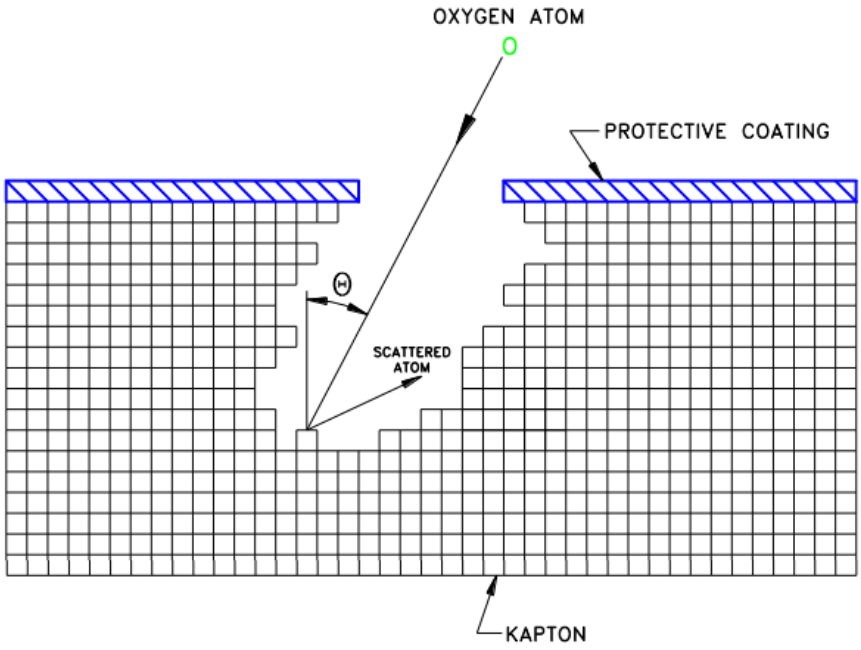

Figure 3.7: Illustration of coated material erosion on contact with reactive atomic oxygen. [42]

The interaction of a material with atomic oxygen depends on many factors, such as the energy of the particles, the temperature, the surrounding components, the number of incoming particles, etc. [42]. Therefore, it is very challenging to model and predict the consequences and extent of the contamination. Each situation is different, and to measure the effects of atomic oxygen as accurately as possible, it is necessary to test specific components in the exact configuration in which it will be used in orbit.

3.2 Air Breathing Ion Thruster

Previous sections outlined several criterias and information that an engine should meet in order to be a suitable candidate for use in *air-breathing* (AB) mode.

- It should have the lowest possible power consumption
- It should have the highest possible specific impulse
- It must be able to ionize residual atmospheric gases (primarily oxygen and nitrogen)
- It must be able to develop a thrust up to units of mN to suppress the effect of atmospheric drag

Several conclusion can be made from looking at the table 2.1 and the charts 2.9. All electrothermal thrusters, represented there by resistojets and arcjets, can be ignored due to their very low specific impulse. FEEP can also be excluded from the theoretical candidates, as despite its high efficiency in the form of the highest specific impulse, it has too little thrust and therefore, not possible for low atmospheric use. Only PPT, HET and Ion thruster remain.

A PPT system adapted to the use of nitrogen, which is present in the atmosphere around the 150 km of altitude, was tested by dropping from a stratospheric balloon. The results of experiments and theoretical calculations indicate that an engine designed in this way is able to develop a thrust of about 5 mN at an altitude of about 25 km [43]. It can therefore be used to control, for example, high altitude airships, but not so much to keep the satellite in the desired orbit at higher altitudes exceeding 100 km.

HET is considered to be the most researched system in the atmospheric use. It provides a good ratio of thrust to power consumption, reaching values between 10-59 mN/kW. On the other hand, the ion thruster, abbreviated ABIT, is more suitable for applications where a lower thrust (less than 10 mN) is sufficient and thus has a lower energy consumption [43]. However, both types of drives has their limits connected with the problem of mechanical erosion of materials. In addition, in the case of ABIT, the acceleration grids are endangered due to the interaction with the atomic oxygen present and the outgoing exhaust velocity particles.

When designing an air-breathing propulsion system (ABIT or different types as well), three issues needs to be addressed.

- Particle capture efficiency
- Ionization efficiency of captured particles
- Erosion of electrodes and other mechanical parts of the engine

Each of these problems is associated with one element of the AB propulsion system. Particle capture efficiency depends on the geometry and material of an inlet, ionization efficiency is defined by the used ionization chamber, where the captured gas particles are stored and the erosion of electrodes or accelerating grids is connected with the last block of an engine and how the ionized particles are leaving the device.

3.2.1 Inlet

The efficiency of particle capture by inlet is most dependent on its shape. In *Jackson, 2017* [5] three basic geometric of the inlet are outlined and capture efficiency simulation was performed, see the picture 3.8 and 3.9. The shape of a truncated pyramid, conical shape and parabolic shape. For each of these shapes with a diameter of 10 cm and a length of 5, 7.5, 10 cm a particle capture simulation was performed using the MolFlow+ software. The simulation results are available for both specular and diffuse reflection.

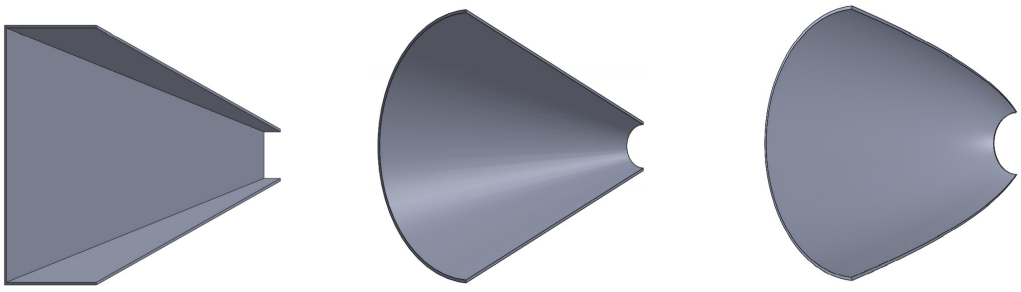

(a) (b) (c)

Figure 3.8: 3D models of three different inlet geometries. (*a*) - Truncuated pyramid, (*b*) - Conical shape, (*c*) - Parabolic shape. [5]

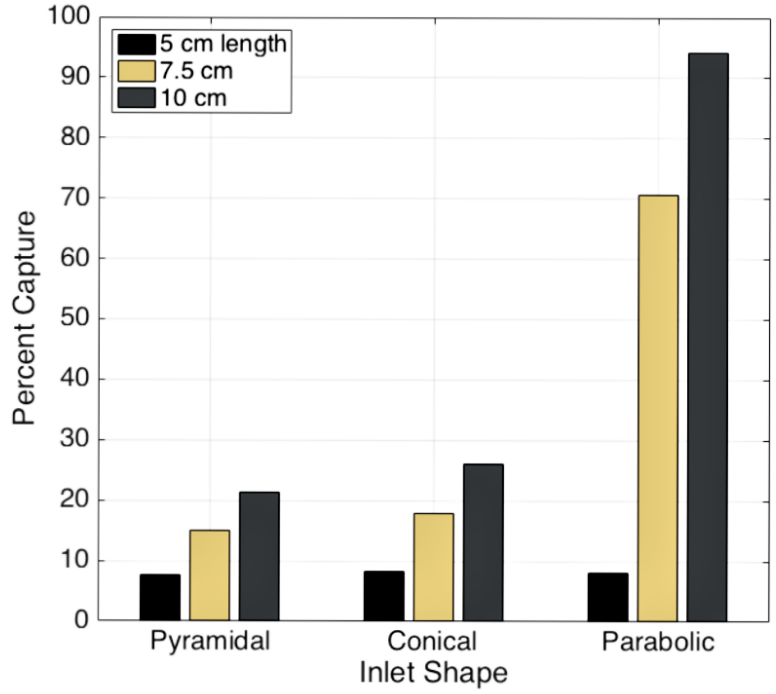

(a)

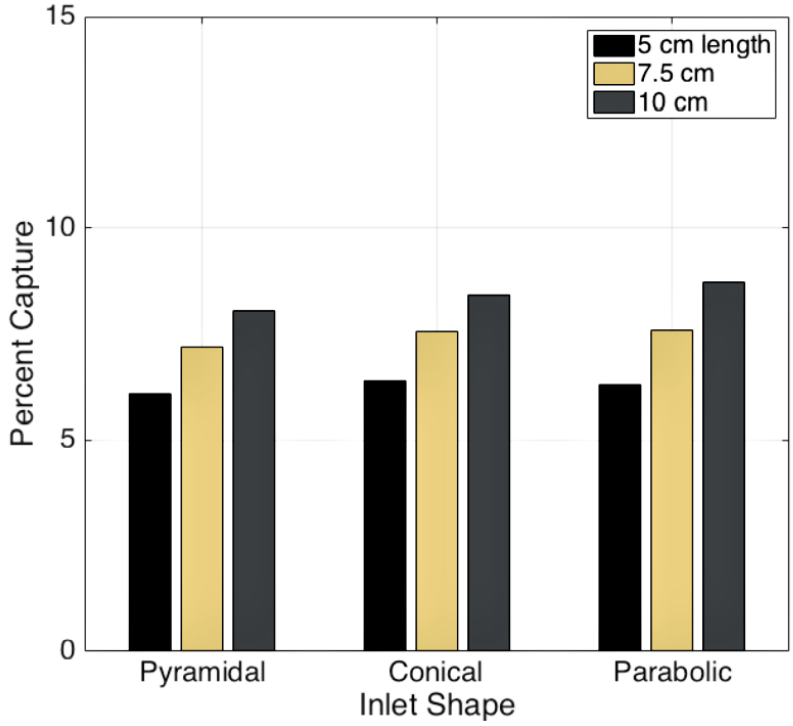

(b)

Figure 3.9: MolFlow+ simulation results of the particle capture efficiency for all three inlet geometries and a) specular b) diffuse reflection. [5]

The graphs show that for the specular reflection, practically only the parabolic shape of the inlet is viable, because it can capture over 90 % of particles at a length and diameter of

10 cm. In diffuse reflection, the values are similar for all shapes, but even here the parabolic shape is slightly above average for the largest size. As explained in the previous section, most interactions of gaseous particles with satellite surfaces in the lower atmosphere are initially following specular reflection rules. However, with increasing material erosion and atomic oxygen contamination, the surfaces degrade. This causes particle reflections to begin to behave diffusely. Thus, if the inlet initially has a capture efficiency of about 90 %, it can be assumed that over time the value will fall below 10 % or even lower. To increase the capture efficiency of diffuse reflection, the nozzle outlet diameter can be increased. In previous simulations, an outlet diameter of 2 cm was taken into account. For a diameter of 3 cm, the capture efficiency is already around 20 % and if the diameter of the outlet was above 6 cm, the efficiency of capture at diffuse reflection would increase above 50 % [5].

Another possible solution to the problem of low capture efficiency during diffuse reflection is the prevention the erosion and contamination of the inlet material. The rate of absorption of atomic oxygen in a material is strongly dependent on the material itself [30]. Therefore, the project *Discoverer* [29] is conducting experiments to find a suitable material that would limit the interaction with atomic oxygen. The most advanced experiment is a mission called SOAR (*Satellite for Orbital Aerodynamics Research*), being developed at the University of Manchester. The mission goal is to transport a small satellite constructed from new materials to the ISS (*International Space Station*) and to test their resistance to interactions with atomic oxygen and overall aerodynamic behavior in low orbit for a duration of several months [30]. The SOAR mission is planned for early 2021.

3.2.2 Ionization chamber and Acceleration grid

As outlined in Chapter 2, there are several ways to ionize a captured propellant. It is worth mentioning the use of a hollow cathode for electron injection and electron cyclotron resonance (ECR). Both methods can also be used for AB drives.

At first, the hollow cathode method was preferred for its simplicity and considerable experience in conventional electric drives. However, due to its disadvantage in the form of material erosion, there is an effort to move towards the cathode-free principle, ie ECR [21].

In addition to a non-existent cathode that could wear out, ECR technology also has a second advantage, which is being less energy-intensive. However, both methods have one major disadvantage, which is the strong dependence on the density of the propellant to be ionized. In the case of ECR, ionization processes are limited to pressure around 10^{-3} Pa [45].

Ionization efficiency is one of the key parameters of an ionization chamber. In conventional electric drives, where rare gases are most often used as a propellant, the ionization efficiency is around 50 % and can reach up to over 80 % [44]. However, for AB-type drives, which operate with neutral elements of the Earth's atmosphere such as nitrogen and oxygen, the ionization efficiency is much lower. The doctoral thesis *Shabshelowitz, 2013*, which deals with the study of plasma generation using radio waves for AB drives, states that the ionization efficiency of neutral atmospheric gases can be around 10 % [46].

The acceleration grid system is also practically identical to conventional electric ion thrusters. The majority of concepts composes of so-called two or three grid arrangements. In the case of two grids, the first grid has the task of attracting positively charged ions from the plasma, which are then accelerated by the second grid. The third grid in the sequence is called *deceleration grid*. It helps to regulate the velocity of ions to the required exhaust velocity and prevents backstream.

3.2.3 Thrust

The thrust an ABIT can produce is strongly dependent on several factors. In particular, environmental properties such as particle density and composition and engine parameters such as capture and ionization efficiency, available power and voltage.

Thrust equations are aquired from the book *Fundamentals of Electric Propulsion: Ion and Hall Thruster, Goebel D. M. and Katz, I.* [11]. To begin with, it is important to determine the exhaust velocity of ions and their mass flow. These parameters are given by the equations 3.3 and 3.4.

$$v_i = \sqrt{\frac{2qV_b}{M}} \tag{3.3}$$

where q is the elemental charge, V_b is the beam voltage, which is often slightly less than the voltage present on the acceleration grids, and M is the molecular mass.

$$\dot{m}_i = \frac{I_b m_i}{q} \tag{3.4}$$

where m_i is the mass of ions and I_b is the beam current obtained from the equation 3.5.

$$I_b = \frac{1}{2} n_i q v_a A T_g \tag{3.5}$$

here n_i is the ion density, A is the acceleration grids area, T_g is the grid transparency and v_a is the velocity of ions in the gap between grids. The grid transparency most often ranges from 70 to 80 % [11] and the velocity of the ions in the gap depends on the distance between the two grids, the voltage used, and the mass of the ions. Often exhaust velocity is used instead.

Using the values obtained, it is then possible to calculate the resulting thrust from the equation 3.6.

$$T = \sqrt{\frac{2m_i}{q}} I_b \sqrt{V_b} \tag{3.6}$$

The thrust calculated in this way is an ideal value that will be reduced by ram drag in a real environment, similar to the propulsion units used in aircrafts ε_{ram}, the efficiency of particle capture η_z and the efficiency of ionization η_i.

The ram drag is expressed by the relation 3.7

$$\epsilon_{ram} = \frac{g_o I_{sp} - v_{orbit}}{g_o I_{sp}} \tag{3.7}$$

where v_{orbit} is the orbital velocity of the spacecraft and I_{sp} is the specific impulse obtainable from the equation 3.8.

$$I_{sp} = \frac{1}{g_o}\sqrt{\frac{2q}{m_i}V_b} \tag{3.8}$$

where g_o is the gravitational acceleration.

With knowledge of all the factors that affect the thrust calculation, a final equation for the thrust that takes into account mentioned efficiencies and the environmental impact can be constructed.

$$T = \eta_z \eta_i \epsilon_{ram} \sqrt{\frac{2m_i}{q}} I_b \sqrt{V_b} \tag{3.9}$$

Looking at the graph 3.2, it is clear which elements most influence the level of thrust at given altitudes. For altitudes up to about 170 km, these are nitrogen molecules. Above that line, atomic oxygen molecules predominate, and from an altitude of 450 km, hydrogen atoms are dominant. The elements affect the value of the thrust not only by their mass but also by their ionization potential. Molecules, or light elements such as hydrogen and helium, generally have a higher ionization potential, which means that more energy needs to be supplied for successful ionization. In the case of molecules, such as oxygen, the difference between the ionization potential of atomic and molecular oxygen is up to twofold.

Based on the previous paragraphs, it is clear that thrust, as well as atmospheric drag, is dependant on the density of the atmosphere, thus even the value of solar activity. Figure 3.10 shows this dependency for minimum, maximum and average value of solar activity for the past solar cycle. It can be stated, that the value of atmospheric drag is affected more than thrust by the solar activity, especially in higher altitudes.

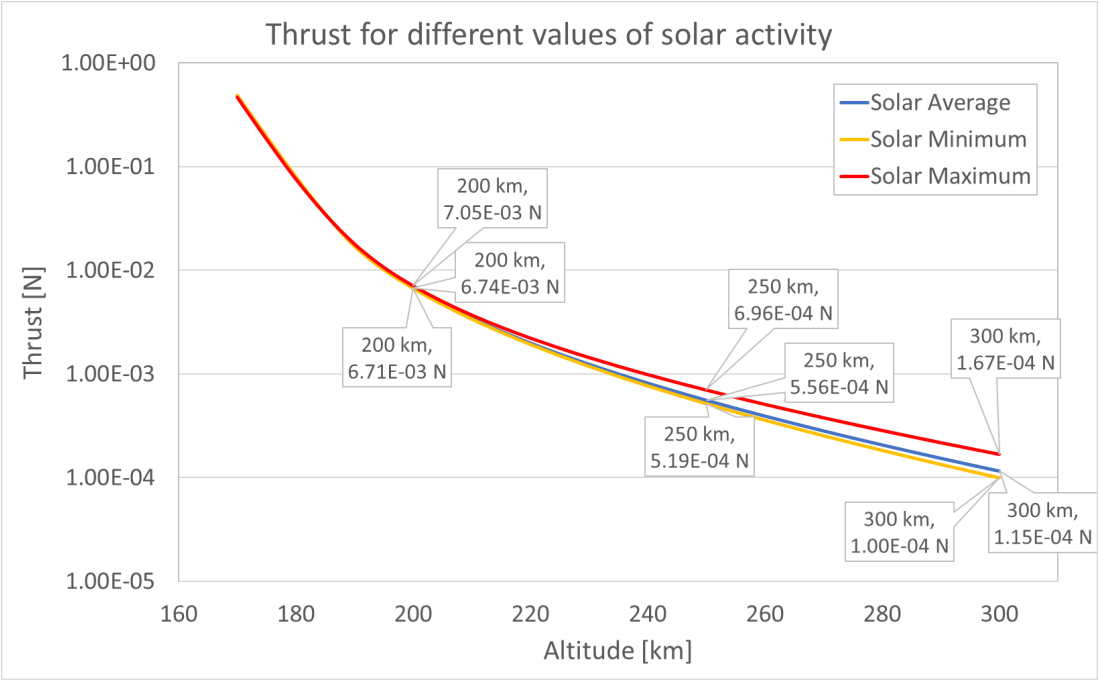

(a)

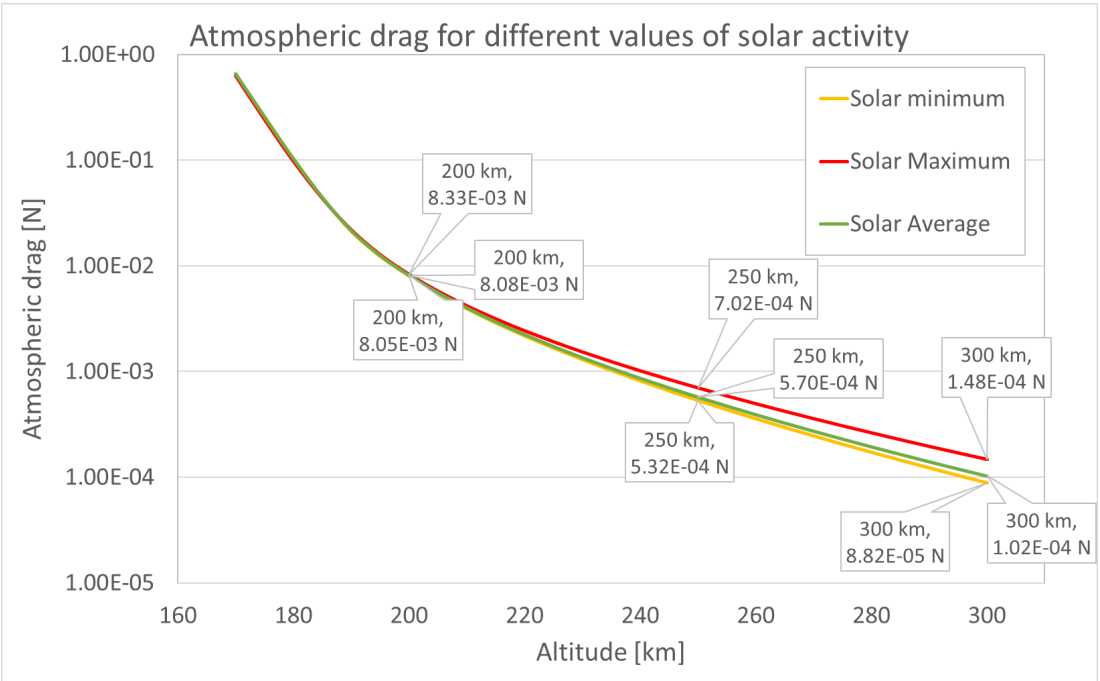

(b)

Figure 3.10: The thrust value of AB drives and atmospheric drag of a 6U CubeSat during different values of solar activity.

The achievable thrust can be further compared with various quantities and thus it is possible to analyze the performance and utilization of the drive. It is also needed to take into account limited amount of energy that a propulsion unit can use. Such an analysis is performed in the Chapter 7.

3.3 SpaceLab Air-Breathing Engine Concept

3.3.1 Concept description

The engine designed by the Czech company SpaceLab is currently in the concept phase with initial experiments being conducted. It is previously outlined *Air-Breathing Ion Thruster (ABIT)* type. First steps were taken in the direction of ionization chamber development. Alongside the ionization chamber, a new mathematical plasma model was developed and used to measure the method of plasma ionization.

A cylindrical shape was chosen for the ionization chamber. The plasma inside the chamber is created by the ECR technology. The concept operates with a three-grid design, where the first grid is put on the potential ground, the second acceleration grid will be operated at a voltage of about 500 V and the third deceleration grid serves as reverse current protection [45].

During the experiment, a metal plate called the collector was placed behind the chamber, to which accelerated ions impact, and thus it is used to measure the beam current. Surrounding the ionization chamber it can be found a series of coils that have the task of keeping the plasma inside the chamber, for limiting the contact of the plasma with the chamber surface. At last, planar electrodes are used to generate an alternating electric field with a frequency of 435 MHz. The strength of the resulting field inside the ionization cylinder is 22 mT [45]. The magnetic field frequency was chosen experimentally to achieve the highest possible resonance between the generated field and the cyclotron frequency of electrons inside the chamber, which will gain the necessary energy for the subsequent ionization of other elements due to resonance.

3.3.2 Simulation and experiments

The experiment carried out in cooperation with the Aviation Research and Testing Institute (VZLÚ) focused on measuring the beam current generated and thus the ability to successfully ionize the elements [45]. A mixture of oxygen and nitrogen in the ratio of 22 % and 78 % was chosen as the propellant, which roughly corresponds to the distribution of substances in the Earth's atmosphere up to a height of 100 km. Using vacuum pumps, the ionization was measured for different pressure values and the ideal pressure conditions for plasma ignition were evaluated. The results were compared with a plasma model developed by SpaceLab for this purpose.

According to the results, the mathematical model of the plasma is almost identical to the data obtained from the experiment. A small deviation was observed around the maximum value of generated current. In the mathematical model, the maximum current occurs at about twice the pressure of a real experiment. The deviation is most likely due to the method of measuring pressure in the experiment, where the pressure was measured before and after the chamber, but no probe was available directly inside the chamber. Thus, it can be stated that the maximum of the generated current occurs at a pressure of about 50 mPa [45].

The degree of ionization also depends on the chamber pressure. Detailed calculations from the plasma model show that at the input power Pin = 10 W the maximum ionization level occurs also around 50 mPa pressure. For pressures lower than 1 mPa, it is already difficult to ignite the plasma. On the other hand, for higher pressures above the level of 1 Pa, which corresponds to an altitude of about 100 km, the density is so high that the ionization level decreases again. This can be explained by insufficient power for the source is no longer powerful enough to compensate for the energy lost by electrons during non-ionization collisions. The ideal conditions for operating this type of drive, therefore, appear to be at a pressure around 10-100 mPa [45].

The developed plasma model was also used to calculate the current and current density for variable geometric configurations and different amounts of energy consumption. Firstly, different geometries were considered, taking into account radius sizes in the range of 0.3 cm to 10 cm and the length of the cylinder from 10 cm to 150 cm. The results are that to obtain a higher current it is desirable to have a shorter configuration with a larger radius [45].

The same conclusion was reached when examining the obtained current for different delivered power levels. Although the current density is saturated from a certain level, especially for larger radii, the total current still increases significantly with further increase in radius [45].

The interim results show that the drive is able to keep plasma ignited at a chamber pressure up to 10 mPa, with an ideal performance around 50 mPa. The ionization chamber in the form of a hollow cylinder itself has a compression factor of about 30 and an added inlet in the future will have a compression factor of up to 200 [45]. As can be seen from the graph 3.11, at such values of the compression factors, the altitude limit for the use of a given engine is up to the altitude of 190 km, respectively 280 km when using the inlet.

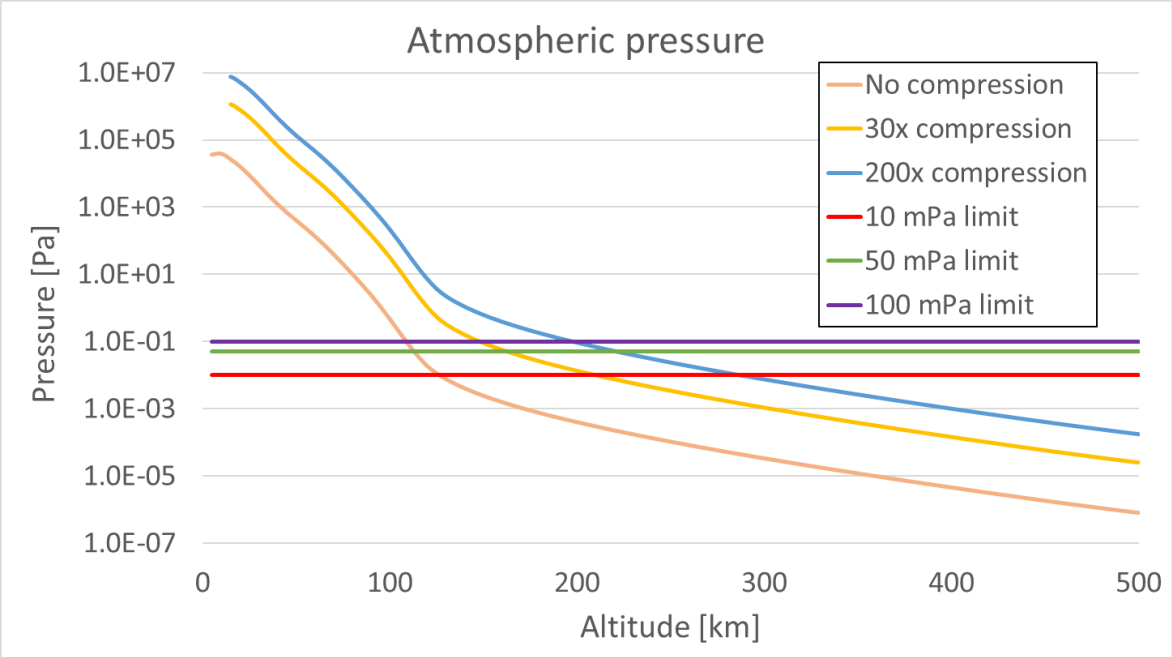

Figure 3.11: Pressure values in the Earth's atmosphere.

According to the study *Di Cara, Gonzales del Amo, 2007* [28], which deals with the general usage of air-breathing drives, it follows that to maintain sufficient thrust for drag compensation at an altitude of 200 km satellite requires about 10 W of power. Lowering the altitude by another 30 km increases energy consumption by one order of magnitude. To maintain the satellite in orbit at an altitude of 170 km, it would require the power of an order of 100 W. Therefore, the altitude region between 190 km and 280 km seems optimal for the use of air-breathing propulsion in CubeSat missions. A detailed analysis supported by calculations will be presented in later chapters.

3.4 Summary

In this chapter, it was outlined what effect the residual atmosphere has on the flying body at orbital velocity. In the VLEO region, these are mostly elements of nitrogen and atomic oxygen, which cause atmospheric drag and degradation of the spacecraft's materials. Engines based on the AB principle can utilize these residual gases to generate plasma and subsequent thrust, which compensates the drag and keeps the spacecraft in stabilized orbit. However, such drives encounter large limitations on both sides of the orbit altitude. Mainly pressure and power limitation.

In terms of the minimum feasible altitude, the value is about 200 km, where the atmospheric drag of CubeSat satellites reaches a magnitude of about 10^{-4} N, which is the value of the thrust, which is technically possible to achieve with the AB drive at power consumption up to 10 W. At the same time, at an altitude of 250 km, the air pressure is around 10^{-4} Pa, which represents a value that, with suitable compression, is adequate for the ignition of plasma in the ionization chamber. Higher altitudes no longer meet the requirements for pressure in the ionization chamber and the ionization level decreases rapidly. It can therefore be stated that for CubeSats, air-breathing type of propulsion can be used in orbit range from 200 km to 250 km.

Chapter 4

Payload

Contents

Before the beginning of any space mission design process, it is important to realize what is to be achieved and what resources or payload is needed for it. As part of the cooperation between CTU and SpaceLab company, which develops ABIT propulsion system to be used, it was decided to focus on monitoring sources of soft X-rays in the Earth's atmosphere. These can be so-called *terrestrial gamma-ray bursts* or *aurora borealis*. Because soft X-rays are absorbed by the atmosphere, VLEO is desirable for their observation. The use of a *Medipix* type detector with optics based on the *Lobster Eye telescope* principle is proposed for X-ray observation. It is a unique solution offering large field of view (FOV) typically 30 square degrees or even more while maintaining still reasonable resolution of order of few arcmin.

This chapter aims to explain the principle of operation of proposed payload and its comparison with alternative methods. At the same time, it summarizes the detailed parameters of a specific device that is planned to be used for the future space mission and outlines the possibilities of its integration into CubeSat satellites.

4.1 X-ray optics

Unlike conventional optics, where a set of mirrors is used to reflect incoming photons, X-rays are reflected from the mirror surfaces only at a very small angle, typically less than 1 degree.

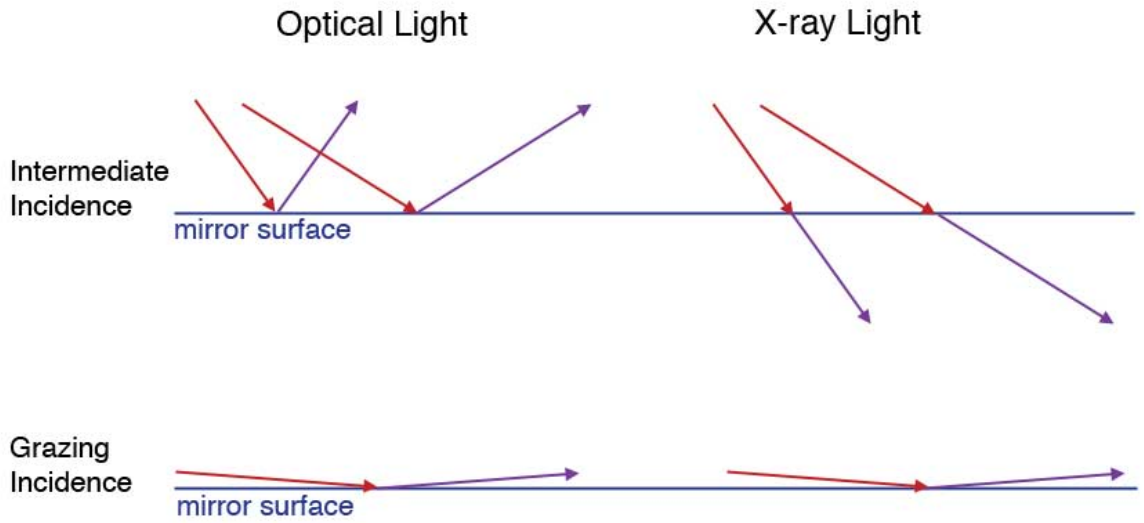

Figure 4.1: The difference between reflection of visible light and X-ray beams. [48]

It was therefore necessary to invent new optical systems to observe it. The *Grazing Incidence* mirror arrangement shown in 4.2 is often used for X-ray observation. Two sets of reflective surfaces are used to focus the beam, one is parabolic and the other hyperbolic. Due to the large angle of inclination of the mirrors, an empty space is created in the middle of the optical system. The problem is usually solved by using cylindrical mirrors, which are nested in layers, see Fig. 4.3 [48].

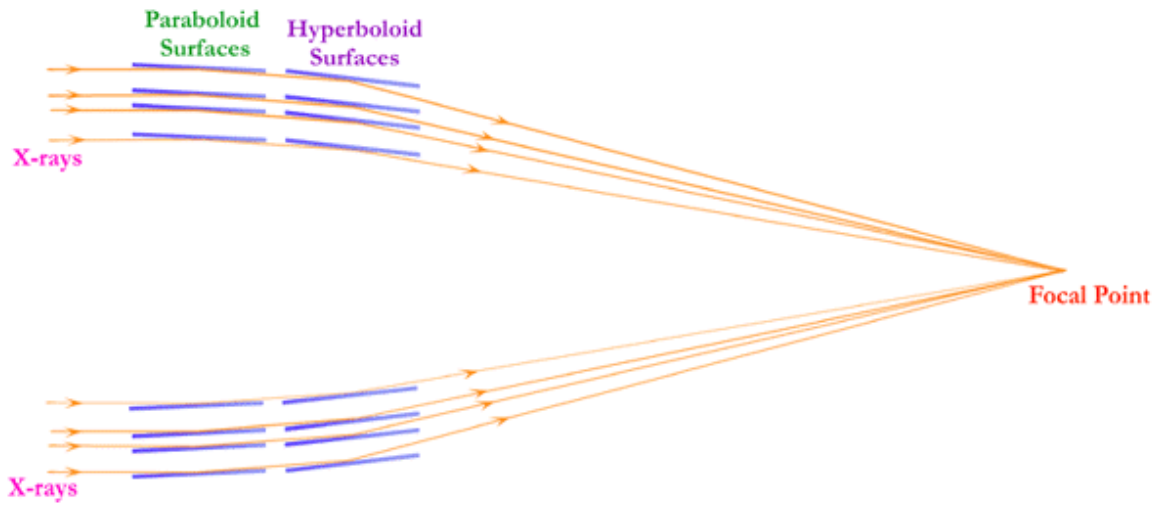

Figure 4.2: Grazing Incidence optic schema. [47]

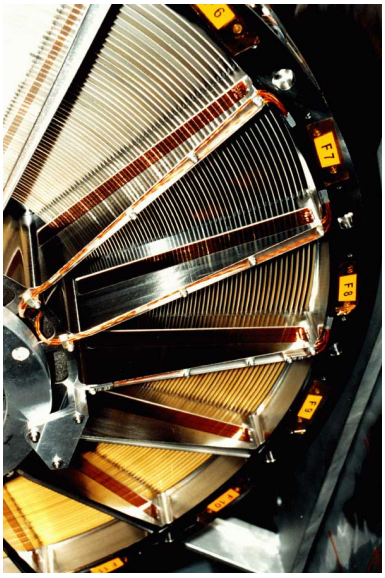

Figure 4.3: Close up of a mirror arrangament inside the X-ray telescope XMM-Newton. [48]

Several space missions have been conducted to observe X-rays in space in the past. It is worth mentioning the last two major missions *Chandra X-ray Observatory* and *X-ray Multi-Mirror Mission (XMM-Newton)*.

4.1.1 Chandra X-ray Observatory

The *Chandra* observatory was launched into orbit on July 23, 1999, by the space shuttle Columbia. It is one of the largest and most expensive projects NASA has ever conducted [49]. The observatory's role is to capture soft X-rays with energies between 1 keV and 10 keV

generated by large supernovae, inside black holes and the centers of galaxies. The set of four cylindrical mirrors embedded in each other with a focal length of 10 m and a resolution of up to 0.3 arcsec was constructed for this purpose.

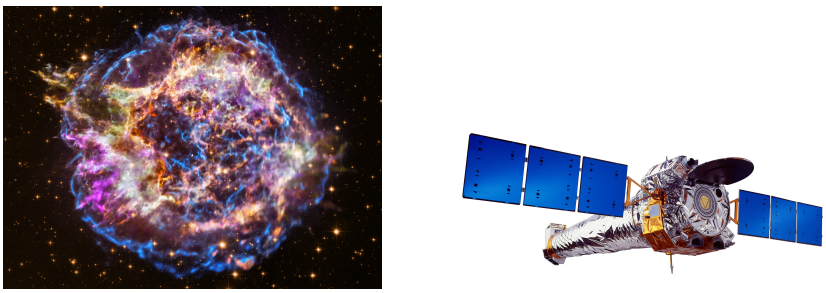

(a) (b)

Figure 4.4: *a* - Supernovae Cassiopeia A captured by the Chandra observatory [49]
b - Chandra observatory illustration [50]

4.1.2 XMM-Newton

In the same year, 1999, ESA also launched its X-ray observatory into orbit, using the Ariane 504 rocket. The planned lifespan of the mission is to end in 2022 and should be replaced by the year 2030 by a new *Advanced Telescope for High Energy Astrophysics - ATHENA* observatory. The focal length of the XMM-Newton telescope is 7.5 m and the resolution is about 10 arcsec [51].

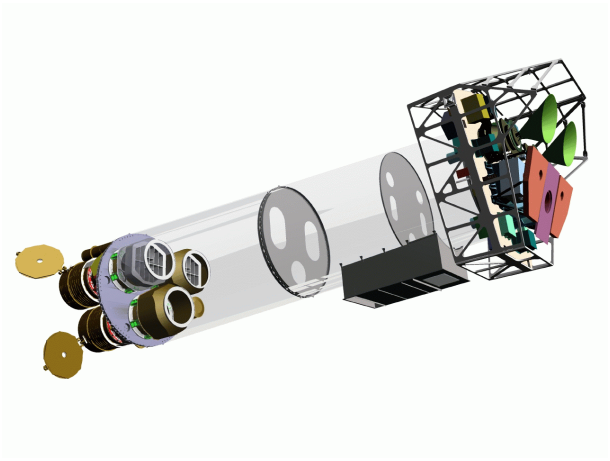

Figure 4.5: XMM-Newton obervatory illustration [51]

4.2 Lobster Eye optics

Grazing incidence optics has typically a very high resolution, reaching up to one angular second. However, the disadvantages of these systems are the high production cost, the small field of view and the requirement for a high focal length, i.e. the large dimensions of the device.

Therefore, a new system was designed that is based on the functionality and principle of real lobster eyes. The optics, designed in 1975 and referred to as the *Schmidt Lobster Eye* (SLE) type, takes on the geometric arrangement of the reflecting surfaces in the lobster eyes [54] [52]. In contrast to the *Grazing Incidence* optics, it adds another set of reflective surfaces that are perpendicular to the first row. The beam is thus directed in both axes. The system can be imagined as a system of square tubes that focus the incoming particles towards the detector, as shown in the picture 4.6.

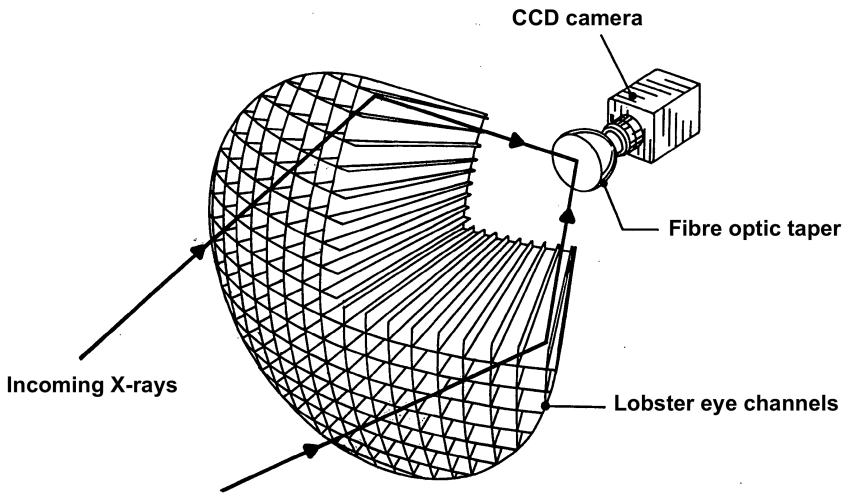

Figure 4.6: Lobster Eye X-ray telescope diagram [53]

Although SLE optics has a lower resolution than other variants of X-ray telescopes, it excels in the size of the field of view and the compactness of the entire system. Individual SLE optics can achieve field of view values of up to 6° x 6° and because of their compactness, it can be combined into larger systems, where the field of view can be increased even more by connecting more modules in series. At the same time, it is relatively easy to adapt the entire system for sizes corresponding to small satellites and CubeSats [56].

A modification of the developed prototype of the Lobster Eye X-ray telescope, which is marked with the code P-25 and was manufactured by Rigaku Innovative Technologies Europe s.r.o., was designed in collaboration with the Czech Technical University. The proposed model has a focal length $f = 289\ mm$ and can be placed in a volume of about 10x10x30 cm, which corresponds to a 3U CubeSat. It has the field of view 7.2° x 7.9° and a resolution of 1 arcmin [56]. It uses gold-coated plates with a thickness of 100 µm. Number of reflecting surfaces is 100 per set with a gap of 0.8 mm between the central planes to reflect the rays. The second variant allows for the number of 72 reflective surfaces per set, gaps of 1.1 mm and a thickness of 280 µm. Both variants have similar optical properties [56].

The focused beam impinges on the surface of the Medipix detector made by Advacam, which has a sensitive area of 14 mm x 14 mm. This detector is generally used to detect energetic particles such as neutrons, ions or X-ray particles. It can capture X-ray particles with energy above 3 keV and it has time resolution up to 1.6 ns [57].

The entire system of optics and detector weighs approximately 1 kg, consumes about 2 W of power and, as mentioned, can be integrated into a CubeSat type 3U measuring 10x10x30 cm [56] [58]. However, a stabilization system is required for proper operation. The design of the optical system envisages the use of a stabilization star tracking system. It can be integrated into a 1U module with dimensions of 10x10x10 cm. Also systems such as communication, control and energy system are needed for a complete solution. These can be placed in a 2U module with a size of 20x10x10 cm. Thus, a complete payload and support subsystems can be integrated into 6U or larger CubeSats, as shown in the following 3D model [56].

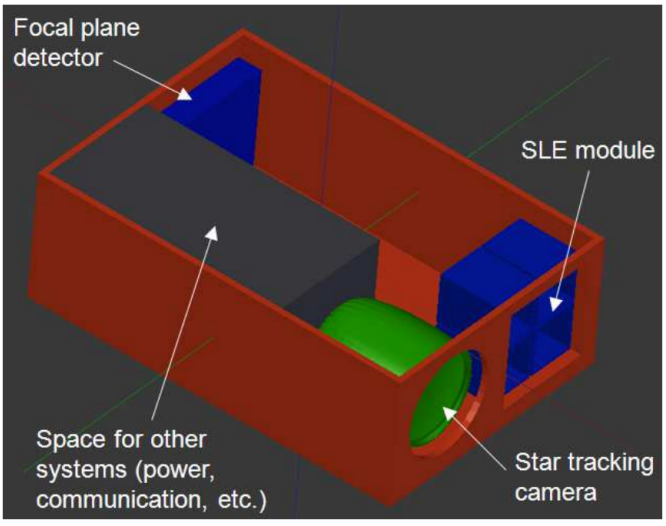

Figure 4.7: 3D model of 6U size CubeSat with integrated X-ray detector and telescope, including other supporting instruments [56]

Chapter 5

Space Mission Design

Contents

A detailed analysis of a space mission is a key document without which space travel would not be possible. It indicates the goal for which the rocket is sent into space, the way in which the goal will be achieved, the means needed to do so, and last but not least, the political and economic analysis. The resulting document should thus serve as a guide both for engineers and designers in development and for politicians and investors in deciding and approving the intention to carry out the mission.

Most of the information in this chapter is drawn from the comprehensive book *Space Mission Analysis and Design by W.J. Larson and J. R. Wertz [6].* This book is considered a universal tool for planning and designing any future space mission and is based on more than 40 years of experience with space flights and their design. Most of the arguments are focused on space missions with large satellites, but the basic principles can be easily applied to missions for small satellites and CubeSats.

5.1 Space mission analysis and design process

For most space mission designs, it is advantageous to proceed from head to toe. This means to first set a goal and a broad concept of what is expected of the final mission, then focus on the selection of individual components and using the iterative process reach the ideal solution. The involvement of members from as many teams as possible is expected, as everyone must set their expectations, limiting factors and bring their experience to the issue in order to adequately select the appropriate components that as a whole will meet the desired goal. At the same time, it is important to keep in mind that it is not just a matter of meeting the goal at all costs, but of making it as effective as possible. In the case of space missions, it is mostly about price. Space is expensive and price is the limiting factor for almost all ambitions in the space industry.

5.1.1 Space Mission Life Cycle

A space mission has typically 4 phases, which can be referred to as the life cycle.

- Concept exploration - An initial study to determine the general objective of the mission and the necessary components
- Detailed development - The formal phase of mission design, where the individual components are described in detail, together with the design of hardware and software for the necessary prototype testing
- Production and deployment - Construction of the necessary hardware and software and deploying it into space
- Operation and support - Daily operation, maintenance and technical support of launched satellites, together with the subsequent end of the life cycle in the form of deorbitation or return to the Earth's surface

This work will, for obvious reasons, focus only on the first and part of the second phase. The design of hardware, subsequent launch into space and operation of the device goes far beyond the scope of this diploma thesis.

5.2 Designing the Mission Concept

5.2.1 Mission statement and Mission Objectives

At the beginning of each mission design must be a brief statement. A statement that describes the exact purpose of the mission. It states the problem and its solution without any details. In a few lines, a reader should understand the importance and purpose of the planned mission, as well as the qualitative measure against which success will be measured.

This statement is a key step and it is necessary to keep returning to it and evaluating whether the planned mission really meets what was originally requested.

Mission statement then specifies the tasks and objectives that the mission is to meet. They are divided into primary, which must be met at all costs, and secondary, which serve to achieve additional goals. Additional goals do not have to be only technical or scientific in nature, e.g. socio-political. For example, the secondary objective can be considered to be the improvement of political relations in a given region, and thus the relocation of production to the selected area.

5.2.2 Baseline Mission Concept and System Drivers

If the mission objectives with subsequent mission requirements and limitations are outlined, it is time to focus on the mission concept. A mission concept is a basic set of decisions that indicate how the mission will be carried out. It describes a wide selection of choices for every space segment shown in the figure 5.1. Ideally, several options are outlined for each segment, from which different concepts are subsequently formed. These are decided in later design stages based on their ability and effectiveness to meet the stated mission objectives and requirements.

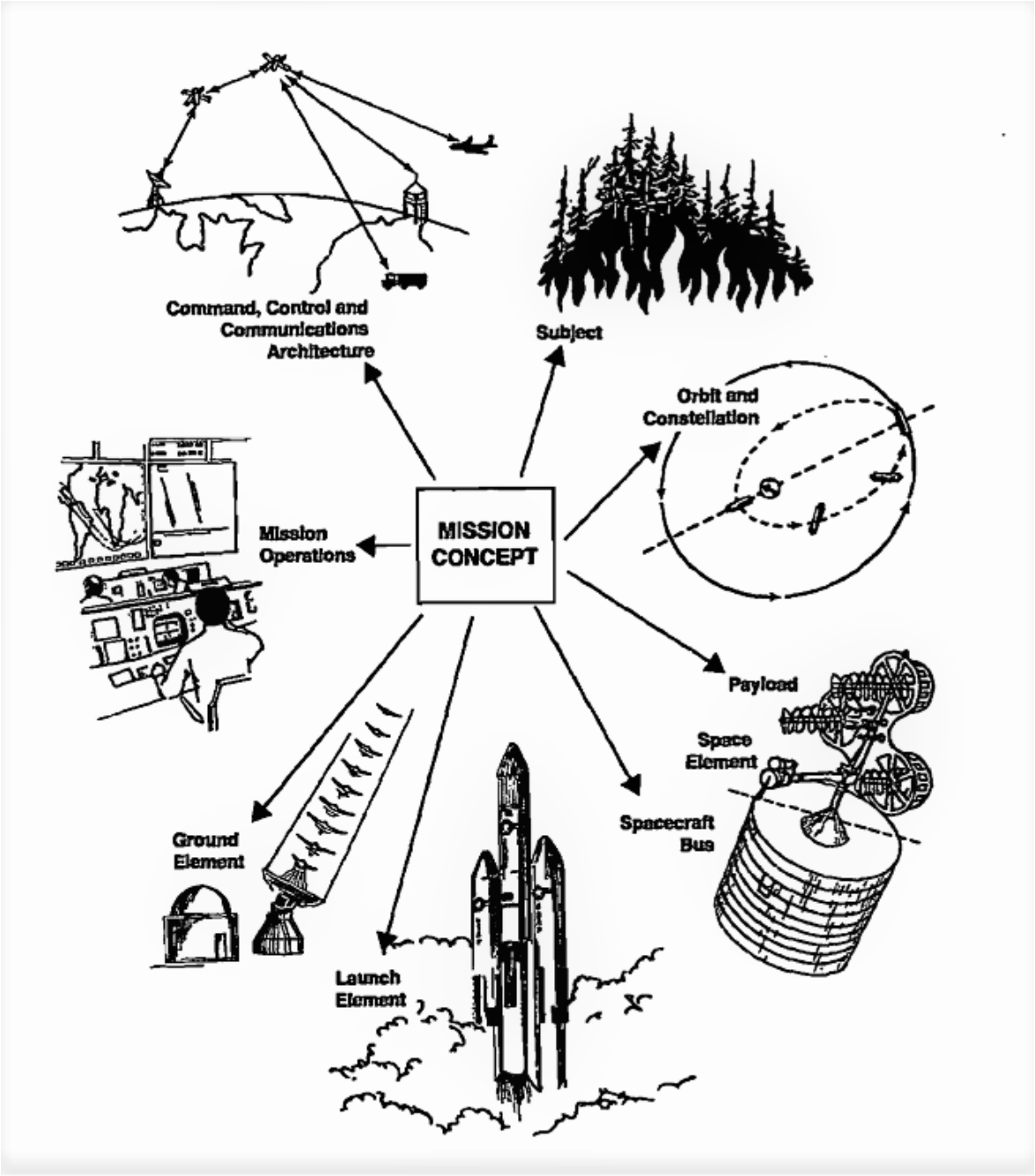

Figure 5.1: Space mission architecture. Eight segmets, which together creates a comprehensive design of any space mission. [6]

After defining the initial concept, it is useful to find key parameters, the so-called *System Drivers*. These are elements and subsystems that can be controlled and changed while fundamentally affecting the performance, cost, risk, or mission timeline. For each identified system driver, it is necessary to determine its own constraints and what limitations it can cause.

Subsequently, there is a more detailed analysis of individual space segments, finding specific technical solutions, and evaluating different concepts. When all design analyzes are complete, the baseline concept decision phase begins. The final decision on which mission concept will be chosen is not always based on quantitative parameters alone. It is a combination of optimal performance, low cost, acceptable risk, and political decisions. The analyzes carried out during the previous design process serve primarily to provide as much information as possible before making a final decision. After selecting the baseline concept, it is advised to return and go through the design process again, with a higher degree of knowledge and specification.

In the following chapters, the baseline concept of a small satellite space mission to VLEO will be proposed using the presented theoretical foundations and analysis from the Chapters 3. - 5. Emphasis will be placed on the satellite's power system and the propulsion unit configuration. The goal of this baseline concept will be to demonstrate feasibility of an air-breathing propulsion station keeping. And it can also serve as a starting point for further development of viable space mission for monitoring of X-ray triggers in the Earth atmosphere.

Chapter 6

Space Mission Software

Contents

For needs of the particular space mission design and analysis, an algorithm was created within this diploma thesis which includes important calculations presented in this work. This algorithm aims to show the key parameters and variables needed for decision-making in the design of a space mission using an air-breathing propulsion to the user. These are primarily functions in table 6.1, expressed as interactive graphs showcased in this section. The code was written in Python and open-source JupyterLab [59] development environment was used for implementing the code. Aquired CSV files with computed data were used in the Chapter 7.

Comparison of atmospheric drag and available thrust.
Amount of atomic oxygen interacting with the surface of a satellite.
Orbit decay curve.
Thrust-to-Drag (T/D) ratio.

Table 6.1: Functions of the algorithm that can be used for mission analysis.

6.1 Atmospheric drag and achievable thrust

In the Chapter 3 the equations for atmospheric drag (3.2) and the achievable thrust (3.9) were presented and explained. It can be seen that the drag depends primarily on the ram surface and the value of the drag coefficient. Thrust, on the other hand, is affected by particle capture and ionization efficiencies as well as grid voltage. Both quantities, drag and thrust, depend on the environment, which changes significantly with an orbit altitude and with solar activity. For these reasons, it is possible to change the value of solar activity, the value of both drive efficiencies, the voltage on the acceleration grids, and the value of the drag coefficient directly in the interactive graph.

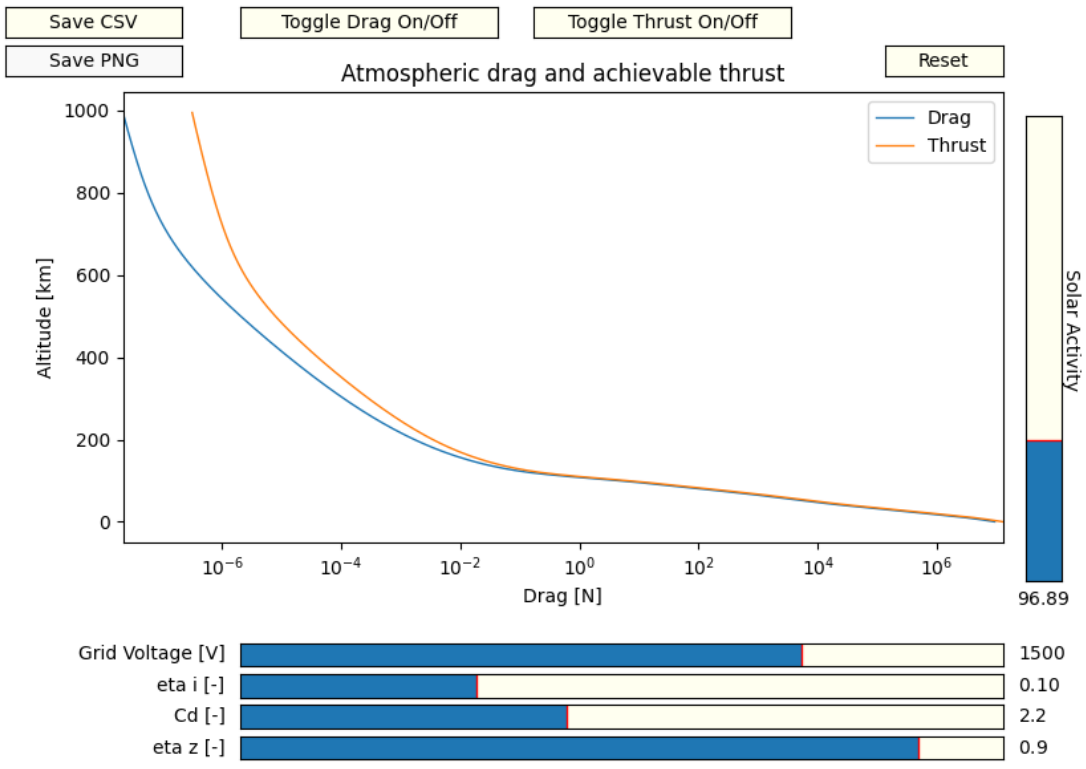

Figure 6.1: An interactive graph displaying the value of atmospheric drag and achievable thrust for a given size of the ram surface and variable parameters of solar activity, grid voltage, drag coefficient and engine efficiencies.

6.2 Thrust-to-Drag ratio plot

The curve of the T/D ratio is simply another interpretation of the values from the previous calculation. With the same variable parameters, this ratio can easily show the ability of the engine to compensate for a given drag. The graph 6.2, *part a* shows the T/D ratio curve depending on the orbit altitude, which is an important parameter in the design of the space mission. In contrast, the *part b* shows the same ratio as a function of the capture efficiency value, as a key parameter in designing the air-breathing engine itself.

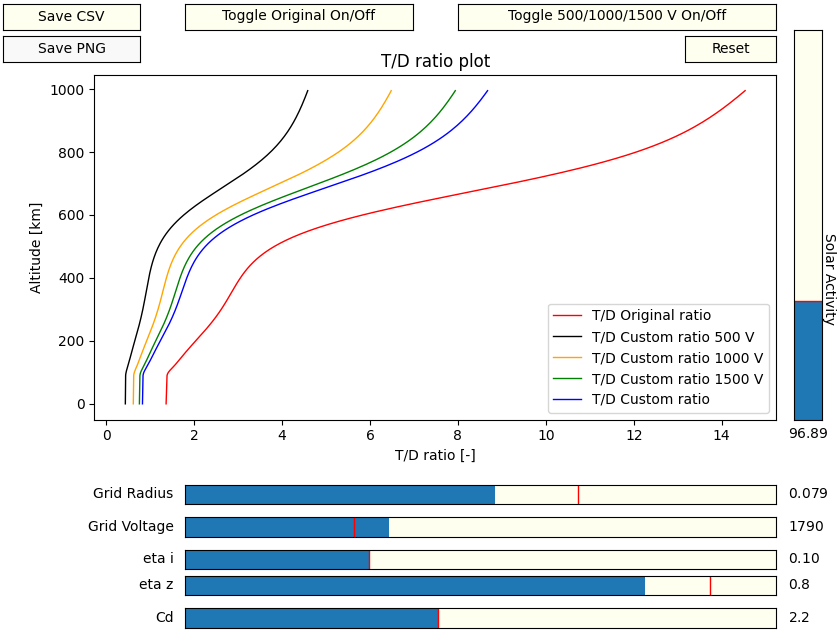

Figure 6.2: *a)* Interactive graph showing the T/D ratio as a function of orbit altitude

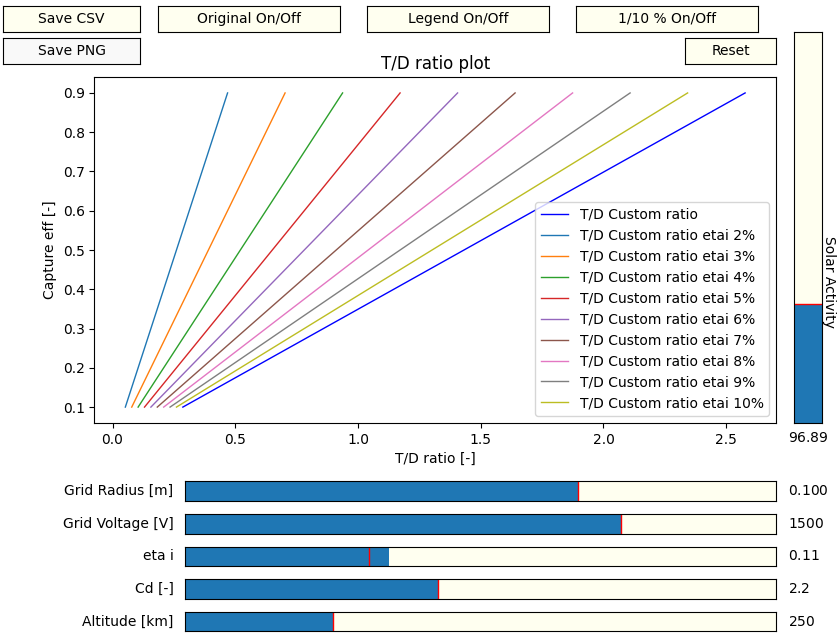

Figure 6.2: *b)* Interactive graph showing the T/D ratio as a function of particle capture efficiency

6.3 Atomic oxygen amount

In another interactive graph, the number of atomic oxygen particles interacting with the ram surface of a flying body can be observed. This value depends primarily on the size of the ram surface, orbital velocity, and the surrounding environment, ie the orbit altitude and the value of the solar activity. At the same time, it is directly proportional to the time spent in orbit. The data obtained are for information purposes only, to evaluate the risk of contamination of satellite surfaces by atomic oxygen.

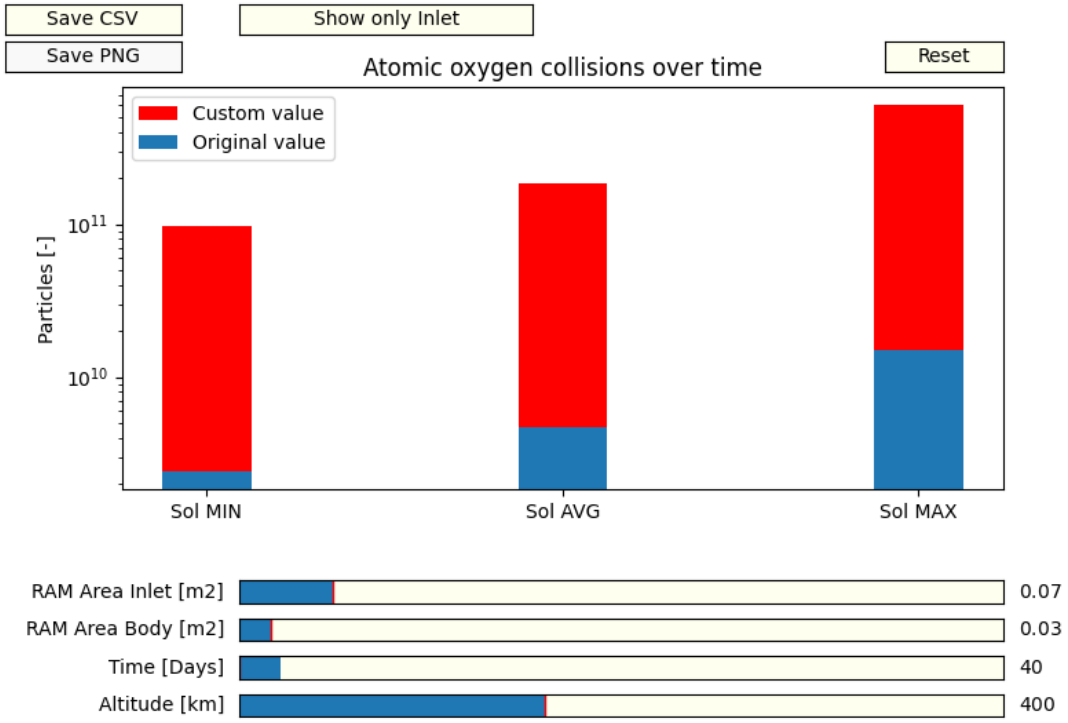

Figure 6.3: Interactive graph showing the number of atomic oxygen particles reacting with a flying body with a selected ram surface, at the selected altitude and for different values of solar activity

6.4 Orbit decay

The last interactive graph shows the orbit decay curve. It is obtained from the equations 6.1 - 6.4.

$$P = 2\pi\sqrt{\frac{a^3}{GM}} \tag{6.1}$$

$$dP = 6\pi\frac{a^2 D}{GMm} * dT \tag{6.2}$$

$$P_{new} = P - dP \tag{6.3}$$

$$a_{new} = \sqrt[3]{\frac{P_{new}^2 MG}{4\pi^2}} \tag{6.4}$$

Here *P* represents the orbit period, *dT* is the measured time period, *G* is the gravitational constant, *M* is the mass of the Earth, *D* is the atmospheric drag that can be reduced by an added thrust from the propulsion unit, *a* is the orbit altitude including the radius of the Earth and *m* is the mass of the satellite. Knowledge of the decay rate is especially valuable for calculations of the orbit altitude decrease due to short-term shutdown of the engine, or in general the stability of the orbit at the selected altitude and with an available thrust.

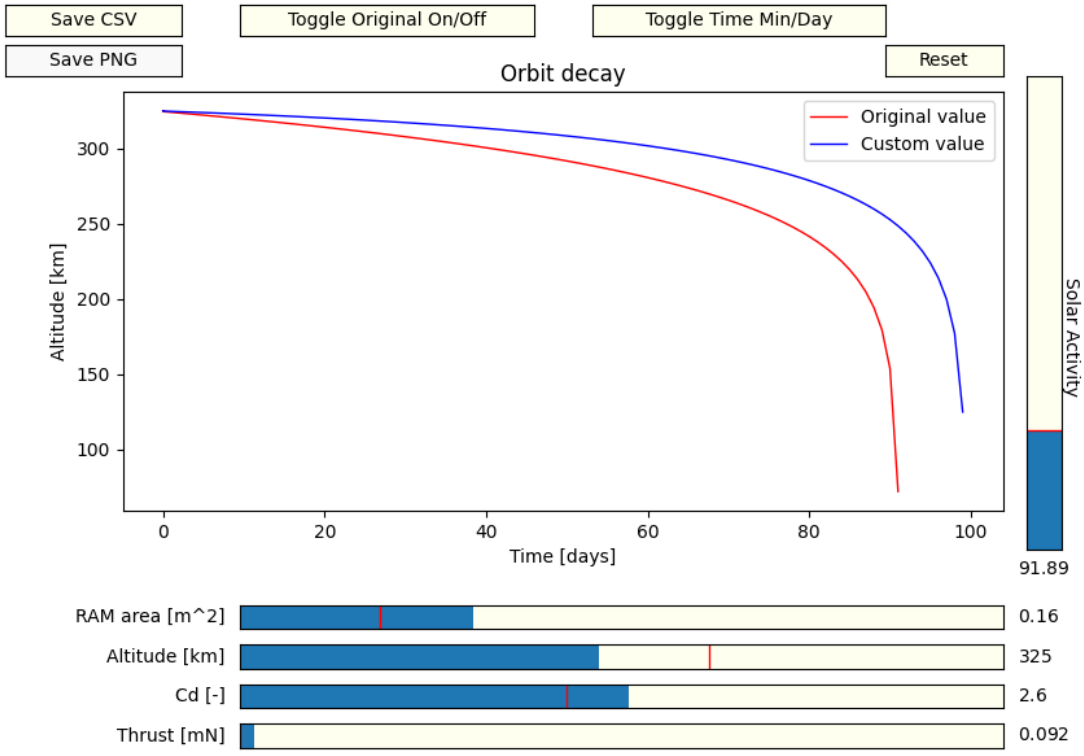

Figure 6.4: Interactive graph showing the orbit decay curve for variable initial altitude, ram surface, available thrust, solar activity and drag coefficient.

This tool, created within this diploma thesis, was further used for the analysis of the designed space mission, which is described in the Chapter 7.

Chapter 7

CubeSat Mission Design and Analysis

Contents

7.1 Mission Statement

This diploma thesis aims to present a viable space mission using the proposed air-breathing propulsion in a Very Low Earth Orbit. Due to the characteristics of this study, namely University involvement, CubeSat satellites are considered as an inexpensive alternative still able to provide valuable scientific data. Using the mission design framework presented in the Chapter 5, baseline concept of the mission will be presented. This will serve as a basis for the decision whether a CubeSat mission with air-breathing propulsion is feasible.

The first step is to formulate a brief description of the mission called *Mission Statement*.

Mission Statement
There are several potential sources of X-rays in the Earth's atmosphere. Current satellites and detectors have a very small field of view and are therefore unable to monitor beam sources over a longer time horizon and a large area. Proper monitoring of X-ray sources in the Earth's atmosphere is important for full understanding of their nature and expansion of knowledge about the issue. At the same time, X-ray monitors can be used to complement large X-ray detectors in space, to monitor sources such as black holes and supernovae.

Table 7.1: Mission statement.

7.2 Mission Objectives

Using the mission statement, mission primary and secondary objectives can be deduced.

Primary Objective
Detect and monitor X-ray sources in the Earth's atmosphere, focused mainly on the polar regions. (Monitoring of an auroral X-ray emission)
Secondary Objectives
Expand the capabilities of X-ray detection in orbit
Demonstrate the capabilities of CTU to design and develope a space mission using the CubeSat satellite
Demonstrate new capabilities of air-breathing drives for station keeping of the satellite

Table 7.2: Mission primary and secondary objectives.

The secondary objectives are mainly focused on gaining knowledge and hands-on experience with space hardware. In the Czech Republic, a handful of attempts have been made to build a

CubeSat satellite, but most of them have failed due to the lack of funding [60]. Since 2017, Czech Republic managed to launch two CubeSats and the third is waiting for the official rocket launch date [61]. However, none of these cases were considered a student project and it can be stated that for astronautics students the current opportunities for gaining relevant experience are very limited. For this reason, the project to study and to design a new CubeSat satellite at the CTU is key to the development of Czech astronautics and the education of a new generation of students.

At the same time, the aim is to demonstrate the feasibility of the air-breathing propulsion and to obtain valuable data on its operation in a real environment.

It has already been outlined that the critical problem of most CubeSat projects in the Czech Republic is connected with funding. At the same time, the proposed mission is not strictly time-constrained. For these reasons, the mission characteristic was chosen for the lowest possible cost, even at the cost of a significant prolongation of development. The use of air-breathing propulsion remains the key element, even though it will not be the cheapest possible solution to meet the primary objective of the mission.

Mission characteristic
Mission with the lowest possible development and deployment costs using air-breathing propulsion for station keeping.

Table 7.3: Mission characteristic.

7.3 Mission Phases

The proposed space mission will be in several different phases during its lifetime. The phases follow each other chronologically and briefly describe the ideal course of the mission from launch to deorbit process.

Phase 1 - Deployment
Satellite deployment into orbit altitude of 300 km.
Phase 2 - Controlled descent
Gradual descent by natural orbit decay to the desired altitude.
Testing of the controls, housekeeping and payload data collection tests, and engine performance tests.
Duration: 1 month
Phase 3 - Stabilization maneuver on VLEO
Stabilization maneuver using its own propulsion system to compensate for atmospheric drag.
Phase 4 - Monitoring
X-ray sources monitoring in the Earth's atmosphere and recording the high-energy phenomena with continuous atmospheric drag compensation and station keeping.
Duration: $>$5 years.
Phase 5 - Deorbit
Shutdown of the propulsion system, spontaneous deorbit and controled unassembly in the atmosphere.
Duration: Several days.

Table 7.4: Proposed mission phases.

7.4 Baseline Concept

After defining the fundamentals of the space mission in the form of mission objectives and characteristics, it is possible to outline the baseline mission concept. It serves as a starting point for further specification, development, and comparison with other alternatives for each segment of the mission shown in figure 5.1.

Segments presented here are the subject, payload, spacecraft bus, the selected orbit, power system, and the onboard propulsion unit.

7.4.1 Subject, Payload and Spacecraft Bus

The subject of interest and payload were described in more detail in the Chapter 4.

Subject
Auroral X-rays in the polar regions of the Earth.
Soft X-rays with energy below 5 keV.
Payload
Medipix X-ray detector made by Advacam using a small Lobster Eye optical module.

Table 7.5: Payload baseline concept.

The design takes into account the 6U CubeSat satellite, which has external dimensions of approximately 100x200x300 mm. This design of a spacecraft bus is appropriate for housing the X-ray detector as well as the rest of the subsystems, as shown in the fig. 4.7. Three units are dedicated for payload, one unit for the star-tracking system, and the other two units for support systems such as the on-board computer, communication unit, inertial senzors, and power management system. Due to the characteristic of the mission, ie monitoring the Earths

atmosphere, it is needed for the spacecraft bus, shown in fig. 4.7, to be aligned with the optics pointing down. That means that the ram area of the body is 0.03 m^2. For drag calculations, it is needed to include the ram surface of the propulsion unit, which is externally strapped onto the spacecraft bus and is dependent on the inlet radius.

Spacecraft bus
Outer dimensions: 100 x 200 x 300 mm
Support systems: 3 units
Payload: 3 units
Ram area: 0.03 m^2 + Inlet area

Table 7.6: Spacrecraft bus baseline concept.

7.4.2 Orbit

A polar orbit is required to observe auroral X-rays. In addition, the choice of a polar orbit with an inclination around 98 ° is a so-called sun-synchronous polar orbit, in which solar radiation hits the orbital plane under the constant angle. Such a phenomenon can be used for constant irradiation of solar panels and thus greater and more stable power generation. Sun-synchronnous orbit inclination is dependant on orbit altitude and can be calculated from the equation 7.1.

$$\cos i = -\frac{2}{3}\frac{\dot{\Omega}}{J_2\sqrt{\frac{GM_e}{a^3}}(\frac{R_e}{a(1-e^2)})^2} \tag{7.1}$$

where *G* is the gravitational constant of Earth, *Me* is the mass of the Earth, Ω is the rate of revolution of Earth around the Sun, J_2 is the zonal harmonic coefficient and it is equal to 1.08263 * 10^{-3}, *a* is the semi-major orbit axis, *e* is the eccentricity and *i* is the inclination. The rate of revolution of the Earth around the Sun is calculated by 7.2.

$$\dot{\Omega} = \frac{2\pi}{365.242\ days} = 1.72 * 10^{-}2\ rad/day = 1.99 * 10^{-}7\ rad/sec \tag{7.2}$$

Finally, the inclination for sun-synchronnous orbit around the VLEO area is rouglhy 96.5°. After the satellite is launched on a stable LEO polar sun-synchronous orbit, a phase of spontaneous orbit decay to an altitude of 250 km occurs. When the required altitude is reached, the propulsion unit is ignited to compensate for atmospheric drag, which ensures a stable circular VLEO orbit.

Depending on the selected orbit, a precise value of atmospheric drag can be determined. The value of drag also depends on the size of the total ram area of the satellite and the inlet. The ram area of the satellite was defined as one side of a 6U CubeSat with an area of 0.03 m^2. The graph 7.1 shows the atmospheric drag at an altitude of 250 km for different sizes of the inlet. The mentioned area of the satellite is also included in the drag calculation.

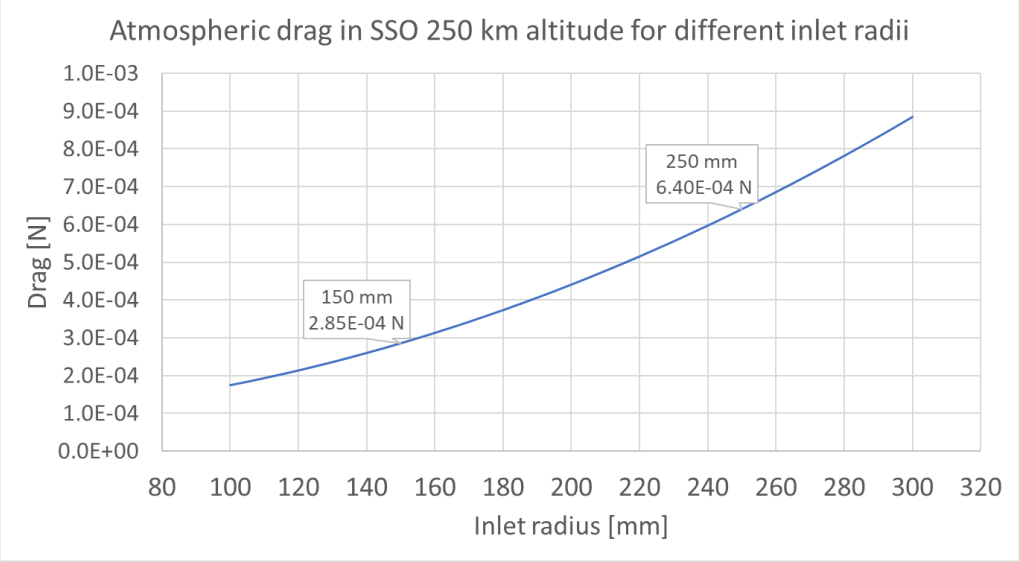

Figure 7.1: Corresponding atmospheric drag in 250 km orbit for the satellite ram surface 0.03 m^2 and different inlet dimensions.

Orbit
Polar sun-synchronous orbit with an altitude of 250 km and an inclination of 96.5°.
With increasing inlet contamination, the increase of orbit up to 280 km is available.
Atmospheric drag: 0.2 - 0.9 mN depending on the size of the inlet.

Table 7.7: Orbit baseline concept.

7.4.3 Power System

The power system is used to produce, store, distribute and control electricity flow in the satellite. A set of solar panels with a suitably selected battery and power distribution unit is used for this.

7.4.3.1 Solar panels

Solar panels must be selected according to the required output and available space. Various technologies are available to choose from, but in space applications, only the technology with the highest efficiency is favored. It is a GaAs Triple-junction technology that achieves efficiency in a real environment of over 30 % [63].

In orbit near the Earth's surface, the solar constant is approximately 1368 ± 5 W/m^2. At the same time, the Earth's atmosphere reflects about 30 % of incoming solar radiation which is called albedo, and the Earth's surface itself emits energy of about 240 W/m^2 [64] [65]. The total energy incident on the surface of the satellite is thus about 2000 W/m^2. The position of the satellite and its solar panels must also be taken into account. In the case of a polar sun-synchronous orbit, the solar panels are positioned almost perpendicular to the incoming solar rays. Thus, this source is dominant and, conversely, the source from the earth's surface is significantly reduced due to the large incident angle.

Commercially available solar panels for CubeSats with triple-junction technology have an efficiency of about 30 % and an effective area of 30 cm^2 [66]. With the solar constant in orbit close to Earth being around 1400 ± 5 W/m^2, the power of one solar panel with the mentioned parameters is roughly 1.2 W.

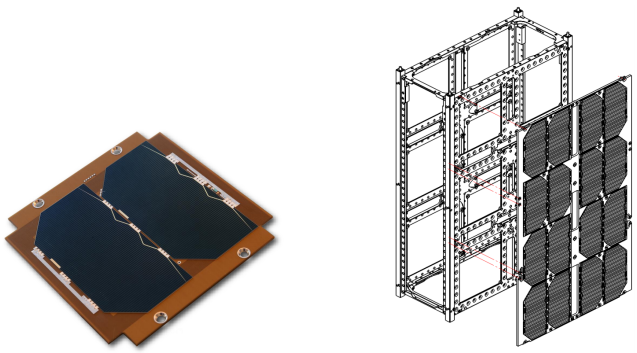

(a) (b)

Figure 7.2: *a* - Single unit composed of two solar cells.
b - Solar array of 16 solar cells that can be mounted on a 6U CubeSat. [66]

A 6U CubeSat orbiting in a sun-synchronous orbit will have only one side constantly irradiated, ie an area of 220 x 340 mm. Up to 16 solar panels can be placed on such an area, which can generate up to 19.2 W of power [66]. At the same time, it is possible to develop a deployable mechanism that can extend additional solar panel area from the sides of CubeSat. A commercially available solution offers, for example, the ”accordion” method, where additional areas are deployed from the narrow side of the 6U Cubesat and it allows the addition of up to another 12 panels, see fig. 7.3. Using this mechanism from both sides of the CubeSat, the system will expand to 40 panels with a power output of up to 48 W. The deployable field of the panels should be as thin as possible to affect the atmospheric drag as little as possible.

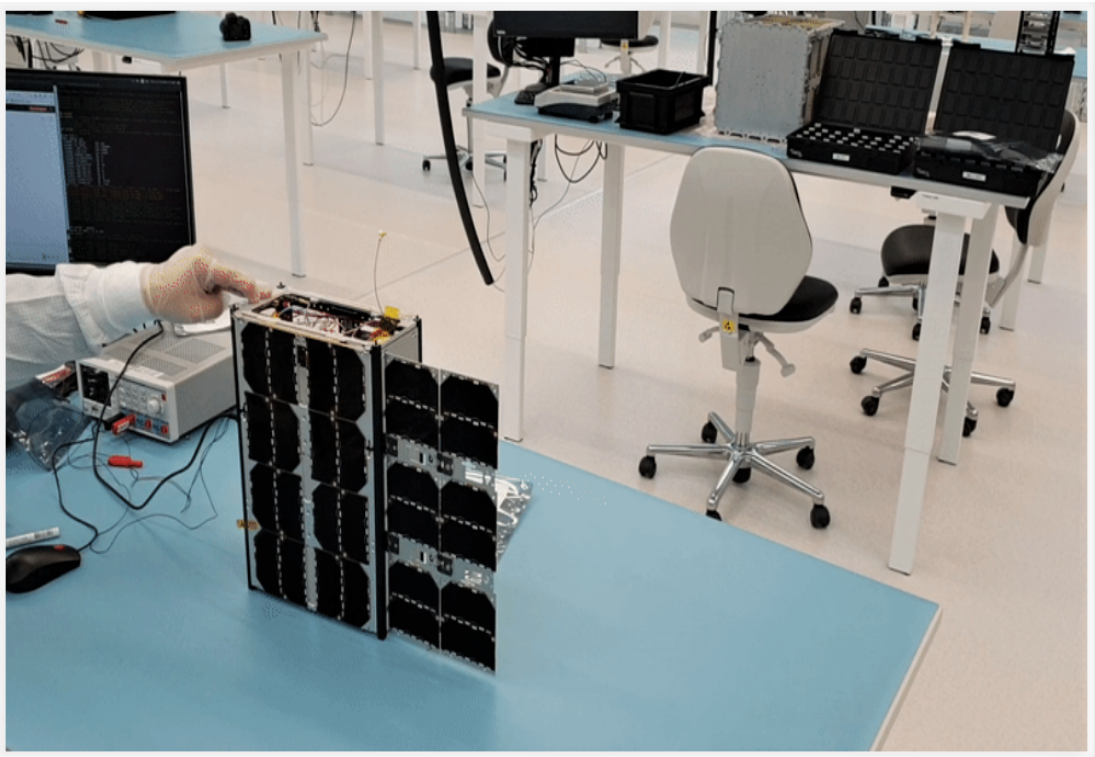

Figure 7.3: Deployable mechanism mounted on a 6U CubeSat. Developed by GomSpace [66].

In the selected sun-synchronous orbit at an altitude of 250 km, one orbit takes about 89.4 minutes, of which the satellite is in the Earth’s shadow for 36 % of its time, ie about 32 minutes [68]. With a mission duration of 2 years, the total number of cycles, and thus the battery charging cycles, is around 11 800. For a mission duration of 5 years, the number is close to 30 000 cycles.

During the designing process of a power system, it is necessary to find out how much energy

the satellite will need when moving in the shade, how much energy it can generate during the sun phase, and if it is able to recharge the battery pack for the next orbit cycle.

Another option for ABIT control is available here. It is an option of a thrusting mode. The simplest way is continuous thrusting, where the engine compensates for the drag continuously throughout the orbital cycle, ie even in the shadow phase. This mode leads to lower thrust requirements but sets greater demands on the energy system, which must be able to supply enough energy for the satellite even during the shadow phase, which is taken solely from the battery pack.

The second mode is a combination of an active phase in which the drag is compensated and an inactive phase in which the engine is switched off. In this case, switching off the engine can be timed with the shadow orbit phase, thus reducing the demands on the energy system. However, in the active phase, it is necessary to develop a higher thrust to maintain the desired orbit, as there was a slight orbit decay. The article *Di Cara, 2007* [28] outlines that the ideal ratio between the active and inactive phase is 5/6. That means the propulsion unit is switched off for 1/6 of the orbit time. For the case of the selected SSO at an altitude of 250 km, the inactive phase period is approximately 14.9 minutes, and the active period is 74.5 minutes.

The following figure 7.4 shows a comparison of the energy needed to maintain a stable orbit in the continuous atmospheric drag compensation mode and in the 5/6 alternating mode.

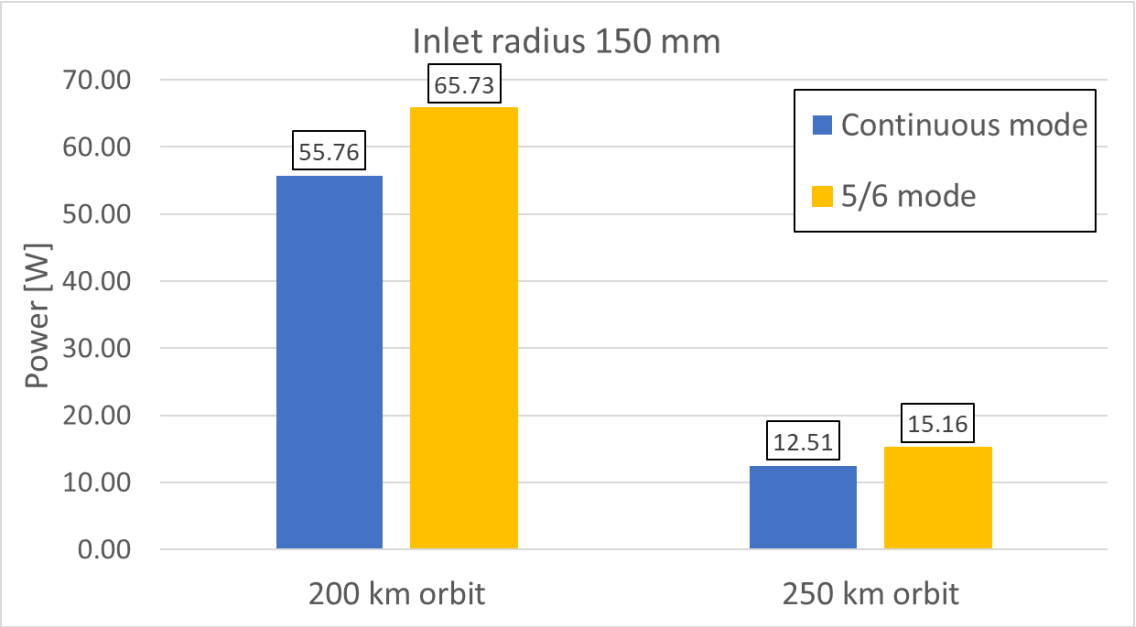

(a)

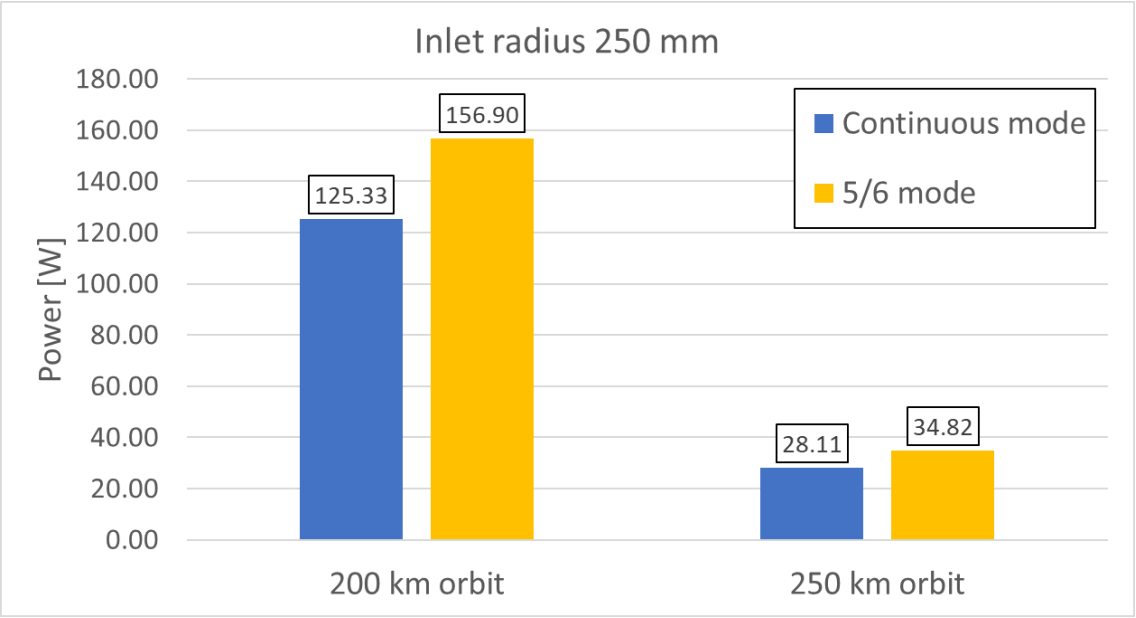

(b)

Figure 7.4: Energy needed to maintain a stable SSO orbit in continuous compensation mode and in alternating mode for orbit altitudes of 250 km and 200 km.
a) Inlet radius 150 mm *b)* Inlet radius 250 mm

The figure 7.5 outlines the satellite's power consumption during the shadow phase and the value of the energy generated per orbit cycle for different values of the total power consumption using the solar array specified above. The graph 7.6 shows the difference between these two values.

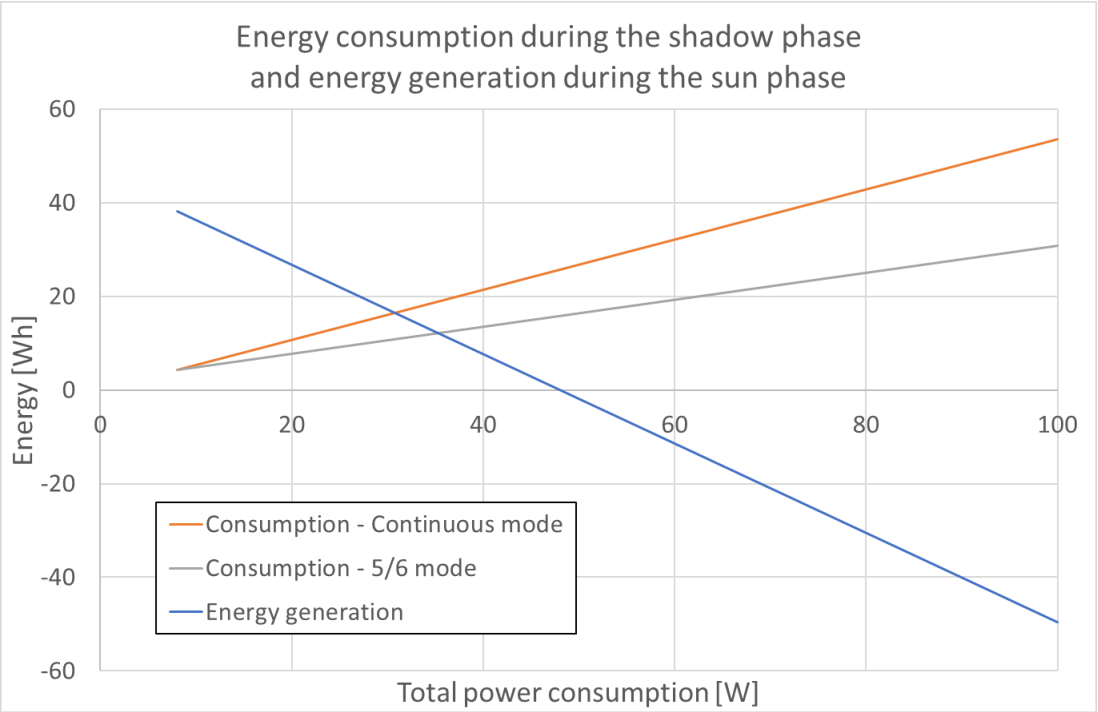

Figure 7.5: Satellite power consumption while going through the shade in a sun-synnchronous orbit at an altitude of 250 km and available generated power during the sun phase with variable total power consumption.

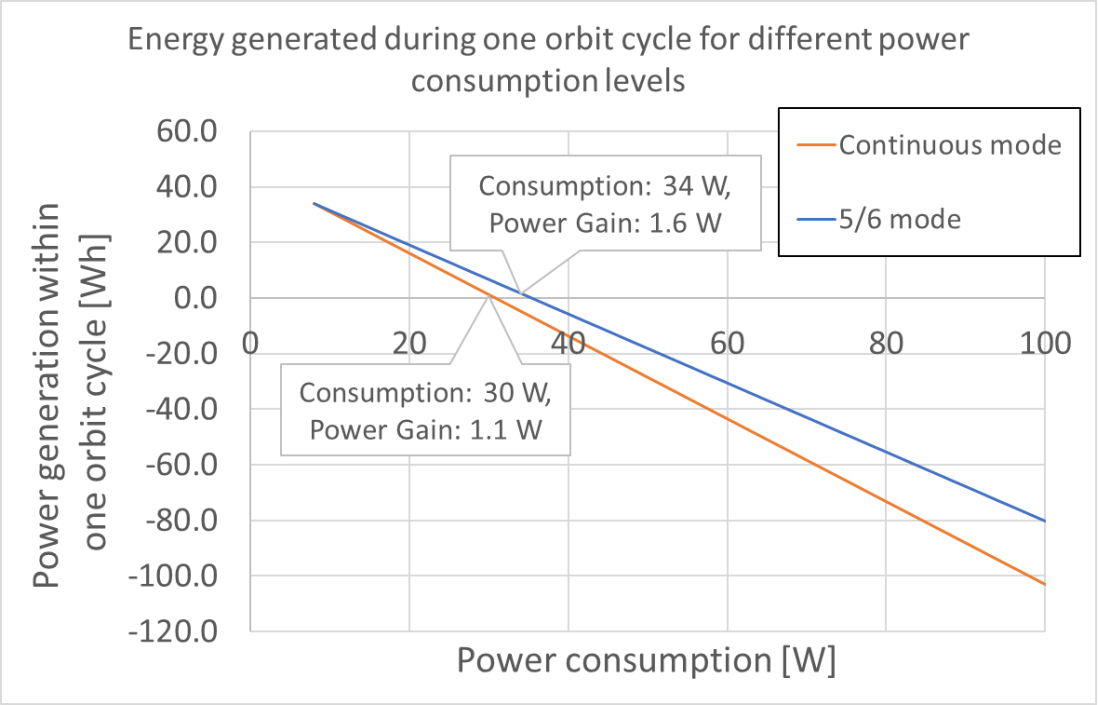

Figure 7.6: Available power gained from solar panels during one orbit around the Earth depending on the level of total power consumption.

It is clear that for the designed solar panel field with a power output of 48 W, it is necessary to keep the satellite power consumption below 30 W for continous thrusting mode and

below 34 W for 5/6 thrusting mode. For these values, the system is in the balance. During the sun phase of the orbit, the satellite is able to generate enough energy for the subsequent flight in the Earth's shadow. The selected payload has a consumption of about 2 W, while communication and stabilization systems reach the consumption of 6 W. Thus, around 22 W, resp. 26 W of power is available for the electric engine.

7.4.3.2 Battery pack

The battery needs to be selected based on mostly two data. Capacity and charge cycle life. One charge cycle represents discharging the battery from a fully charged state to any lower capacity value and recharging again. The difference between the original state of charge and the state of discharge is referred to as the depth-of-discharge *DoD* [67]. DoD for most types of batteries strongly affects the resulting charge cycle life. Therefore, it is desirable to design an accumulator that exceeds the power consumption need to avoid high DoD values.

The commercially available batteries commonly used for CubeSats are based on Lithium-Ion technology. While maintaining DoD values in the range of about 15 %, their capacity decreases by 25 % after 10 000 charging cycles, resp. by 30 % after 30 000 cycles [66].

Using a commercially available battery proposed specifically for 6U CubeSats with a capacity of 10.4 Ah at a nominal voltage of 7.2 V, the unit is capable of delivering 75 Wh. At a set consumption of 30 W, the satellite will discharge by 21.5 % during the shadow phase of the orbit. From the previous conclusions, it follows that the battery pack with a capacity of 75 Wh will degrade to a capacity approximately of 50 Wh after two years of active mission and it is thus sufficient for the continuous operation of the satellite.

7.4.3.3 Power management unit

The brain of the whole energy power system is the power management unit, which connects the power supplied from the solar panels to the battery and subsequently to the CubeSat subsystems. The goal is to get the best performance out of the solar panels while maintaining

the constant voltage required by the satellite subsystems. At the same time, optimal battery utilization and current protection of satellite systems are desirable. All of this should be accomplished with the least possible complexity of the solution and minimal power losses. Current and voltage levels are controlled using DC / DC converters. Although it is possible to design a system with different number and position of converters, the paper *Osman, 2012* [69] explains that the ideal solution for CubeSat systems is to use two converters positioned as shown in the block diagram 7.7.

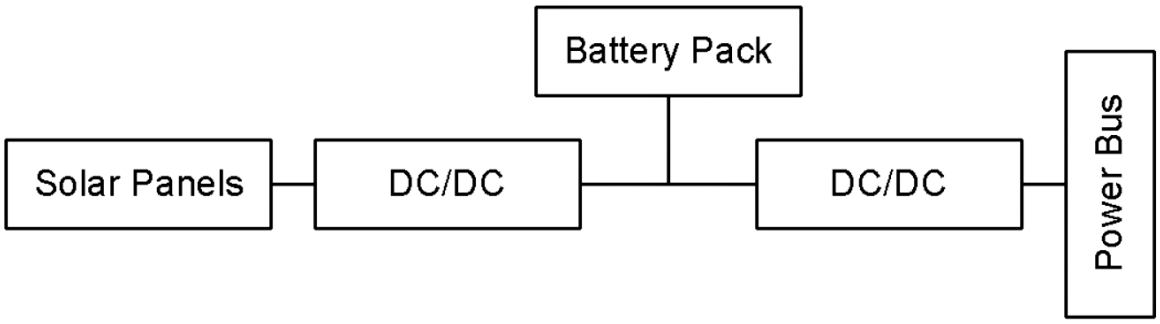

Figure 7.7: Block diagram of a power management unit with two converters [69].

In this circuit, the first converter, between the solar panels and the battery pack, serves to control the ideal operation of the solar panels. Such a unit is called *Max Power Point Tracking Converter - MPPTC*. The second converter between the battery pack and the satellite systems serves to maintain the stable voltage required for the systems to function properly and is referred to as the *Power Conditioning Converter - PCC*. It is advisable to use a different type of converter for each of them, because of their different needs. The diagrams for MPPTC and PCC converters are shown in the figure 7.8.

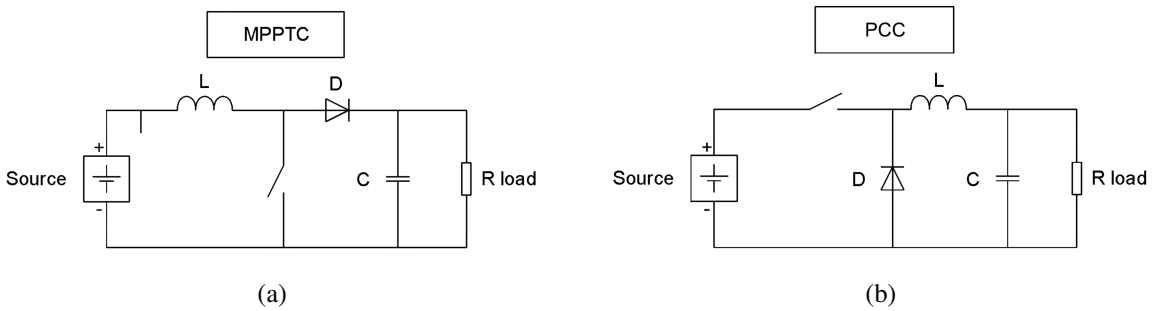

Figure 7.8: Diagrams of DC/DC converters [69].
a) MPPTC *b)* PCC

The last part of the unit is the current protection. It can be implemented as a mere passive

resistor or an active component. Active current protection is more advantageous in terms of power losses. Its diagram is shown in the figure 7.9. The block diagram of the whole power management unit is then in the figure 7.10.

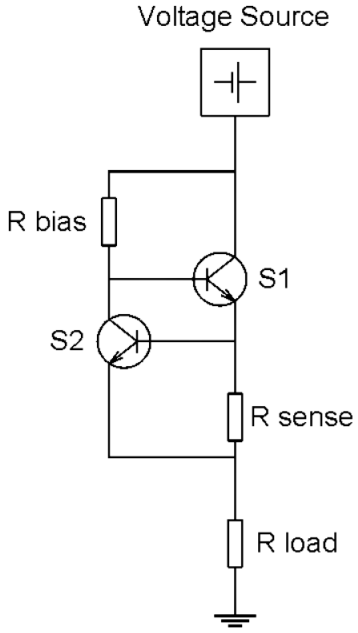

Figure 7.9: Diagram of an active element for current protection of satellite subsystems [69].

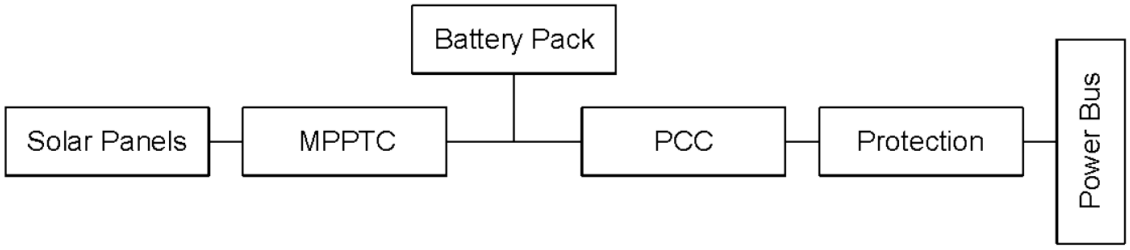

Figure 7.10: Block diagram of the complete power management unit including protection circuits [69].

7.4.3.4 Power System Summary

The proposed power system for the 6U CubeSat has 40 solar panels based on triple-junction technology with an efficiency of 30 % and an effective area of 30 cm^2. Such an arrangement can provide up to 48 W of power. The selected battery pack has a capacity of 10.4 Ah at a nominal voltage of 7.2 V. It is expected that the capacity will decrease by about 30 % for the duration of the mission.

As previous paragraphs outlined, it is possible to choose alternating thrusting mode, where drag is being compensated only for 5/6 of the orbit duration. Figures 7.4 and 7.6 show that when using 5/6 mode in an SSO orbit at an altitude of 250 km with selected solar panel arrays, up to 4 W can be obtained in the energy budget. However, there will be increased consumption of the propulsion unit, depending on its geometry. For a smaller configuration with an inlet radius of 150 mm, the consumption is increased by 2.66 W and for a larger inlet with a radius of 250 mm by 6.72 W. Thus, it can be stated that at a height of 250 km for an inlet size of 150 mm, the 5/6 mode is slightly more advantageous, but it is not the case for larger inlet dimensions.

Therefore, the consumption of the whole CubeSat system should not exceed the value of 34 W, resp. 30 W, of which about 8 W is for the payload and support systems consumption and 26 W, resp. 22 W, for the consumption of the propulsion unit. However, it will be necessary to take into account the possible degradation of solar panels, which may reduce their efficiency due to the presence of atomic oxygen particles or mechanical failure. Furthermore, convertors in the power management unit can cause approximately 10 % power loss [70]. Therefore, it would be appropriate to design the propulsion system so that the total consumption of the satellite does not exceed 25 W of which only 17 W would be used for propulsion.

7.4.4 Propulsion Unit

To maintain a stable orbit in the VLEO region, many problems need to be addressed. A closer look at the VLEO issues is described in the Chapter 3.

Depending on the selected orbit altitude, it is necessary to choose the engine parameters so that it can generates sufficient thrust. Parameters that can be modified directly or indirectly are:

ABIT parameters
Inlet dimensions
Acceleration grids dimensions
Acceleration grids voltage
Capture efficiency
Ionization efficiency

Table 7.8: Main engine parameters, that can be modified to obtain needed performance.

There are two key indicators. Specifically, it is the *Thrust-to-Drag (T/D)* ratio, and the *Thrust-to-Power* ratio. If not specified otherwise, the average value of the solar activity, which equals 92.1 F10.7 flux units, was used for all the following calculations.

7.4.4.1 Thrust-to-Drag ratio (T/D)

The graph 7.11 displays the T/D ratio for a 6U CubeSat with the ram surface of 0.03 m^2. The curve shows the ratio value for the orbit altitude from 170 km to 270 km. The values for three different values of voltage on the acceleration grids 500 V, 1000 V, 1500 V, and two different geometric configurations of the engine with an inlet radius to the radius of the acceleration grids 150 / 100 mm and 250 / 167 mm are shown. The remaining parameters match the drag coefficient Cd = 2.2, ideal efficiency values of ionization 10 %, and capture 90 %.

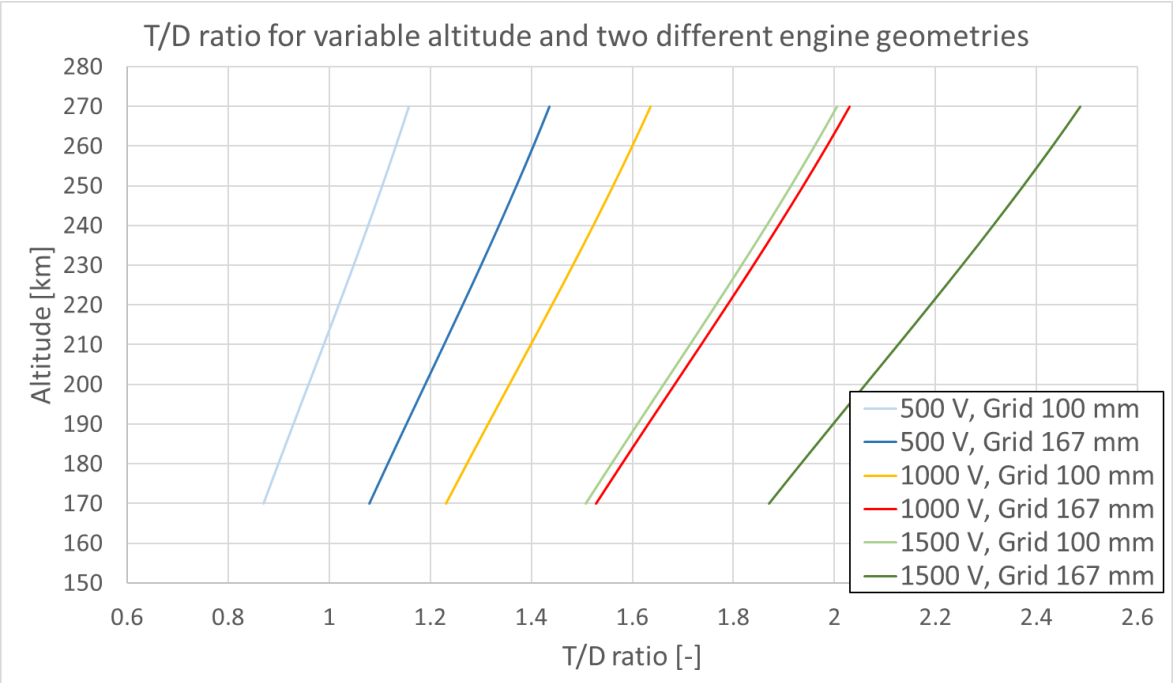

Figure 7.11: T/D ratio for altitudes from 170 to 270 km.

As shown in the plot for a radius of accelerating grids of 100 mm and voltage on the grids 500 V, the T/D ratio becomes positive up from an altitude of 210 km. For higher voltage, as well as for larger geometric configurations, this indicator is positive from altitudes even below 170 km. For all of these cases, however, the ideal situation was taken into account, with high values of both key engine efficiencies.

Hence, it is important to investigate the engine performance while reducing the capture efficiency which occurs over time with the absorption of atomic oxygen into the material of an inlet. Figure 7.12 shows Thrust-to-Drag ratio curves for orbit altitude 200 km, acceleration grids radius 100 mm and 167 mm, grid voltage 1500 V and ionization efficiency from 2 % to 10 % while gradually reducing the capture efficiency. The same graphs for 1000 V and 500 V grid voltage values can be found in the appendix.

It can be seen from the figure for 1500 V that for the initial capture efficiency of 90 %, the T/D ratio had a value greater than one with an ionization efficiency greater than 6 %. However, the capture efficiency decreases during the mission. The rate of decline depends on the material used, where the selection of a suitable alloy is currently the subject of research in the project Discoverer [30]. Yet, it can be assumed that the capture efficiency may drop down

to 40 % or 50 % during the duration of the mission. With this in mind, the T/D ratio matches the required value greater than one only for $\eta_i > 9$ %. In the case of 1000 V grid voltage, only the values of the ionization efficiency $\eta_i \geq 8$ % are viable, even at a high capture efficiency. And finally, for a 500 V grid voltage, thrust does not reach values higher than drag even for high ionization and capture efficiencies.

The second examined engine configuration was for the inlet radius 250 mm and the acceleration grids radius 167 mm. In this case, the relative size of the radii remains the same as in the previous case. Again, the T/D ratio was calculated for the orbit altitude 200 km and the same grid voltage values.

Calculations show that even if there has been an increase in the inlet, and thus in the entire ram surface area of the satellite, the available increment in the acceleration grids area will compensate for this fact. For all voltage levels, the T/D ratio is higher, but it still applies that when using a 1500 V voltage while decreasing the capture efficiency down to 50 %, it is necessary to achieve a high degree of ionization, specifically $\eta_i > 8$ %.

As the orbit increases to 250 km, higher values of the T/D ratio are visible in the figure 7.13 for all cases, as expected. However, there is no fundamental difference and the conclusion remains similar. When using a voltage of 1500 V in the configuration of an inlet radius of 150 mm and an acceleration grids radius of 100 mm, ionizing efficiency is required $\eta_i > 7$ % and for the second, larger, configuration $\eta_i > 6$ % for capture efficiencies around 50 %.

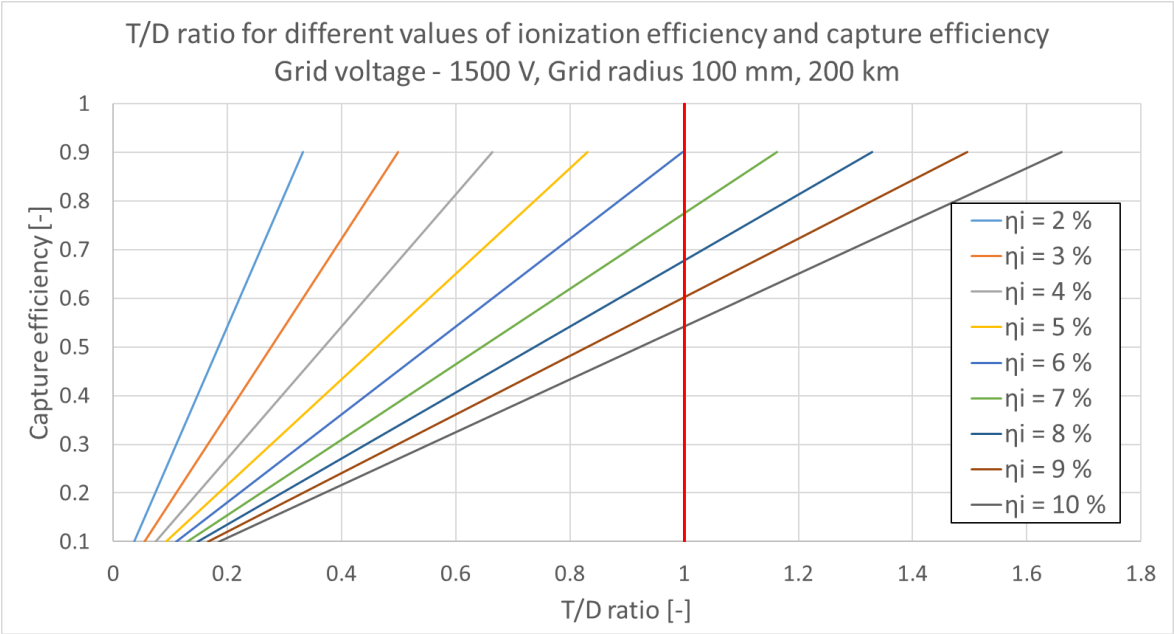

(a)

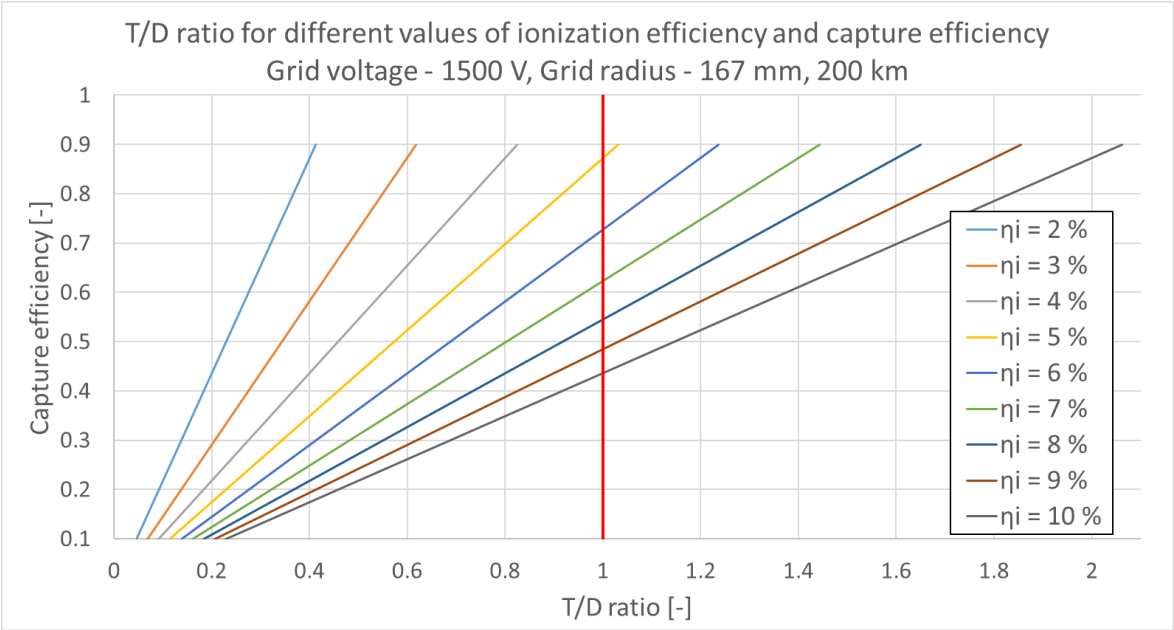

(b)

Figure 7.12: T/D ratio values for variable capture efficiency at an orbit altitude of 200 km for different ionization efficiency values.
a) - 150 mm inlet radius and 100 mm acceleration grids radius, *b)* - 250 inlet radius mm and acceleration grids 167 mm radius

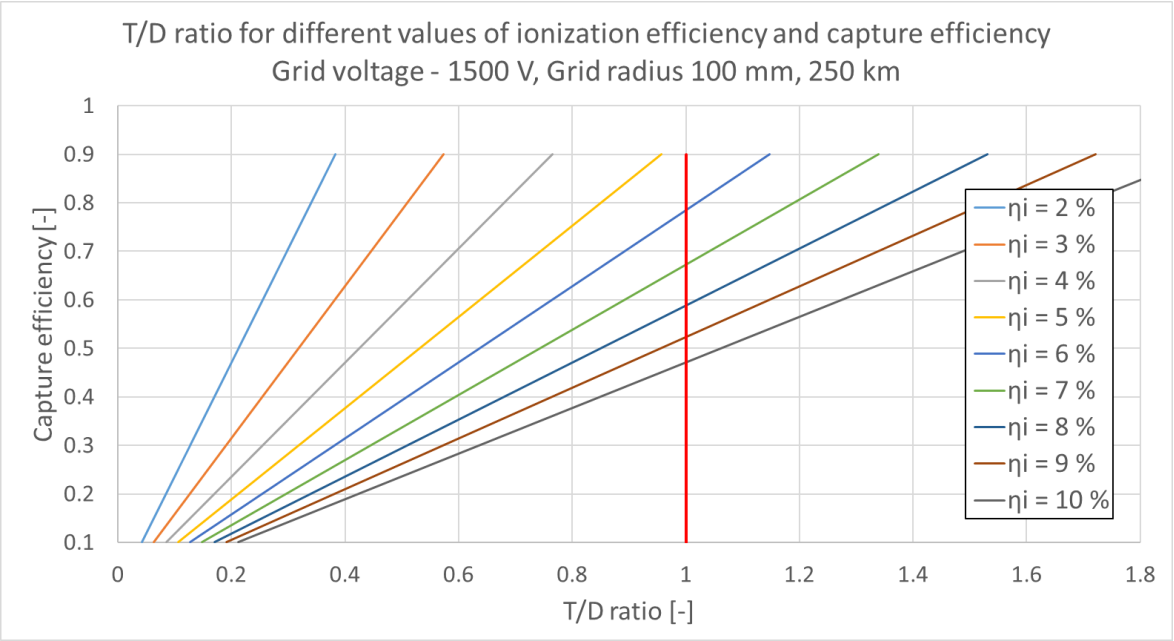

(a)

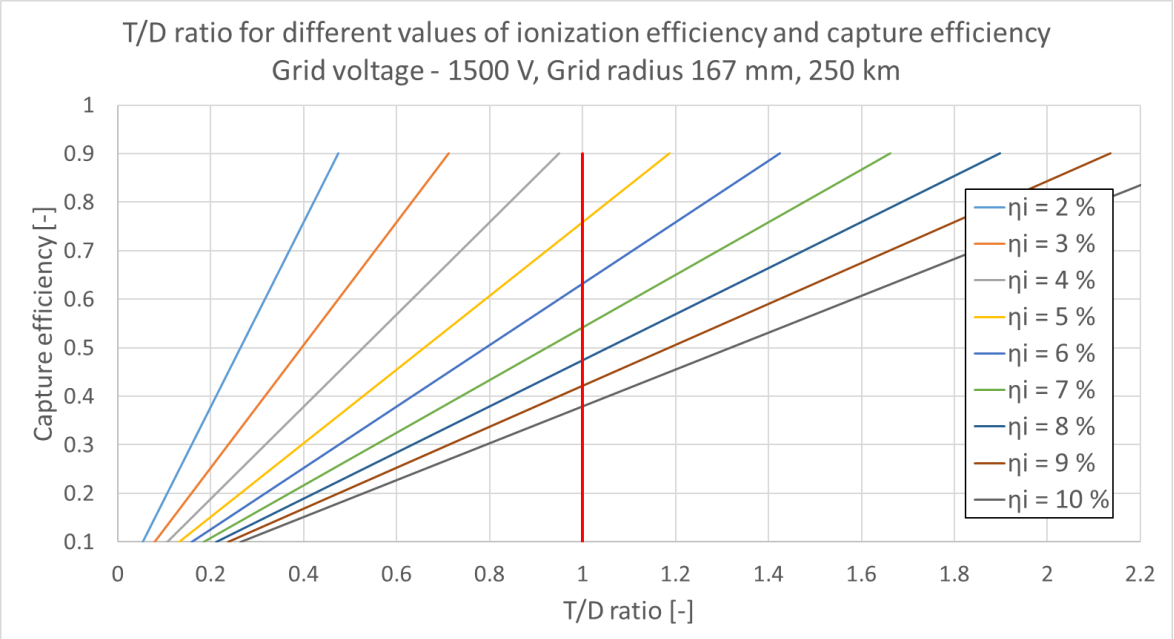

(b)

Figure 7.13: T/D ratio values for variable capture efficiency at an orbit altitude of 250 km for different ionization efficiency values.
a) - 150 mm inlet radius and 100 mm acceleration grids radius, *b)* - 250 inlet radius mm and acceleration grids 167 mm radius

7.4.4.2 Thrust-to-Power ratio (T/P)

The next way of evaluation of the engine performance relates the achievable thrust to the required power. From the article on SpaceLab experimental propulsion [45], it is possible to deduce the values of the Thrust-to-Power ratio for different geometric configurations with which the research operated, namely different values of radii and lengths of the ionization chamber. For easy comparison with previous calculations, the configuration with a radius of 150 mm and a length of 100 mm was chosen. For these dimensions, the Thrust-to-Power ratio reaches 30.08 mN/Kw [45].

The resulting T/P ratio can be related to the value of atmospheric drag for different altitudes and sizes of the inlet, ie also the ram surface areas and the areas of the acceleration grids. The following plot shows the power required for drag compensation at the altitudes relevant to the usage of the ABIT drive. It is clear that for a 6U CubeSat with an engine that has an inlet radius of 250 mm, and a combined ram area of 0.226 m^2, over 100 W is needed at an altitude of 200 km to develop the required thrust and about 30 W for an altitude of 250 km. When the engine size is reduced to an inlet radius of 150 mm, the drag and thus the required power decreases. For the drag compensation at a 200 km altitude, 55 W is needed, and only 13 W is enough for 250 km altitude.

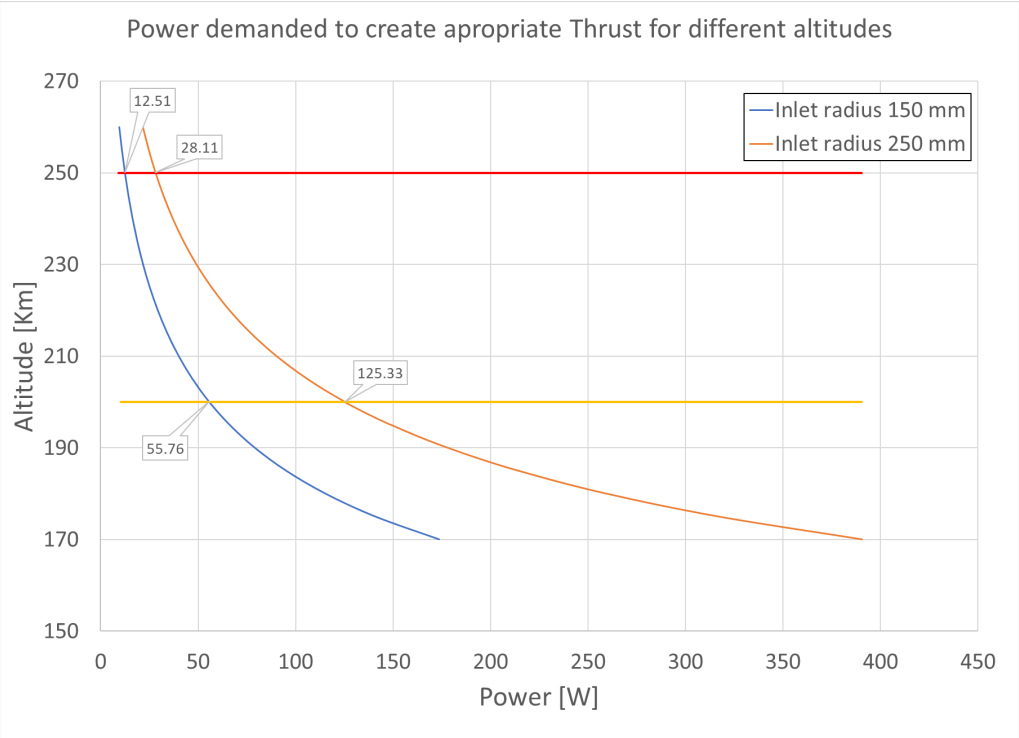

Figure 7.14: Power required to compensate for atmospheric drag on the VLEO with a thrust-to-power ratio of 30.08 mN/kW for two different sizes of ABIT engine inlet and 6U CubeSat.

With the knowledge of available power for propulsion purposes, see section 7.4.3, and engines thrust per unit of power efficiency, the graph that shows relationship between atmospheric drag, achievable thrust, altitude and inlet dimension can be plotted.

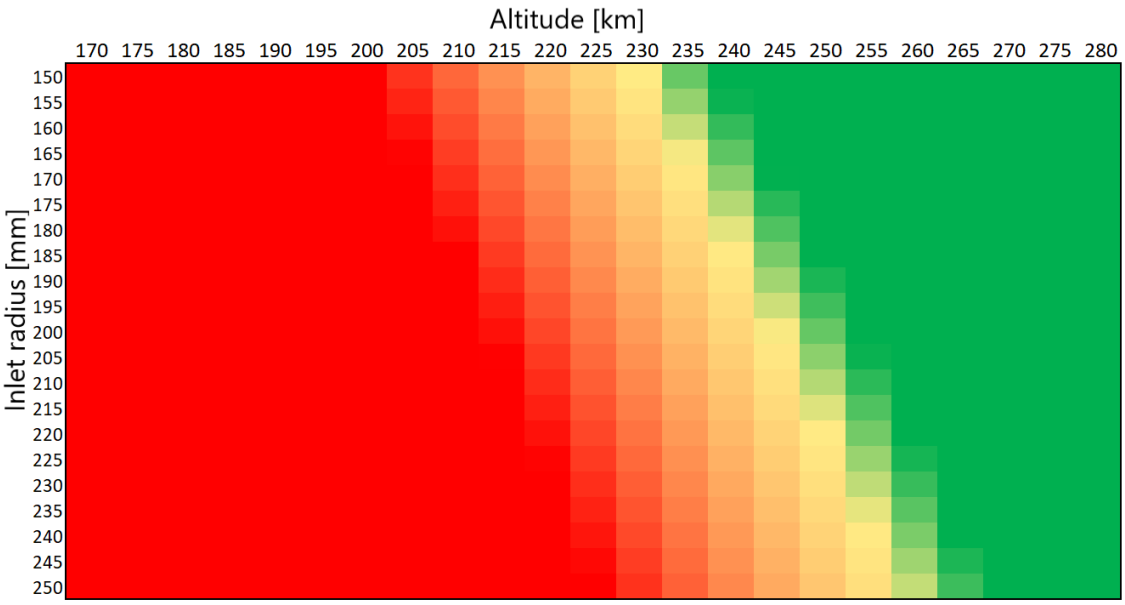

Figure 7.15: Comparison of atmospheric drag and achievable thrust ploted against altitude and inlet dimensions. The *green area* represents feasible region, the *yeallow area* is the limit line and the *red area* represents drag overcoming achievable thrust.

It is clear that the available power is sufficient to generate enought thrust for drag compensation at the altitude of 230 km with the inlet radius of 150 mm. On the other side of the spectrum, using the inlet radius 250 mm will allow drag compensation only above the 255 km of altitude.

Depending on the size of the inlet used, a value of the accumulated particles of atomic oxygen on the surface of the inlet can be added. As mentioned, the exact degree of contamination and absorption depends on the material used and it is the subject of ongoing research. For this reason, only the amount of atomic oxygen particles that come into contact with the inlet material for the duration of the mission, 5 years, is presented, regardless of the subsequent reaction. The result is shown in the figure 7.16.

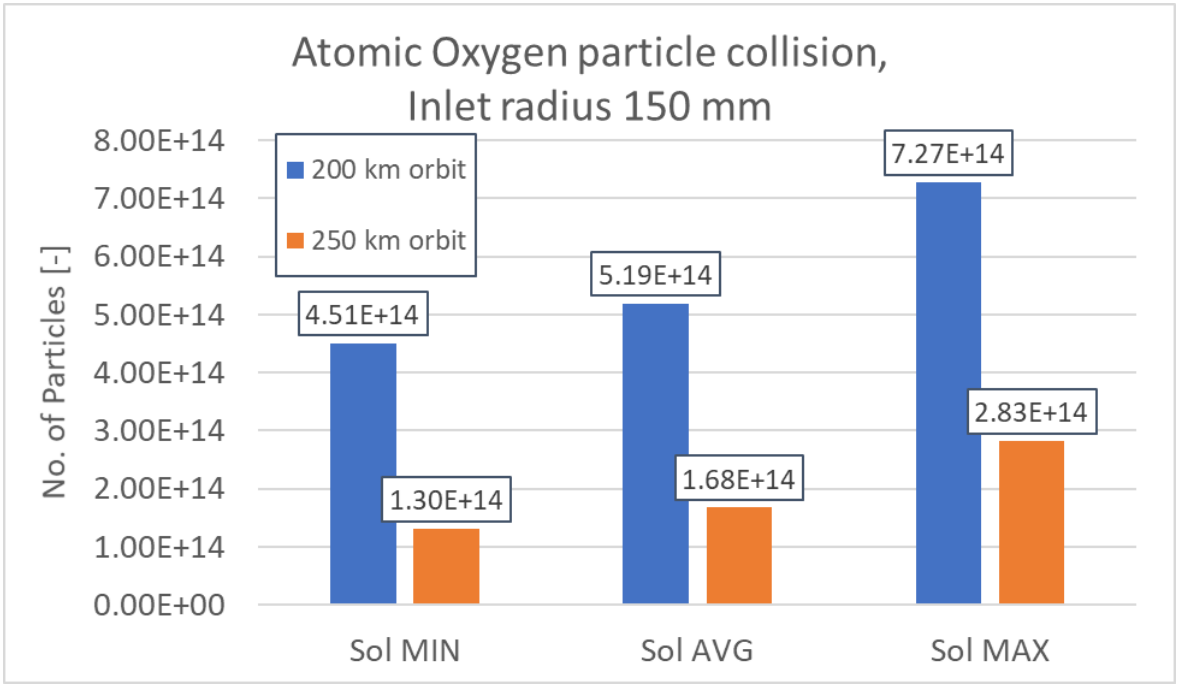

(a)

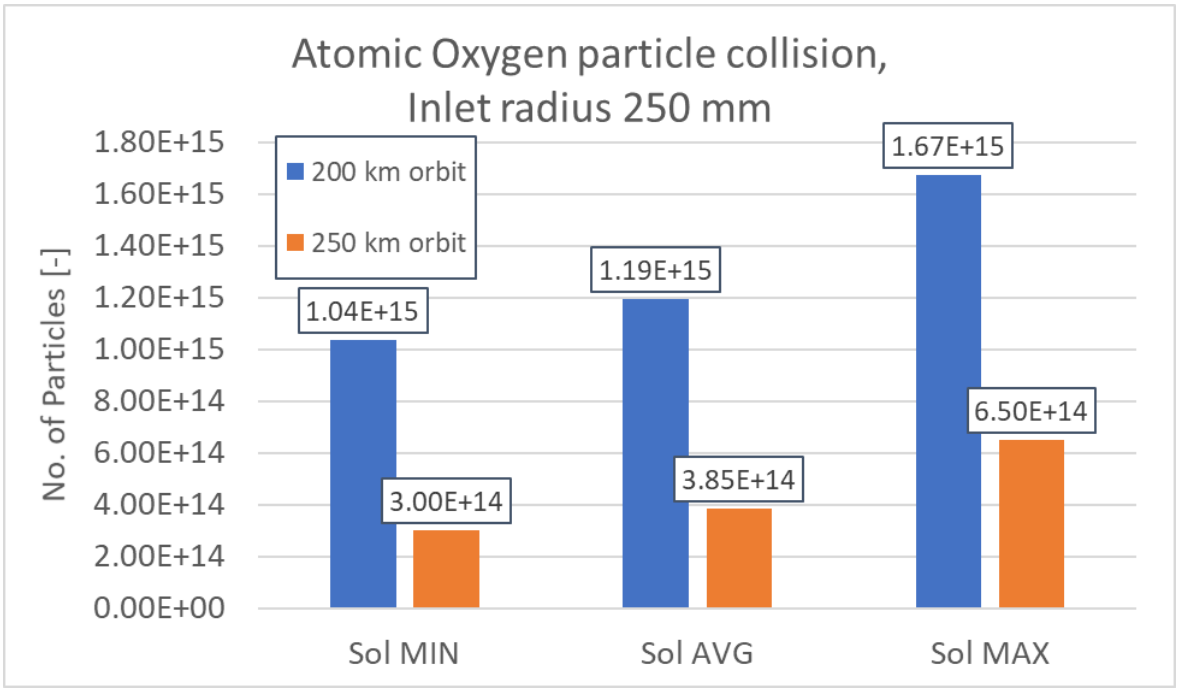

(b)

Figure 7.16: An amount of atomic oxygen particles reacting with the material of the inlet at an orbit altitude of 200 km and 250 km for the duration of the mission - 5 years. *a)* - Inlet radius 150 mm, *b)* - Inlet radius 250 mm

7.4.4.3 Propulsion Unit Summary

It can therefore be stated that for the proposed mission of Earth's atmosphere X-ray monitoring, it is possible to use an air-breathing propulsion unit if it meets the following parameters. It is mainly a degree of ionization of at least 9 % and a capture efficiency of at least 50 %. However, for a sufficient value of the thrust, it is necessary to have higher voltage on the acceleration grids. The proposed value of 1500 V seems to be sufficient while maintaining the rest of the parameters. At the same time, for the VLEO region, ie an altitude of about 200 km to 250 km, it is necessary to develop a thrust of the orders of 10^{-3} N and 10^{-4} N with available energy of about 17 W created by solar panels. This corresponds to the required thrust efficiency per unit of power between 58.8 mN/kW and 5.88 mN/kW. The proposed drive from SpaceLab achieves the value of 30.08 mN/kW, therefore it meets this condition. The critical indicators for the SpaceLab drive will therefore be the capture and ionization efficiencies.

Propulsion system
Inlet dimensions: 150 - 250 mm.
Accelerating grids dimensions: 100 - 170 mm.
Accelerating grids voltage: 1500 V.
Ionization degree: 9 %.
Capture efficiency: 90 - 50 %.

Table 7.9: Propulsion system baseline concept.

7.4.4.4 Propellant break-even point

An important analysis in the design process of a mission using an air-breathing engine is a comparison with the classic version of electric propulsion. From the theoretical description of the ABIT propulsion, it is clear that with increasing height, the advantage of conventional electric propulsion will prevail, as such a large amount of fuel will not be needed to keep the satellite in a stable orbit. The altitude level at which classic electric propulsion becomes more advantageous is called *propellant break-even point*.

The experimental ion thruster called MiXi, which is being developed at the University of California, USA, was selected for this comparison. It is a micro ion thruster with a diameter of 30 mm [71]. It is being developed in order to implement a suitable and reliable propulsion system for 6U CubeSats. The exact engine parameters are summarized in the table 7.10.

MiXi engine parameters
Diameter: 30 mm
Specific impulse: 3000 s
Achievable thrust: 1.43 mN
Power: 30 W
Propellant type: Xenon

Table 7.10: MiXi engine parameters [71].

The MiXi engine can develop a thrust of up to 1.43 mN at a power consumption of 30 W. The value of the specific impulse reaches 3000 s and it uses compressed xenon as a propellant [71]. Xenon is stored in a propellant tank at a pressure of about 100 bar. At such pressure, the density of the gas is saturated, as shown in the figure 7.17.

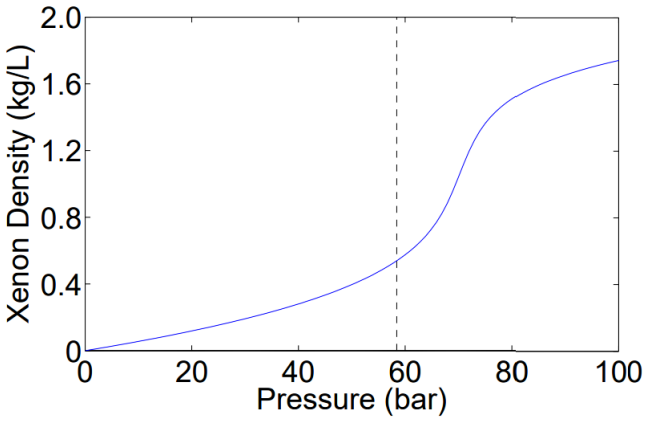

Figure 7.17: Density of xenon for different pressure levels [72].

The same geometric configuration was chosen for the analysis of the performance of the air-breathing engine as well as the selected MiXi thruster. Thus 6U CubeSat with a ram surface of 0.03 m^2 and attached cylindrical AB engine with an inlet radius of 150 mm and a length of 200 mm. In the case of the MiXi engine, a propellant tank of the same dimensions is externally mounted to the spacecraft bus instead of the engine. The usable volume of a xenon tank with such selected dimensions is difficult to calculate due the need to find the ideal thickness of the tank wall and additional structures inside the tank for proper propellant storage. For these reasons, a commercially available xenon propellant tank made by Cobham with a radius of 453.5 mm, a length of 336.5 mm and an internal volume of 268 l was selected [73]. Its internal volume was then proportionally adjusted for a tank of the required dimensions. This theoretical pressure vessel thus has an internal volume of about 8.71 l into which 15.25 kg of xenon can fit at a pressure of 100 bar.

Using the value of the specific impulse, it is possible to calculate how many kilograms of propellant are needed to compensate for atmospheric drag. The graph 7.18 outlines the required mass of the propellant for the duration of the mission of 2 years for different orbital altitudes. In addition, curves for theoretical engines with a lower specific impulse and the volume limit of the selected propellant tank are plotted as well.

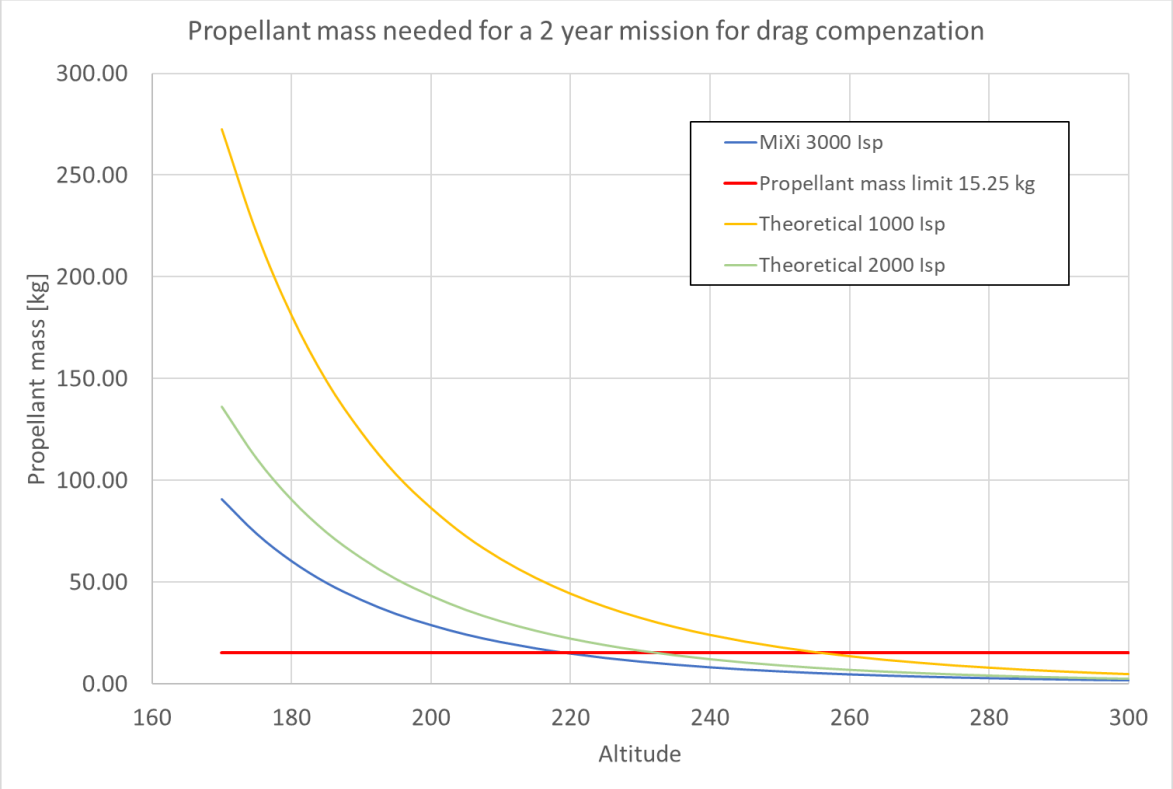

Figure 7.18: Required propellant mass to compensate for atmospheric drag at different altitudes using the MiXi engine for 2 years mission lifespan.

It is evident that for the selected propellant tank with 15.25 kg of xenon, the MiXi drive is able to compensate the atmospheric drag for 2 years from the altitude of 220 km. For lower orbits, the selected amount of propellant is insufficient. Engines with a lower specific impulse encounter lack of propellant in orbits lower than 235 km for a specific impulse of 2000 s, and 255 km for a specific impulse of 1000 s, respectively.

The graph 7.19 expresses the required amount of propellant for the three selected orbit altitudes over a different time horizon. It is shown there that for a given propellant mass limit, it is possible to compensate the atmospheric drag at an altitude of 200 km for about 12 months. For an altitude of 250 km it is already up to 5 years and for an altitude of the orbit 300 km and above it is more than 10 years.

Ultimately, the graph 7.20 presents a comparison of the energy expended to create the required thrust between the MiXi engine and the selected ABIT engine. It is clear that the power required by the MiXi engine is considerably less than that power required by the ABIT engine. For an orbit altitude of 250 km the difference is around 4.1 W and for the altitude of 200 km the difference is up to 20 W.

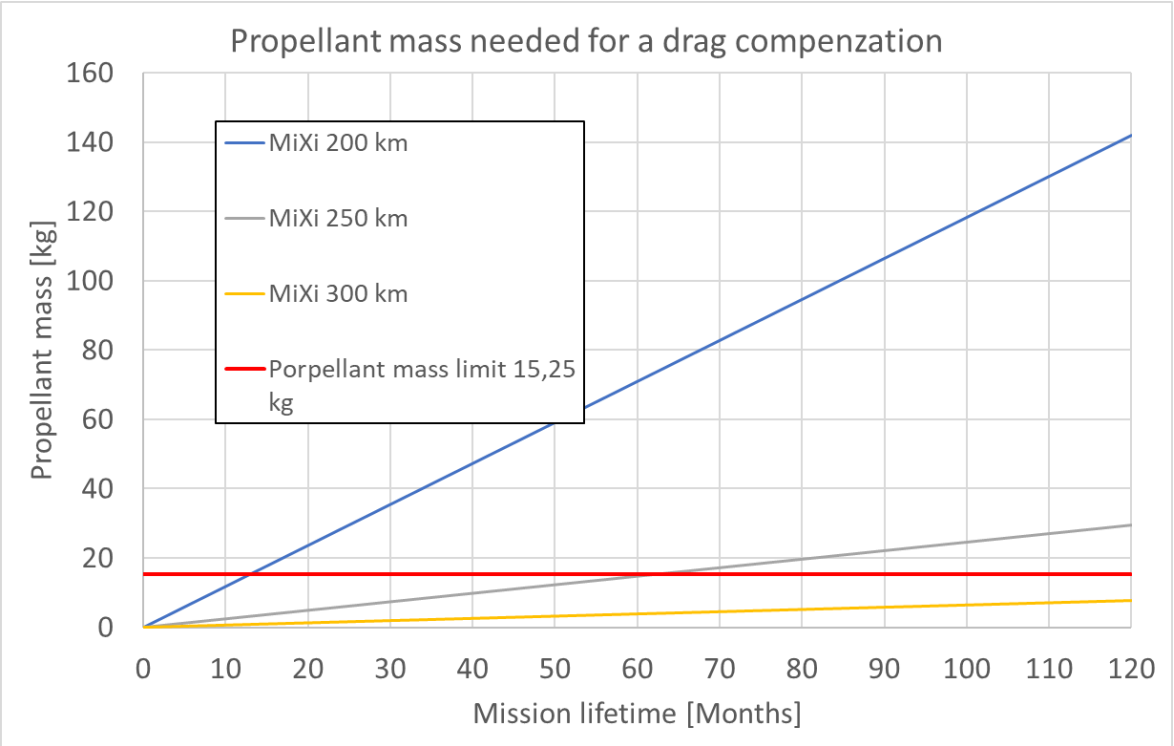

Figure 7.19: Required propellant mass for atmospheric drag compensation at altitudes of 200 km, 250 km and 300 km using MiXi engine

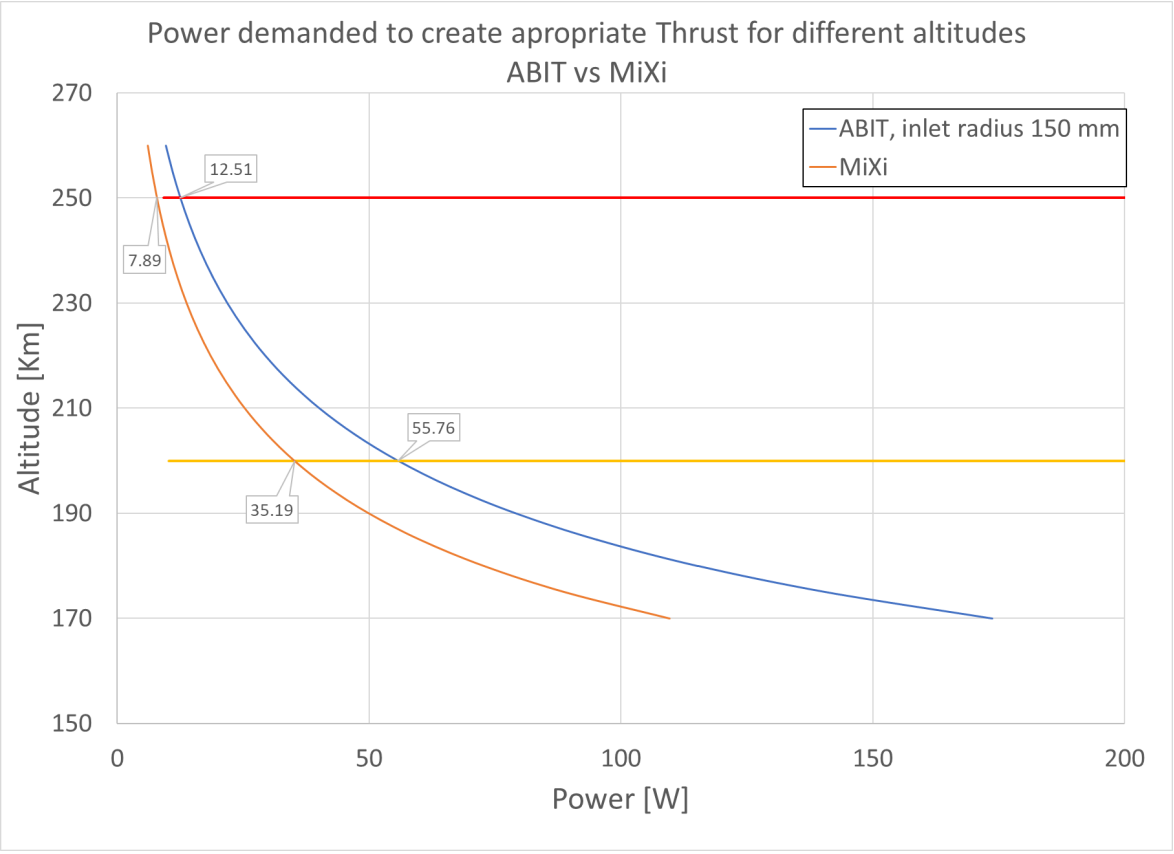

Figure 7.20: Power required to create the appropriate thrust needed to compensate for atmospheric drag. Comparison of MiXi and ABIT engine.

Based on the presented data, it can be stated that the selected MiXi engine with given propellant tank dimensions is more advantageous under certain conditions due to the high achievable thrust and relatively low power consumption. It depends mainly on a combination of a suitable orbit altitude and mission lifetime. Given the geometric configuration of the propellant tank, it follows that the MiXi is more advantageous from the orbit altitude of 220 km with a mission lifetime of 2 years. For longer missions, the minimal altitude of the orbit where MiXi is usable is already increasing. For example, for missions longer than 5 years, due to the limited amount of propellant, it is more advantageous to use an air-breathing type of propulsion for all regions below 250 km.

It should be noted that MiXi engine is currently only in the experimental phase and reaches excellent values, mostly of the specific impulse, achievable thrust and consumption per unit of power. The competitive ion thruster designed for CubeSats made by Busek co., called BIT-3, already has about half the value of the specific impulse and about four times less efficiency in terms of consumption per unit of power, see table 7.11 [74]. Thus comparison with the proposed ABIT drive would be more in favor of air-breathing technology.

	MiXi	***BIT-3***
Diameter:	30 mm	25 mm
Specific impulse:	3000 s	1400 s
Achievable thrust:	1.43 mN	0.66 mN
Power consumption:	30 W	56 W
Propellant type:	Xenon	Ionide

Table 7.11: MiXi and BIT-3 comparison [71] [74].

7.5 Summary

The baseline concept of a space mission in VLEO to measure and monitor X-ray sources in the Earth's atmosphere was designed. To successfully achieve the mission's objectives, the 6U CubeSat satellite with its propulsion system unit in the form of an air-breathing ion thruster was chosen. The mission was designed to meet the basic requirements arising from the mission statement and the chosen objectives of the mission. The active mission time was originaly chosen to be at least 2 years, which is considered the limit of the feasibility of conventional electric propulsion for drag compensation [28], but as the comparison in the section 7.4.4.4 shows, 5 years lifespan is more appropriate. All the designed elements should be capable of such a prolongation. It is desirable to exceed the lifetime limit of a classical electric propulsion capabilities for demonstration purposes of viability of air-breathing technology as a competitive alternative.

In the baseline concept, the mission schedule was roughly designed, the spacecraft bus was described, the payload and the mission subject were selected. The satellite's power subsystem and air-breathing propulsion unit have been described and analyzed in more detail. It was shown for which dimensions, performance parameters, and atmospheric environment it is theoretically feasible to operate the unit, based on data aquired from interactive tool, described in Chapter 6, and data from available mathematical simulations.

Chapter 8

Conclusion

Within this work, an analysis of the space mission to VLEO using an air-breathing (AB) propulsion to maintain a constant orbit of the CubeSat satellite was performed. The theoretical foundations presented in the Chapters 2 - 5, which describe the principle of classical and air-breathing electric propulsion, risks associated with the VLEO region, X-ray optics and space mission design process, were used to construct a comprehensive view of the issue of space missions in very low Earth orbits and its possible solution. The performed analysis, which is based on these bases, should answer, or at least direct the subsequent research in the following topics:

- Is the proposed spacecraft developed by SpaceLab usable for a space mission to measure X-ray sources in the Earth's atmosphere?
- In which area of the atmosphere is the application of AB engines feasible?
- What parameters must be achieved for real and commercial use?
- What is the usability of AB engines compared to conventional electric propulsion?

8.1 Feasible region of use for AB engines

The initial determination of the feasible region of AB engines results primarily from the limited amount of power and the density of atmospheric particles.

For the ideal functioning of an air-breathing unit it is necessary to achieve a particle pressure in the ionization chamber between values of 10 - 100 mPa, see Chapter 3. This value corresponds to the altitudes between 110 - 125 km without any added compression system, or 190 - 280 km with a compression factor of 200, which should be provided by a suitably selected inlet.

The amount of available power is analyzed in section 7.4.3. The value of available power for the propulsion unit using the selected satellite and geometry is sufficient enough to compensate for atmospheric drag at a minimum altitude in the range of 230 - 255 km, see graph 7.15.

Thus, it can be stated that AB propulsion with selected parameters, such as available power and satellite size, is usable in the altitude range from 230 km to 280 km. Results are strongly dependent on the size of the satellite and engine inlet used, the available power and the propulsion efficiency in terms of power consumption per unit of thrust.

8.2 Required parameters of an AB engine

A subsequent take on the AB propulsion issue shows the values of key parameters of the air-breathing engine, which must be achieved in its design to develop sufficient thrust. The following values of selected parameters were used within the performed analysis:

Inlet radius	150 mm and 250 mm
Accelerating grids radius	100 mm and 167 mm
Accelerating grids voltage	500 V, 1000 V, 1500 V
Ionization efficiency	2 - 10 %
Capture efficiency	10 - 90 %

Table 8.1: Values of selected engine parameters that were used for the analysis.

For the analysis of different values, the created tool with interactive graphs described in the Chapter 6 can be used.

The calculations show that the geometric configuration of the engine again strongly influences the resulting performance. Mostly radius of an inlet and acceleration grids. Two possible configurations were analyzed. *Small configuration* with an inlet radius of 150 mm and an acceleration grids radius of 100 mm and *Large configuration* with an inlet radius of 250 mm and a grid radius of 167 mm. It can be seen that while maintaining the same ratio of the two radii, *large configuration* is more advantageous in terms of achievable thrust related to atmospheric drag.

The table 8.2 summarizes the required ionization level values for atmospheric drag compensation when the capture efficiency drops to 50 % for both analyzed configurations, at different values of grids voltage and two selected orbits from the VLEO region.

Small configuration	Altitude 200 km	500 V	-
		1000 V	-
		1500 V	η_i >10 %
	Altitude 250 km	500 V	-
		1000 V	η_i >10 %
		1500 V	η_i >9 %
Large configuration	Altitude 200 km	500 V	-
		1000 V	η_i >10 %
		1500 V	η_i >9 %
	Altitude 250 km	500 V	-
		1000 V	η_i >9 %
		1500 V	η_i >8 %

Table 8.2: Summary of desirable levels of ionization in propulsion unit.

If it is not possible to reach these values of the ionization level, it is necessary to compensate the missing performance with a higher voltage, improving the capture efficiency, or changing the geometric configuration.

8.3 Comparison of classical and AB electric propulsion

An experimental MiXi ion thruster with a propellant tank of the same size as the proposed AB propulsion unit was chosen for the analysis. With known parameters of MiXi thruster, which are listed in the table 7.10, it was calculated the amount of propellant is sufficient to compensate for atmospheric drag for 2 years above the altitude of 220 km. It was also shown that it is possible to operate the given engine at an altitude of 250 km for up to 5 years.

Thus, it can be considered that for a space mission at an altitude below 250 km, it is more advantageous to use an air-breathing propulsion, mainly for space missions lasting longer

than 5 years. This conclusion is roughly identical to the conclusion presented in the article *Di Cara, 2007* [28], where the author came to the conclusion that classical electric propulsion is usable for drag compensation at altitudes below 250 km only for a maximum period of 2 years. The difference in the time range is most likely due to the selected engine, ie MiXi, as it has excellent parameters of specific impulse and energy consumption in its category and the engine was not available at the time of mentioned article publication.

At the same time, it should be noted that a linear relationship between the maximum available thrust, power consumption and specific impulse was used in the calculations for lower values of thrust. This was due to the missing power consumption data and a specific impulse for different thrust values.

8.4 X-ray monitoring feasibility

From the theoretical basis, it is clear that in order to successfully perform the mission of monitoring X-ray atmospheric emission, it is necessary to operate a satellite in the lowest possible orbit. The analysis shows that it is possible to keep the selected satellite in a stable orbit at an altitude of approximately 230 to 280 km using an AB propulsion that meets the above-mentioned criteria. This altitude is unquestionably more advantageous for measuring X-ray atmospheric and auroral sources than the commonly available orbits on the LEO, ie altitudes above 400 km.

8.5 Discussion

It is possible to follow up on the performed analysis not only by a doctoral study of electric propulsion, but also by refining the presented calculations and generalizing the results. It was mentioned that many calculations were performed for one or two specific scenarios, with a fixed geometry of the satellite and the propulsion unit. This was due to the limitation of variable parameters and simplification of calculations for the given goal of the work, ie the use

of ABIT for a space mission, which aims to monitor X-ray sources in the Earth's atmosphere. It is therefore possible to generalize the initial parameters and create a comprehensive study of the usability of the air-breathing propulsion.

For this purpose, a tool with interactive graphs, described in the Chapter 6, was created. However, this is an early version, which was used primarily for the purposes of this work. For a comprehensive analysis of the issue, it is necessary to implement more advanced functions and improve the existing ones. The difficulties may arise from the strong interconnection of all segments of the space mission that affects each other. The strongest link is evident between the satellite's power system, the propulsion unit, and the selection of orbit.

At the same time, there is a problem with the lack of experimental data. The air-breathing technology is still in its infancy and many experimental, as well as theoretical data, are still completely missing. The greatest progress in this industry is promised by the already mentioned project *Discoverer* [29], or private companies such as SpaceLab, developing their own air-breathing ion propulsion.

8.6 Future prospects of the technology

Throughout the whole thesis, it was emphasized that for the most part, the issue of air-breathing propulsion is still not a fully understood topic, hence it is necessary to answer many questions before the real and commercial use will be available. The most significant obstacles, as this thesis also demonstrates, are mainly the subject of available power, ie power efficiency of the propulsion unit, ionization efficiency in the ionization chamber and capture efficiency, which depends on the shape and material of the inlet.

Due to the current state of the technology and knowledge about the issue, which is at the level of theoretical studies and initial laboratory experiments, it is suitable topic for subsequent research in postgraduate studies. Subsequent research should focus on improving the ionization process and implementation of the propulsion system into the satellite design.

List of Figures

List of Tables

Bibliography

[1] Orbitální dálnice: Kolik umělých družic obíhá kolem Země? — 100+1 zahraniční zajímavost. [online]. [15.10.2020]. Available at: https://www.stoplusjednicka.cz/orbitalni-dalnice-kolik-umelych-druzic-obiha-kolem-zeme

[2] Satellite Database — Union of Concerned Scientists. [online]. [10.05.2021]. Available at: https://www.ucsusa.org/resources/satellite-database

[3] How many satellites orbit Earth and why Space Traffic Mgmt is crucial [online]. [17.10.2020]. Available at: https://www.geospatialworld.net/blogs/how-many-satellites-orbit-earth-and-why-space-traffic-management-is-crucial/

[4] Daniel Oltrogge, Kyle Leveque, *An evaluation of cubesat orbital decay*, Conference on Small Satellites, USA, 2011

[5] Stephen W. Jackson, *Design of an Air-Breathing Electric Thruster for CubeSat Applications* [Master thesis], University of Colorado, 2017

[6] Larson W. J., Wertz, J. R., *Space Mission Analysis and Design*, Microcosm Inc., Netherlands, 3rd ed. , 1999

[7] Hugo Nguyen, Johan Kohler, *The merits of cold gas micropropulsion in state-of-the-art space missions*, 2002

[8] *Tactical Propulsion and Controls*, Alliant Techsystems, ATK Space Propulsion Products Catalog, 2008

[9] How much do rockets pollute? - Everyday Astronaut [online]. [17.10.2020]. Available at: https://everydayastronaut.com/rocket-pollution/

[10] Christophe Koppel, Gary Quinsac, *Electric Thruster Selection Criteria*, 8th European Conference for Aeronautics and Space Sciences (EUCASS), 2019, DOI:10.13009/EUCASS2019-805

[11] Goebel D. M., Katz L., *Fundamentals of Electric Propulsion: Ion and Hall Thrusters*, JPL Space Science and Technology Series, John Wiley & Sons, Inc., 2008

[12] Ethan Dale, Benjamin Jorns, Alec Gallimore, *Future Direction for Electric Propulsion Research*, Aerospace 2020, 7, 120, 2020, doi:10.3390/aerospace7090120

[13] Tsuyohito Ito, Nicolas Gascon, W. Scott Crawford, Mark A. Cappelli, *Futher Development of a Micro Hall Thruster*,American Institude of Aeronautics and Astronautics, Standford University, 2006, 10.2514/6.2006-4495.

[14] Edgar Y. Choueiri, *A Critical History of Electric Propulsion: First Fifty Years (1906-1956)*, AIAA-2004-3334, Princeton University, New Jersey, 2004

[15] MEK - Mala encyklopedie kosmonautiky a Space HotList [online]. [10.11.2020] Available at: https://mek.kosmo.cz/sondy/usa/ds1/index.htm

[16] Neil Antoson, *Electric Propulsion*, University of Colorado-Boulder, ASEN 5053, 2007

[17] Ian J. E. Jordan, *Electric Propulsion: Which One For My Spacecraft?*, JHU, Whiting School of Engineering, 2000

[18] Michael Meng-Tsuan Tsay, *Two-Dimensional Numerical Modeling of Radio-Frequency Ion Engine Discharge* [Doctoral Thesis], Massachusetts Institute of Technology, 2010

[19] Pasquale M. Sforza, *Thoery of Aerospace Propulsion (Second Edition)*, Chapter 13 - Space Propulsion, Butterworth-Heinemann, 2017, Pages 669-711, ISBN 9780128093269

[20] Edgar Y. Choueiri, Robert G. Jahn, *Electric Propulsion*, Encyclopedia of Physical Science and Technology 3rd ed., Volume 5, 2003, DOI: 10.1016/B0-12-227410-5/00201-5

[21] Foster E. John, Patterson J. Michael, *Microwave ECR Ion Thruster Development Activities at NASA Glenn Research Center*, AIAA–2002–3837, 38th Joint Propulsion Conference and Exhibit, 2002

[22] hall thrusters – Parabolic Arc. Parabolic Arc – All Space All the Time [online]. [12.11.2020] Available at: http://www.parabolicarc.com/tag/hall-thrusters/

[23] W. P. Wright, P. Ferrer, *Electric micropropulsion systems*, Progress in Aerospace Sciences, Volume 74, 2015, Pages 48-61

[24] Pavel Kubeš, *Impulsní silnoproudé výboje a jejich diagnostika*, Skriptum FEL ČVUT, Praha, 2004

[25] Koizumi H., Roysuke N., Komurasaki K., *Plasma acceleration processes in an ablative pulsed plasma thruster*, DOI:10.1063/1.2710454, AIP Publishing, Japan, 2007

[26] Komurasaki & Koizumi Laboratory [online]. [12.11.2020] Available at: http://www.al.t.u-tokyo.ac.jp/ppt_e.html

[27] QinetiQ - Solar Electric Propulsion, [online]. [25.11.2020] Available at: https://www.qinetiq.com/en/what-we-do/services-and-products/solar-electric-propulsion

[28] Di Cara D., Gonzales del Amo J., Santovincenzo A., Carnicero Dominguez B., Arcioni M., Caldwell A., Roma I., *RAM Electric Propulsion for Low Earth Orbit Operation: an ESA study*, 30th International Electric Propulsion Conference, IEPC-2007-162, Florence, Italy, 2007

[29] DISCOVERER [online]. [cit. 10.05.2021]. Available at: https://discoverer.space/

[30] N.H. Crisp, A. Macario-Rojas et al., *Investigation of Novel Drag-Reducing and Atomic Oxygen Resistant Materials in Very Low Earth Orbit using SOAR (Satellite*

for Orbital Aerodynamics Research), 71st International Astronautical Congress (IAC), The University of Manchester, England, 2020

[31] N.H. Crisp, P.C.E. Roberts et al., *The Benefits of Very Low Earth Orbit for Earth Observation Missions*, Progress in Aerospace Sciences 117 (2020), 10.1016/j.paerosci.2020.100619

[32] D. González, V. Cañas, J. Becedas et al., *Modelling and Simulation of Very Low Earth Orbits*, 8TH EUROPEAN CONFERENCE FOR AERONAUTICS AND SPACE SCIENCES (EUCASS), 2019

[33] F. Romano, Y.-A. Chan, G. Herdrich et al., *RF helicon-based inductive plasma thruster (IPT) design for an Atmosphere-Breathing Electric Propulsion system (ABEP)*, Acta Astronautica (2020), doi: https://doi.org/10.1016/j.actaastro.2020.07.008.

[34] National Geographic Society [online]. [cit. 10.05.2021]. Available at: https://www.nationalgeographic.org/encyclopedia/atmosphere-RL/

[35] NRLMSISE-00 Atmosphere Model. [online]. [10.05.2021] Available at: https://ccmc.gsfc.nasa.gov/modelweb/models/nrlmsise00.php

[36] National Oceanic and Atmospheric Administration. [online]. [20.11.2020] Available at: https://www.swpc.noaa.gov/products/solar-cycle-progression

[37] G. E. Cook, *Satellite Drag Coefficients*, Pianet. Space Sci. 1965, Vol. 13, pp. 929 to 946. Pergamon Press Ltd., 1965

[38] Burkhardt, H., M. Sippel, G. Krille, R. Janovksy, M. Kassebom, H. Lubberstedt, O. Romberg a B. Fritsche, *Evaluation of propulsion systems for satellite end-of-life de-orbiting*, 1-11. 10.2514/6.2002-4208, Germany, 2002

[39] Moe K., Moe M. M., *Gas-Surface interactions and satellite drag coefficients*, Planetary and Space Science 53 (2005) 793–801, 2005

[40] Fisher, Jan. *Optoelektronické senzory a videometrie*, Praha, Vydavatelství ČVUT, 2002

[41] Banks B., Rutledge S., Sechkar E., Stueber T., Snyder A., Groh K., Haytas Ch., Brinker D., *Issues and Effects of Atomic Oxygen Interactions With Silicone Contamination on Spacecraft in Low Earth Orbit*, NASA/TM-2000-210056, NASA Glenn Research Center, Cleveland, OH United States

[42] Miller, Sharon K. R., *Tutorial on Atomic Oxygen Effects and Contamination*, Applied Space Environments Conference, Huntsville, Alabama, 2017

[43] Ian K. Johnson, Robert M. Winglee, B. Race Roberson, *Pulsed Plasma Thruster for Atmospheric Operation*, 50th AIAA/ASME/SAE/ASEE Joint Propulsion Conference, AIAA 2014-3403, Cleveland, 2014

[44] Wirz, R., J. Polk, C. Marrese, J. Mueller, J. Escobedo, and P. Sheehan, *Development and testing of a 3cm electron bombardment micro-ion thruster*, International Electric Propulsion Conference, 2001

[45] Mrózek K., Dytrych T., Moliš P., Dániel V., Obrusník A., *Global plasma modeling of an electron cyclotron resonance plasma source in low-pressure nitrogen and oxygen for air-breathing electric propulsion applications*, Czech Republic, 2020

[46] Shabshelowitz, A., *Study of RF Plasma Rechnology Applied to Air-Breathing Electric Propulsion* [Disertation thesis], University of Michigan, 2013

[47] *JILA - Exploring the Frontiers of Physics*, [online]. [26.11.2020] Available at: https://jila.colorado.edu/ajsh/courses/astr1120_03/text/chapter2/L2S9.htm

[48] *X-ray Telescopes Introduction*, [online]. [26.11.2020] Available at: https://imagine.gsfc.nasa.gov/observatories/technology/xray_telescopes1.html

[49] Chandra X-ray Observatory — NASA. [online]. [26.11.2020]. Available at: https://www.nasa.gov/mission_pages/chandra/main/index.html

[50] *CHANDRA X-ray Observatory*, [online]. [26.11.2020] Available at: https://www.chandra.harvard.edu/index.html

[51] *XMM-Newton SOC Home Page*, [online]. [26.11.2020] Available at: https://www.cosmos.esa.int/web/xmm-newton

[52] *Lobsters in Space!* ,[online]. [26.11.2020] Available at: https://spacecentre.co.uk/blog-post/lobsters-in-space/

[53] *Lobster Eye X-Ray Imagining System and Method of Fabrication Thereof*, United States Patent Application Publication, Pub. No.: US 2007/0025512 A1, 2007

[54] W. K. H. Schmidt, *A Proposed X-Ray Focusing Device with Wide Field of View for Use in X-Ray Astronomy*, NUCLEAR INSTRUMENTS AND METHODS 127, 285-292, 1975

[55] Vladimír Tichý, Vojtěch Šimon, René Hudec, Adolf Inneman, David N. Burrows, *NANOX: proposed Nano-Satellite X-Ray Mission*, SPIE Optics + Optoelectronics, Prague, 2013

[56] Vladimír Tichý, René Hudec, Vojtěch Šimon, *Nano-sat lobster eye soft x-ray monitor*, XI Multifrequency Behaviour of High Energy Cosmic Sources Workshop, Palermo, Italy, 2015

[57] ADVACAM First Truly Spectral Imaging Camera - AdvaPIX TPX 3 - ADVACAM, [online]. [26.11.2020] Available at: https://advacam.com/camera/advapix-tpx3

[58] Martin Urban, Ondřej Nentvich, Veronika Stehlikova, Tomas Baca, Vladimir Daniel, Rene Hudec, *VZLUSAT-1: Nanosatellite with miniature lobster eye X-ray telescope and qualification of the radiation shielding composite for space application*, Acta Astronautica 140, 2017

[59] Project Jupyter. [online]. [11.05.2021]. Available at: https://jupyter.org/

[60] Kuneš Michal, *Návrh kosmické mise CubeSat* [Master thesis], ČVUT, Praha, 2016

[61] Třetí český CubeSat se chystá na start – kosmonautix.cz. kosmonautix.cz – Novinky ze světa kosmonautiky [online], [2.2.2021] Available at: https://kosmonautix.cz/2020/10/treti-cesky-cubesat-se-chysta-na-start/

[62] Ground station czCube and GES-ELECTRONICS. CubeSat.cz [online]. [2.2.2021] Available at: http://www.czcube.org/en/stanice/index.html

[63] M. H. Tsutagawa and S. Michael, *Triple junction InGaP/GaAS/Ge solar cell optimization: The design parameters for a 36.2% efficient space cell using Silvaco ATLAS modeling & simulation*, 2009 34th IEEE Photovoltaic Specialists Conference (PVSC), pp. 001954-001957, doi: 10.1109/PVSC.2009.5411544, 2009

[64] Goode P. R., Qiu J., Yurchyshyn V., Hickey J., Chu M-C., Kolbe E., Brown C. T., Koonin S. E., *Earthshine Observations of the Earth's Reflectance*, Geophysical Research Letters, Vol. 28, No. 9, Pages 1671-1674, 2001

[65] Wu Xiao, Yan JunJie, *Estimating the outgoing longwave radiation from the FY-3B satellite visible infrared radiometer Channel 5 radiance observations*, Chinese Science Bulletin, Vol. 56, No. 32: 3480 - 3485, doi: 10.1007/s11434-011-4686-6, 2011

[66] GOMspace — Power Systems . [online]. [14.4.2021] Available at: https://gomspace.com/shop/subsystems/power/default.aspx

[67] *NanoPower Battery - Datasheet*, Document No. 1017178, GOMspace, 2019

[68] Carlos R. Ortiz Longo and Steven L. Rickman, *Method for the Calculation of Spacecraft Umbra and Penumbra Shadow Terminator Points*, NASA Technical Paper 3547, 1995

[69] Ibrahim Tamir Osman, *Design and Implementation of EPS (Electrical Power System) of a CubeSat* [Bachelor thesis], University of Khartoum, 2012

[70] Hairik H. A., Abbas K. A., AbdulAbass A. K., *DC/DC Buck-Boost Converter Efficiency and Power Dissipation Calculation at Operating Points Not Included in the Datasheet*, Journal of Multidisciplinary Engineering Science and Technology (JMEST), ISSN: 2458-9403, Vol. 6 Issue 6, 2019

[71] Stephan A. Samples, Richard E. Wirtz, *Development Status of the Miniature Xenon Ion Thruster*, 36th International Electric Propulsion Conference, Austria, 2019

[72] Collard, T. A., Sheehan, J. P., Gallimore, A. D., *Pressurized Xenon Propellant Management System for the CubeSat Ambipolar Thruster*, 30th International Symposium on Space Technology and Science, Japan, 2015, IEPC-2015-364/ISTS-2015-b-364

[73] Cobham Mission Systems, Composite Pressure Solutions, Space Systems. Cobham Mission Systems, Home [online]. [cit. 27.04.2021]. Available at: https://www.cobhammissionsystems.com/composite-pressure-solutions/space-systems/

[74] O'Reilley, D., Herdrich, G., Kavanagh, D. F., *Electric Propulsion Methods for Small Satellites: A Review*, Aerospace 2021, 8, 22, 2021

Apendix

T/D ratio values for variable capture efficiency at an orbit altitude of 200 km for different ionization efficiency values. Acceleration grids voltage 500 V.

a) - 150 mm inlet radius and 100 mm acceleration grids radius, *b)* - 250 inlet radius mm and acceleration grids 167 mm radius

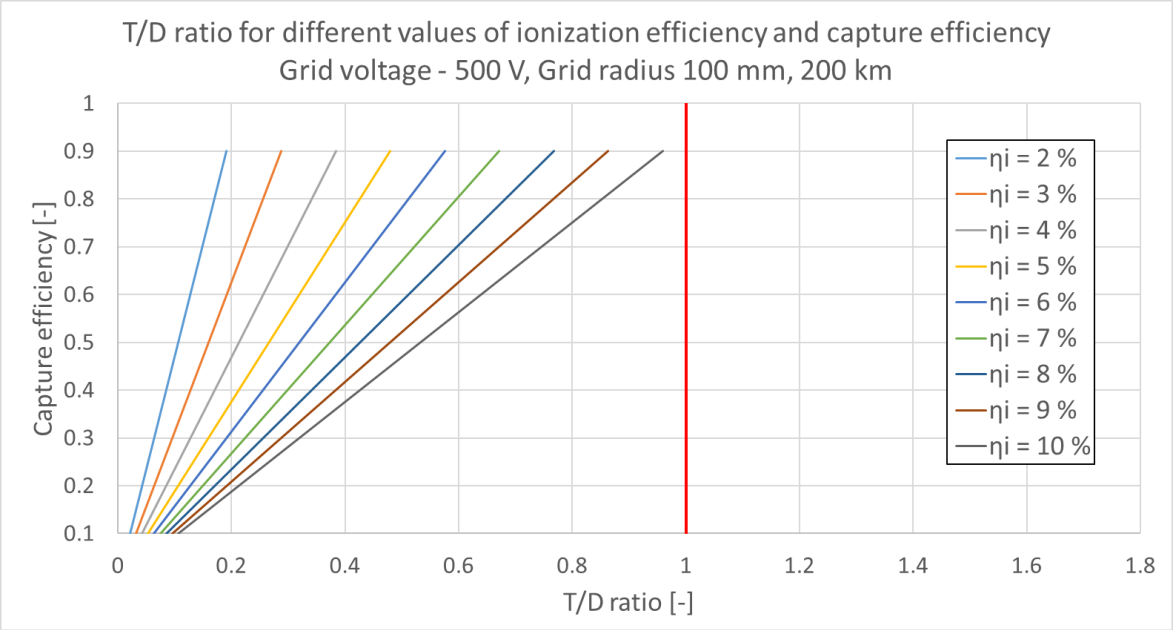

(a)

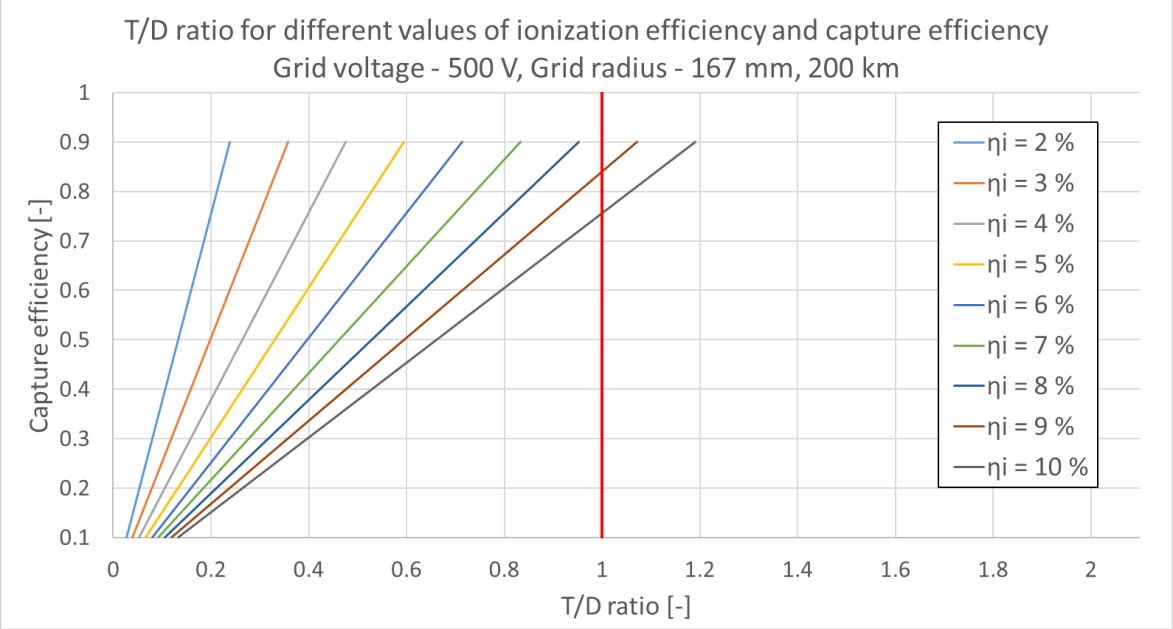

(b)

T/D ratio values for variable capture efficiency at an orbit altitude of 200 km for different ionization efficiency values. Acceleration grids voltage 1000 V.

a) - 150 mm inlet radius and 100 mm acceleration grids radius, *b)* - 250 inlet radius mm and acceleration grids 167 mm radius

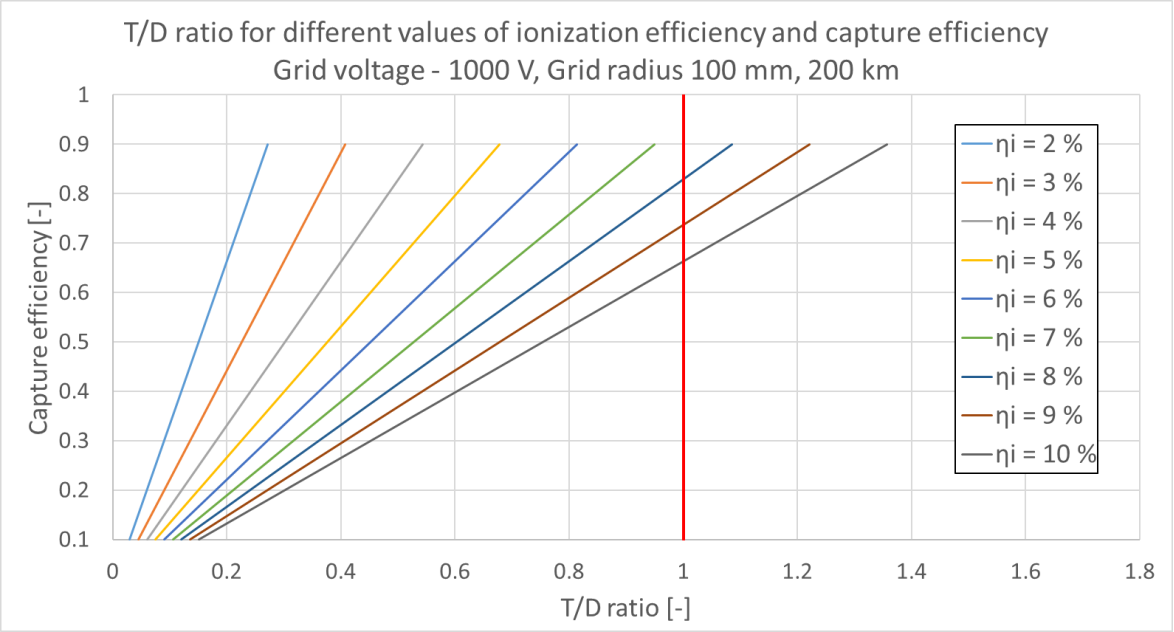

(c)

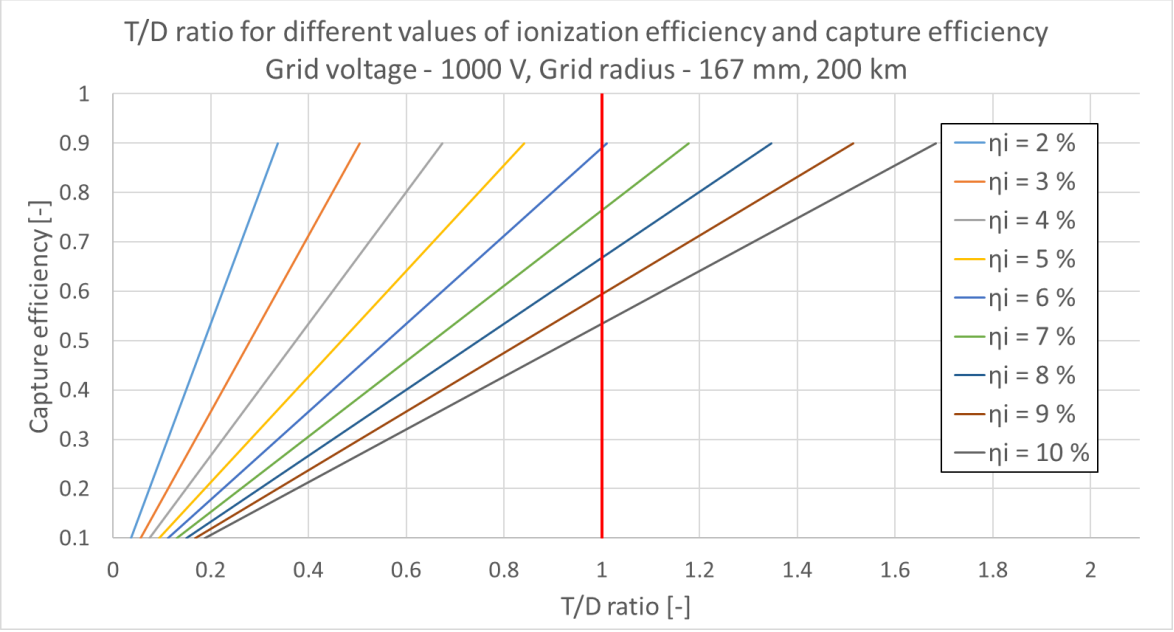

(d)

T/D ratio values for variable capture efficiency at an orbit altitude of 250 km for different ionization efficiency values. Acceleration grids voltage 500 V.

a) - 150 mm inlet radius and 100 mm acceleration grids radius, *b)* - 250 inlet radius mm and acceleration grids 167 mm radius

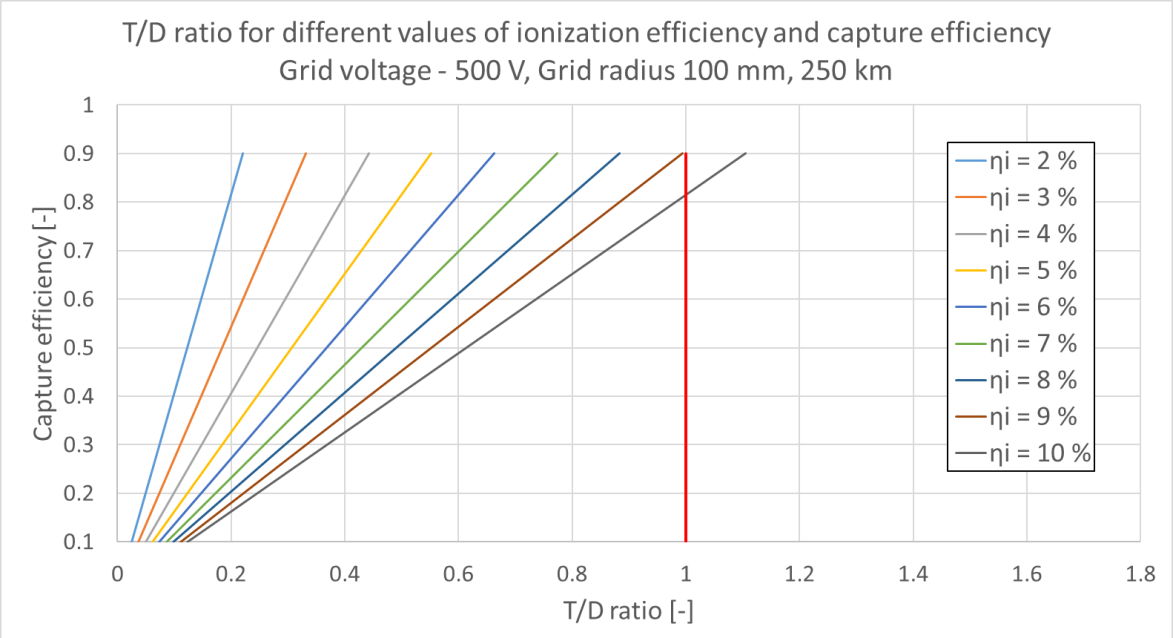

(e)

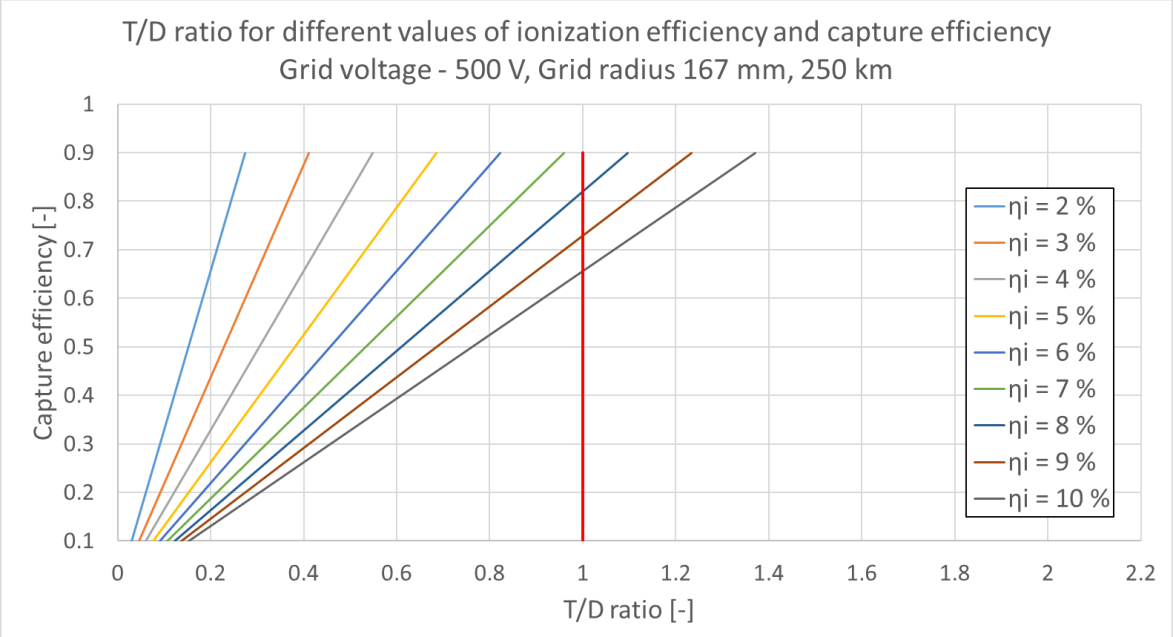

(f)

T/D ratio values for variable capture efficiency at an orbit altitude of 250 km for different ionization efficiency values. Acceleration grids voltage 1000 V.

a) - 150 mm inlet radius and 100 mm acceleration grids radius, *b)* - 250 inlet radius mm and acceleration grids 167 mm radius

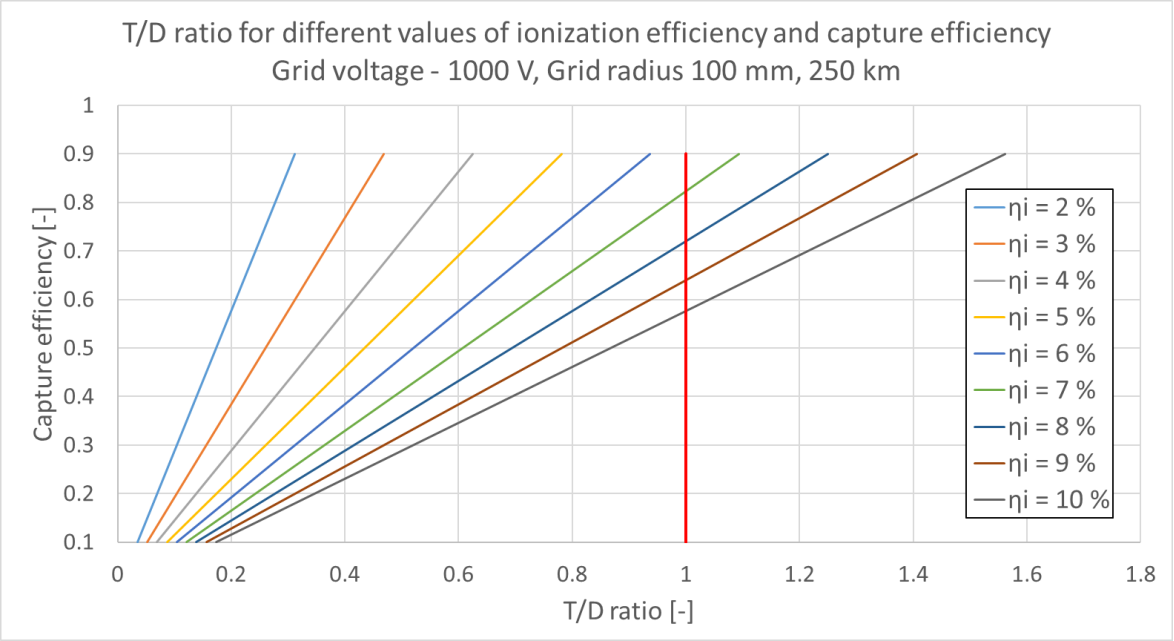

(g)

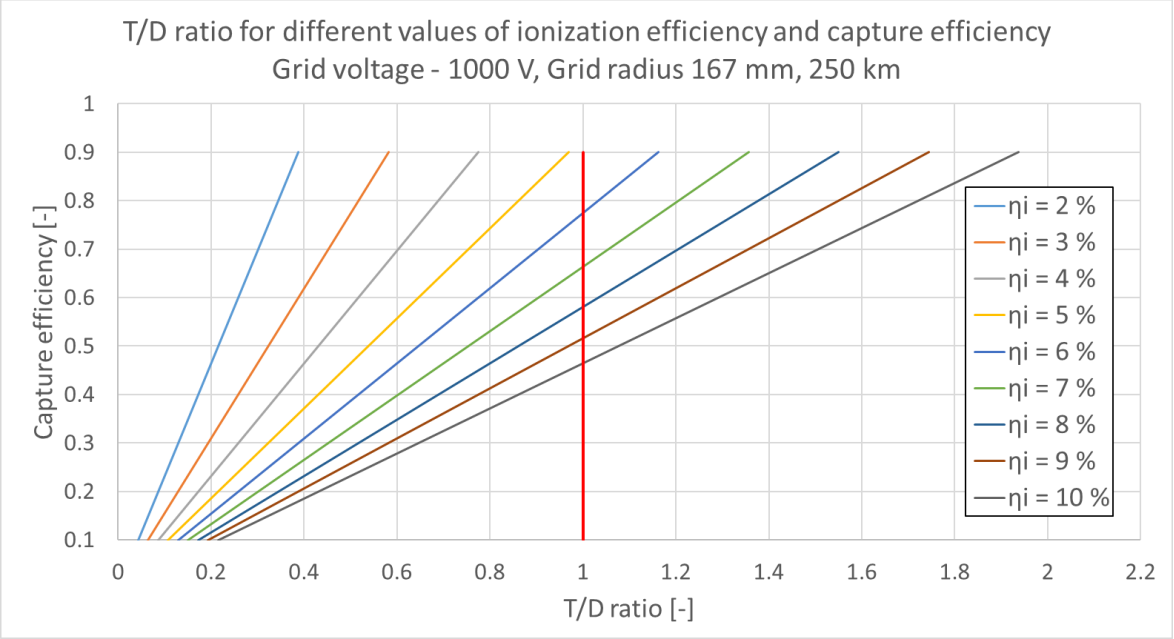

(h)